공학박사 학위논문

Application of Convex Optimization Techniques for Intelligent Electric Vehicles

지능형 전기자동차를 위한 최적화 기법의 적용

2015 년 2 월

서울대학교 대학원

전기·컴퓨터공학부

최 민 음

Application of Convex Optimization Techniques for Intelligent Electric Vehicles
지능형 전기자동차를 위한 최적화 기법의 적용

지도교수 서 승 우

이 논문을 공학박사 학위논문으로 제출함.

2015년 2월

서울대학교 대학원
전기·컴퓨터공학부
최 민 음

최민음의 공학박사 학위논문을 인준함
2015년 2월

위 원 장	최 진 영	(印)
부위원장	서 승 우	(印)
위 원	차 석 원	(印)
위 원	김 성 우	(印)
위 원	Mykel Kochenderfer	(印)

Abstract

Batteries are often damaged by a high peak power and a steep variation of the power since it has a relatively low power density. In order to reduce battery damage, the battery/super-capacitor (SC) hybrid energy storage system (HESS) has been utilized since the SC can act as a buffer against large magnitudes and rapid fluctuations in power. The major objective regarding the battery/SC HESS is to minimize the magnitude/variation of the battery power and the power loss. To achieve the objective, I formulate optimization problems to provide the optimal HESS power using given load operation profiles. In addition, I propose an algorithm using a barrier method and a Multiplicative Increase Additive Decrease method for providing a feasible optimal solution for energy management in HESS.

The battery/SC HESS can be effectively utilized for Electric Vehicles (EVs) because high peak power or rapid charging/discharging occur frequently in driving situations. However, the optimization method proposed in the second chapter cannot be adopted for EVs because it is difficult to obtain the future driving profile in advance. To calculate the optimal power of the battery/SC without the future profiles, I propose a method for computing the reference voltage of the SC based on the characteristic of power-train and the vehicle dynamics. In addition, I formulate the real-time optimization problem that minimizes the magnitude/variation of the battery power and the power loss simultaneously.

To improve the power control for the battery/SC HESS in EVs, it is necessary to know the future motor power in advance. They can be derived from the future speed/acceleration of the vehicle through the method proposed in the third chapter if the future speed/acceleration can be predicted. Fortunately, there are many prediction techniques such as car following models, path planning algorithms and model predictive schemes, which are based on results of target tracking. Therefore, the driving environments, e.g., moving objects, should be accurately estimated.

To improve the multi-target estimation accuracy even if there are many false detections, I propose a robust multi-target tracking scheme based on the GM-PHD filter. The proposed scheme includes the processing step of evaluating multiple states/measurements which is designed to overcome the weight under/over-estimation problem. Furthermore, it includes the step of generating the birth intensity for the next iteration using the measurements not associated with any tracked states. I also show that the proposed method can be extended to nonlinear Gaussian models.

Keywords: Optimal power control, Battery/Super-capacitor, Electric vehicle, Intelligent vehicle, Multi target tracking, Probability Hypothesis Density filter.

Student number: 2008-20990

Contents

1 Introduction **1**

1.1 Background and Motivations 1

1.2 Contributions and Outline of the Dissertation 3

1.2.1 Energy Management Optimization in a Battery/Supercapacitor Hybrid Energy Storage System 3

1.2.2 Real-time Optimization for Power Management Systems of a Battery/Supercapacitor Hybrid Energy Storage System in Electric Vehicles 4

1.2.3 Robust Multi-Target Tracking Scheme against False Detections based on Gaussian Mixture Probability Hypothesis Density Filter 5

2 Energy Management Optimization in a Battery/Supercapacitor Hybrid Energy Storage System **7**

2.1 Introduction 7

2.2 Active Hybrid Energy Storage Systems 11

2.2.1 A Review of Active Hybrid Energy Storage Systems 13

2.2.2 Considered HESS Topology 14

2.3 HESS Energy Management Optimization 15

2.3.1 Notations and Assumptions 15

2.3.2 Minimization of Magnitude/Fluctuation of Battery Power . . 17

2.3.3 Minimization of the Power Loss 21

2.3.4 Minimization of the Dual Objective Functions 22

2.4 Algorithm 23

2.4.1 Computation by Solver 24

2.4.2 Parameter Adjustment Algorithm 24

2.4.3 Analysis of the Total Number of Iterations in the Algorithm . 26

2.5 Simulation Results 28

2.5.1 Review of Previous Approach 29

2.5.2 Simulation Results 32

2.5.3 Adjustment of the Boundary Parameters in the Algorithm . . 33
2.6 Conclusion 34
2.7 Proof of 2^{nd} constraint in $\mathbf{P}_2$ 35

3 Real-time Optimization for Power Management Systems of a Battery/Supercapacitor Hybrid Energy Storage System in Electric Vehicles 36
3.1 Introduction 36
3.2 System Description 40
3.2.1 Powertrain Model 40
3.2.2 Regenerative Braking System 43
3.2.3 Battery/SC Hybrid Energy Storage Systems 45
3.3 Power Control System for HESS 47
3.3.1 Computation of SC Reference Voltage 49
3.3.2 Computation of the optimal SC power 51
3.4 Simulation Result 59
3.5 Conclusion 68

4 Robust Multi-Target Tracking Scheme based on Gaussian Mixture Probability Hypothesis Density Filter 69
4.1 Introduction 69
4.2 Background and Motivation 73
4.2.1 Prediction of Future Driving Profile 73
4.2.2 Brief Overview of The Conventional GM-PHD Filter 74
4.2.3 Problems of the GM-PHD Filter 77
4.3 The Proposed Robust GM-PHD Filter 83
4.3.1 Target Prediction and PHD Update Component Construction 85
4.3.2 State and Measurement Evaluation 86
4.3.3 PHD Updating and Merging 89
4.3.4 Duplication Check 91
4.3.5 Birth Intensity Generation for the Next Iteration 91
4.4 Nonlinear Gaussian Model Extension 92
4.5 Simulation Results 93
4.6 Conclusion 97

5 Conclusion and Future Work 110

List of Figures

2.1 The symbols used for denoting the HESS circuit 11
2.2 The active HESS topologies: (a) SC-only connected through a DC/DC converter, (b) battery-only connected through a DC/DC converter, (c) cascaded connection of the battery/SC using DC/DC converters, and (d) the battery/SC connected through the respective DC/DC converters. 12
2.3 The HESS topology considered in this chapter: Real-time controllers measure the power flows and command the DC/DC converters to adjust the amount of power flow. 14
2.4 The SC equivalent circuit. 14
2.5 The load profiles M1-M6. Time unit: seconds 30
2.6 The simulation results from solving the problem of energy management in the HESS at $\varepsilon_{\text{mag}} = 0.7$, $\varepsilon_{\text{var}} = 0.3$, $\sigma_1 = 26$, $\sigma_2 = 0.8$, $\gamma = 0.001$, and $\delta = 1$. A log barrier penalty function was applied in our algorithm. (a) The battery power obtained by our algorithm and Napoli's strategy, (b) the SC power obtained by our algorithm, (c) the SC energy obtained by our algorithm. 31
2.7 The adjustment of the boundary parameters σ_1 and σ_2 in Algorithm 2. Their initial values were $\sigma_1 = 2$, $\sigma_2 = 0.5$, $\alpha = 2$, $\beta_1 = 2$, and $\beta_2 = 0.5$. Average time of each inner iteration is 0.15 seconds. 34

3.1 Schematic of the system architecture. 40
3.2 Motor efficiency map. According to the torque and rotational speed, the power efficiency is determined. For example, at -50(Nm) and 6000(RPM), the power efficiency is about 95%. 41
3.3 Braking forces varying with deceleration rate [48]. 43
3.4 DC/DC converter efficiency map. 48
3.5 Flowchart of the proposed power control strategy 48
3.6 The power loss of DC/DC converter when $V_B = 300(V)$ and $V_{SC} = 150(V)$. The dashed line is obtained by (3.13) and the solid line is its approximated piecewise linear function. 53

3.7 The operating profile: the speed profile (FTP75) and the power required by the motor. The required power is computed by using the dynamic model described in Section II-A. 59
3.8 The simulation results: the SC power, the battery power, the SC voltage, and the battery voltage. 60
3.9 The battery power from $t = 200$ to 700 computed by the proposed strategy and the other strategies, i.e., the rule-based strategy, the SC voltage control based on the vehicle speed, and the fuzzy logic strategy. 61
3.10 The membership function used in the fuzzy logic strategy for comparison. 62
3.11 The look-up (rule bases) table used in the fuzzy logic strategy for comparison. 63
3.12 The accumulated power loss computed by the proposed strategy and the other strategies, i.e., the rule-based strategy, the SC voltage control based on the vehicle speed, and the fuzzy logic strategy. 64
3.13 The accumulated power loss computed by the proposed strategy with S_α =(0.1481, 0.01481, 1/3000, 1/3000, 0.1481) (solid line), S_α =(0, 0, 1/3000, 1/3000, 0.1481) (dotted line), and S_α =(0.1481, 0.01481, 0, 0, 0.1481) (broken line). 65

4.1 Overall procedure of the conventional GM-PHD filter [54]. 73
4.2 Overall procedure of the proposed robust GM-PHD filter. The steps marked with * are newly proposed in this chapter. 84
4.3 The confirmation score system μ. According to the confirmation score, the corresponding states are categorized into the following states: unconfirmed, confirmed, and lost states. 87
4.4 The PHD updating and merging process. Each cell means the Gaussian term represented by w and m. In the merging process, the Gaussian terms originating from the same target are merged into a single Gaussian term. 90
4.5 NGSIM dataset coverage: US-101 highway [65]. 93
4.6 Measurements obtained with the detection probability $p_{D,k} = 0.9999$ and $\lambda_c = 15$ clutters. 97
4.7 Multi-target tracks estimated by the proposed robust GM-PHD filter scheme with the detection probability $p_{D,k} = 0.9999$ and $\lambda_c = 15$ clutters. 98
4.8 Simulation results with $P_{d,k} = 0.9999$ 107
4.9 Simulation results with $P_{d,k} = 0.9$ 108
4.10 Simulation results with $P_{d,k} = 0.75$ 109

List of Tables

2.1 The SC Characteristics 29

3.1 The Battery Parameters 46
3.2 The Vehicle Parameters 58
3.3 Simulation results 65

4.1 The Notations 99

Chapter 1

Introduction

1.1 Background and Motivations

In recent years, as power electric systems are widely deployed in the transportation areas, the efficient power management has become one of the key issues. In typical power electric systems, a battery has been utilized for the portable energy storage device. Most of the battery devices are composed of a large number of cells to meet the sufficient load power. However, the life of battery can be diminished by a high peaked and fluctuated power that generates excessive heat and makes the internal resistance of battery large.

In order to supplement the weaknesses of battery, the battery/super-capacitor (SC) hybrid energy storage system (HESS) was proposed [1]-[13]. Since the SC has a relatively high power density, it acts as a buffer against high power or variations of the power required by the motor.

When controlling the power flowing through the battery/SC HESS, the following objectives have mainly been considered. First, the magnitude/variation of the battery power should be minimized in order to extend the life of the battery; this is a fundamental goal of the HESS. Second, the power loss should be minimized.

However, the previous researches have not tried to minimize these objectives simultaneously [1]-[13]. To achieve the objectives, I design optimization problems to provide the optimal HESS power using given load operation profiles in the second chapter.

Electric Vehicles (EVs) use batteries to store electric energy. The performance of EVs depends heavily on the battery because it has a large impact on the acceleration and driving distance on a single charge. Because the battery cells can be damaged by high peak power or rapid charging/discharging, which are originated from repetitive acceleration/deceleration of vehicles especially in urban situations, the battery/SC HESS has been adopted for the EVs.

When controlling the power flowing through the HESS in EVs, the State-of-Charge (SoC) of the SC should be adjusted according to future driving profiles [29][35][37]. Before the EV decelerates in near future, for example, the SC should be discharged beforehand in order to receive regenerative braking energy. However, it is difficult to know the future load profiles in advance. In the third chapter, I propose a method for calculating the reference voltage of the SC based on the characteristic of power-train and the vehicle dynamics. In addition, I formulate the real-time optimization problem that minimizes the magnitude/variation of the battery power and the power loss simultaneously.

To improve the power control for the battery/SC HESS in EVs, it is necessary to know the future motor operation profiles in advance. The future motor power of the EV can be computed by the method proposed in the third chapter if the speed/acceleration of the vehicle can be predicted, which are strongly affected by many factors related to driving environment such as traffic lights, lanes, surrounding vehicles, or pedestrians. If these factors can be accurately estimated from the sensor measurements, the future speed/acceleration of the vehicle can be known

in advance through many prediction techniques, e.g., car following models, path planning algorithms and model predictive schemes.

To estimate the multiple environment factors, the Multiple Hypotheses Tracking (MHT) algorithm has traditionally been used to track multiple targets. However, it is not suitable for tracking multiple targets since the MHT algorithm requires a large computational overhead for the track-to-measurement data association process [60]. Recently, the Gaussian Mixture Probability Hypotheses Density (GM-PHD) filter, in which the parameters are updated based on the Kalman filter, has come into the spotlight because it can effectively handle target birth/death without the track-to-measurement data association process [54],[53]. However, the GM-PHD filter is known to have serious problems related to the birth intensity generation and target tractability. In addition, another type of problem, which we call the weight under/overestimation in the fourth chapter, may occur if there are missed detections or measurement clutters. In order to solve these problems, I propose a robust multi-target tracking scheme against the false detections based on the GM-PHD filter in the fourth chapter.

1.2 Contributions and Outline of the Dissertation

1.2.1 Energy Management Optimization in a Battery/Supercapacitor Hybrid Energy Storage System

In this chapter, I investigate the energy management optimization for a battery/SC HESS. First, I propose an optimal energy management scheme for HESS. For the optimal control of the power flow, I suggest two main objectives: minimize the magnitude/fluctuation of power flowing in/out of battery, and minimize the power loss in the HESS. Second, I solve the original non-convex problem by converting it to a convex optimization problem. The optimization is formulated as a penalty

function approximation problem, of which the considered penalty function is convex. The problem for minimizing the power loss from the internal resistance of the SC is formulated as a norm approximation problem, which is also a convex optimization problem. Finally, these two problems are combined into a single problem that has multiple objective functions. Third, I observe that the feasibility and optimality of the solution critically depends on the values of the boundary parameters in the optimization problem. In order to handle this observation, I designed an algorithm that adjusts the boundary parameters based on the multiplicative-increase-additive-decrease (MIAD) principle. I demonstrate that the increase of the computational complexity caused by adapting the MIAD principle is negligible compared to the complexity of an existing optimization solver. The total iteration complexity of the solver is $O(m \log m)$ where m is the number of inequality constraints in the optimization problem.

1.2.2 Real-time Optimization for Power Management Systems of a Battery/Supercapacitor Hybrid Energy Storage System in Electric Vehicles

In this chapter, I investigate the real-time optimization of the power management scheme for the battery/SC HESS in EVs. First, I design a new control framework for the real-time control of the power flowing through the battery/SC HESS in EVs. The framework consists of two parts: one for computing the SC reference voltage based on the load dynamics, and the other for optimizing the power flowing through the HESS. Second, I propose a methodology for computing the reference voltage of the SC considering real-time load dynamics, i.e., the vehicle dynamics, characteristics of the motor, the driving conditions, and the regenerative braking systems. With the proposed method, the SC can handle the future power required by the traction motor even when a future operation profile is not given beforehand. Third, I formulate a

convex optimization problem that minimizes the magnitude/variation of the battery power and the power loss simultaneously. The formulated optimization problem is shown to become an equality constrained problem which can repeatedly be computed by general solvers in polynomial time. The reference voltage of the SC computed by the proposed method is used as a given parameter in the constraints of the formulated problem.

1.2.3 Robust Multi-Target Tracking Scheme against False Detections based on Gaussian Mixture Probability Hypothesis Density Filter

To further improve the power control for the battery/SC HESS in EVs, it is required to obtain the future driving profiles (speed, acceleration) in advance. To obtain the future driving profiles, the driving environment factors such as traffic lights, lanes, surrounding vehicles, or pedestrians should be accurately estimated from the measurements obtained from on-board sensors.

In this chapter, I propose a robust multi-target tracking scheme based on the GM-PHD filter in order to overcome the problems of the conventional GM-PHD filter. The scheme can provide relatively accurate estimates even with numerous false positive/negative detections. The proposed GM-PHD filter consists of five steps, as shown in Fig.4.2: 1) Target prediction and PHD update component construction, 2) State and measurement evaluation, 3) PHD updating and merging, 4) Duplication check, and 5) Birth intensity generation for the next iteration.

I propose a method to evaluate the multiple states and measurements. In the proposed scheme, all states are tagged with the confirmation scores which are updated according to whether or not there are any measurements in the corresponding observation gates. The weights of the states are adaptively determined in different ways based on the updated confirmation score to solve problems related to weight

update. In addition, the measurements not associated with any tracked states are classified and utilized to generate the Gaussian birth intensity.

The states are tracked using the corresponding identities in the proposed robust GM-PHD filter. Accordingly, the states that have different identities do not merge with each other. As a result, the duplicated states may exist depending on the target estimation. For this problem, I also propose a method that finds and removes the duplicated states.

Chapter 2

Energy Management Optimization in a Battery/Supercapacitor Hybrid Energy Storage System

2.1 Introduction

As fossil fuels have been considered a major cause of global warming in recent years, electric energy has received a great deal of attention as a substitute. One of the advantages of electricity is that it can be generated in clean and efficient ways, e.g. solar and wind power. Electric vehicles (EVs) and smart home energy systems are good examples that rely on electric energy, which typically require storage devices such as a battery and a supercapacitor (SC). Since the performance of these applications depends on the electric energy storage devices, it is important to develop an efficient method for the optimal energy management of the battery and SC.

A battery and an SC have different characteristics in their operation. A battery has a relatively high energy density but a low power density compared to an SC. The low power density leads to the following problems: 1) a large number of battery packs are needed to provide sufficient peak power to the electrical systems, and 2) the

life of battery can be diminished through large variations of power flow that generate excessive heat and increase the internal resistance of the battery. In contrast, an SC has a relatively high power density but a low energy density compared to battery. Due to the low energy density, an SC is rarely used alone in energy storage systems.

In order to offset the battery and SC weaknesses, a battery/SC hybrid energy storage system (HESS) has been proposed [1]-[3]. In general, a HESS can be categorized into two types: the passive HESS and the active HESS. The representative characteristic of a passive HESS is the direct connection of the battery and SC in parallel. Although the passive topology is easy to implement in electric systems, the passive HESS shows a restriction in managing the power flow. Because the battery and SC have the same voltage, the power sharing ratio between the battery and SC is determined by their internal resistances. In order to overcome this limitation, bi-directional DC/DC converters are used in the active HESS. The DC/DC converter permits the battery and SC to have different voltages and makes the power flow controllable. In order to effectively control the power flow, several different types of HESS topologies have been proposed [5]-[7]. When the power flow in HESS became controllable through the DC/DC converter, improved schemes for the HESS energy management have been investigated for stable operation of the electric systems. When controlling the power flow in general energy management systems, two kinds of goals are generally considered:

1) The magnitude/fluctuation of the power flowing in or out of a battery needs to be minimized in order to prevent the life of battery from being diminished.

2) The power loss caused by the internal resistance of the SC needs to be minimized in order to extend the battery discharge duration.

Although these two goals are important in designing a HESS, most of the related works [4]-[11] do not consider them or only considered one of them.

Dougal *et al.* [4] analyzed the passive HESS used in pulsed power applications in terms of three terms: peak power, internal losses, and discharge life. Based on their theoretical analysis, the solution used to determine the optimum combination of battery and SC was presented. However, it cannot be applied to an active HESS because the decision parameters are the number of SCs used, not the power flow. Dougal *et al.* [8] also verified that a DC/DC converter can be used to reduce the power fluctuation of the battery in a pulse-operated power system. Their scheme is not appropriate for application to an environment where the battery and SC are connected to a DC bus, because the range of the SC voltage is limited by the direct connection between SC and DC bus. Napoli *et al.* [9] proposed a control strategy for the active HESS in where the battery, SC, and a fuel cell are connected to a DC bus through a multiple input DC/DC converter. In their strategy, there were constraints which set the maximum permissible power and fluctuation of power. The main drawback of their scheme is in that they did not try to minimize the maximum power fluctuation and power value. Lukic *et al.* [10] tried to choose an optimal strategy from given strategies for active HESSs. The given strategies are selected to keep the state of charge (SoC) of the SC constant, to keep the total power constant, and to maximize the SC power. The limitation of this approach is in that the considered parameter in controlling the power flow uses the SoC of the battery and SC, not the power variation. Zhang *et al.* [11] experimented with changing the split ratio of the power between the battery and SC. The considered ratios, i.e., 1/5, 3/3, and 5/1, led to the battery and the SC to be charged or discharged simultaneously. This particular strategy cannot deliver enough power to the loads if the SC capacitance is insufficient.

In this chapter, we investigate the energy management optimization for a battery/SC HESS. The architecture of the active HESS considered in this chapter is

comprised of a battery and multiple SCs, both of which are connected to a DC bus through DC/DC converters. Multiple loads are connected to the DC bus. The loads have a heterogeneous operating profile one with another; some loads may be generators, some other nodes only consume electric energy, and others both consume and generate electric energy. Our contributions can be summarized as follows:

(a) We propose an optimal energy management scheme for HESS. For the optimal control of the power flow, we suggest two main objectives: minimize the magnitude/fluctuation of power flowing in/out of battery, and minimize the power loss in the HESS.

(b) We obtain the optimal solution for controlling the power flow in the HESS by formulating the optimization problem.

(c) We solve the original non-convex problem by converting it to a convex optimization problem. The problem regarding the minimization of the magnitude/fluctuation of the power flowing in/out of battery is formulated as a penalty function approximation problem: a convex optimization problem. The problem for minimizing the power loss from the internal resistance of the SC is formulated as a norm approximation problem, which is also a convex optimization problem. Finally, these two problems are combined into a single problem that has multiple object functions.

(d) We observe that the feasibility and optimality of the solution critically depends on the values of the boundary parameters in the optimization problem. In order to handle this observation, we designed an algorithm that adjusts the boundary parameters based on the multiplicative-increase- additive-decrease (MIAD) principle. We demonstrate that the increase of the computational complexity

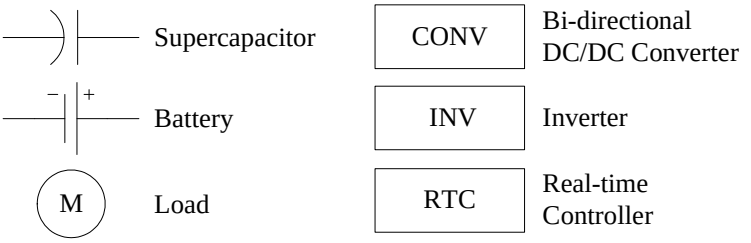

Figure 2.1: The symbols used for denoting the HESS circuit

caused by adapting the MIAD principle is negligible compared to the complexity of an existing optimization solver. The total iteration complexity of the solver is $O(m \log m)$ where m is the number of inequality constraints in the optimization problem.

The remainder of chapter is organized as follows: In Section II, the HESS topologies including the HESS topology considered in this chapter are explained. In Section III, we formulate the optimization problem for the HESS energy management. Section IV presents the algorithm for guaranteeing a feasible optimal solution. The simulation results are shown in Section V. Finally, conclusions are drawn in Section VI.

2.2 Active Hybrid Energy Storage Systems

In active HESSs, energy storage devices are connected to a DC bus through DC/DC converters. The DC/DC converters permit the voltage of the energy storage devices to be different from the DC bus voltage. In regards to the active HESS structures, there are several types of topologies. In this section, we review the existing HESS topologies and introduce the HESS topology considered in this chapter.

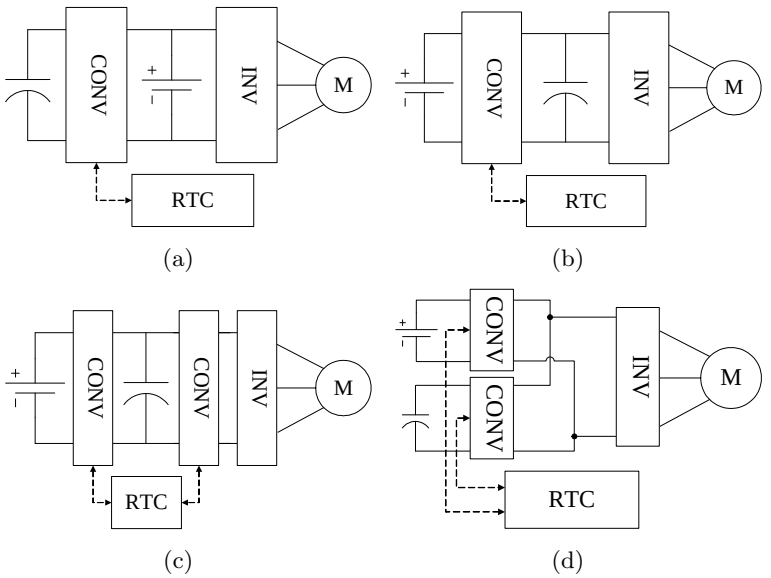

Figure 2.2: The active HESS topologies: (a) SC-only connected through a DC/DC converter, (b) battery-only connected through a DC/DC converter, (c) cascaded connection of the battery/SC using DC/DC converters, and (d) the battery/SC connected through the respective DC/DC converters.

2.2.1 A Review of Active Hybrid Energy Storage Systems

(a) **SC-only connected through a DC/DC converter** (Fig. 2.2(a)): The battery is connected directly to the terminal of the inverter whereas the SC is connected through a DC/DC converter. Due to the direct connection of the battery, the terminal voltage of the inverter can be constantly maintained. When an instantaneous high power is required or absorbed, however, the battery can be severely damaged because there is no buffer between the battery and the inverter.

(b) **Battery-only connected through a DC/DC converter** (Fig. 2.2(b)): The SC is directly connected to the terminal of an inverter whereas the battery is connected through a DC/DC converter. The SC acts as a buffer against a rapid power flow change. As a result, the battery is protected and the power flow can be effectively controlled. However, in this topology, the working range of the SC is limited due to the constantly maintained SC voltage.

(c) **Cascaded connection of Battery/SC using DC/DC converters** (Fig. 2.2(c)): The SC is connected to the inverter's terminal through a DC/DC converter, and the battery is connected to the SC's terminal through an additional DC/DC converter. The DC/DC converter between the inverter and the SC increases the working range of the SC. However the DC/DC converter connected to the terminal of inverter requires a large amount of power for operation because the converter is located at the power flow bottleneck.

(d) **Battery/SC connected through their respective DC/DC converters** (Fig. 2.2(d)): The battery and SC are individually connected to inverter terminal through their own DC/DC converter. This topology shows good performance, especially for the controllability of power flow, because the power flow

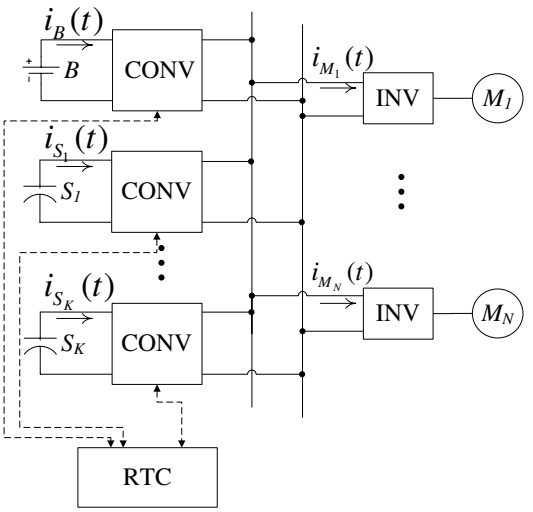

Figure 2.3: The HESS topology considered in this chapter: Real-time controllers measure the power flows and command the DC/DC converters to adjust the amount of power flow.

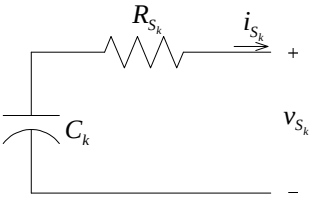

Figure 2.4: The SC equivalent circuit.

can be controlled in parallel according to the power flow control. In addition, this topology is fault tolerant because it can still operate even if failures occur in the battery or the SC. However, the cost for constructing this topology is expensive compared to the other topologies.

2.2.2 Considered HESS Topology

In this chapter, we consider the active HESS topology shown in Fig. 2.3. The considered topology consists of a battery, multiple SCs, and loads. The battery

and each individual SC are connected to the DC bus through their own DC/DC converters. The DC/DC converters are controlled by a real-time controller which measures power flow. The loads are connected to the DC bus through inverters. The SCs support not only wide range of power requirements but also the simultaneous charge/discharge of the loads. As a result, a more flexible power control can be achieved. The power profiles of the loads may be diverse; that is the loads can work as sinks, generators, or both.

2.3 HESS Energy Management Optimization

In this section, we formulate three problems as optimization problems in order to minimize: 1) the magnitude/fluctuation of power flowing in/out of the battery, 2) the power loss induced by the SCs, and 3) both 1) and 2) at the same time. The objective is to determine the battery power and the SC power for an optimal HESS energy management.

2.3.1 Notations and Assumptions

The battery, the set of SCs and the set of heterogeneous loads are denoted as B, $S = \{S_k | k \in K\}$, and $M = \{M_n | n \in N\}$, respectively, where K and N are the number of SCs and loads. The battery power, SC power, and SC energy are denoted as $p_B(t)$, $p_{S_k}(t)$, and $E_{S_k}(t)$. $p_B(t)$ and $p_{S_k}(t)$ are dynamically controlled by the DC/DC converters. We assume that the energy and power are measured using discrete signals with a sufficiently small sampling period Δ. The sampling period is determined by the time resolution of the load power history. The battery has a capacity in watt-hour units, and $\sum_t p_B(t) = p_o$ where p_o is a constant. The SC $S_k (k \in K)$ can be characterized by the following parameters: capacitance C_k, Equivalent Serial Resistance (ESR) of capacitor R_{S_k}, and the maximum capacitor

energy $E_{S_k}^{\mathrm{MAX}}$. Due to the ESR virtually connected with SC as described in Fig. 2.4, power loss is induced in the charging and discharging of the SCs. Although an power loss can be induced by the battery, we ignore it because $p_B(t)$ is relatively small compared to $p_{S_k}(t)$. $E_{S_k}(t)$ can be calculated by the following classic equation:

$$E_{S_k}(t) = -\sum_{\tau=t_0}^{t} p_{S_k}(\tau)\Delta.$$

Load $M_n(n \in N)$ is characterized by the required power $p_{M_n}(t)$. $p_{M_n}(t) > 0$ means that the load only consumes the stored energy; $p_{M_n}(t) < 0$ means that the load always supplies electric energy to the energy storage system.

We assume that the future profile within a certain time interval can be acquired in advance even though the power profiles of the loads are dynamic. The future operation of the loads can be obtained in advance by previewing the working environment. This kind of assumption has been adopted in many applications, e.g., energy management systems for hybrid electric vehicles [14]-[18]. The profile of the future operation of the loads is useful in controlling the instantaneous operation of the HESS. For example, the behavior of a motor in the EV is strongly related to the terrain of the road or the traffic conditions in front of the vehicle. If the EV will be on an uphill road in a few second, the SC in EV needs to be fully charged in order to support acceleration. Similarly, if the EV is due to undergo a downhill course in the near future, the SoC of SC needs to be minimized in order to capture as much of the regenerative energy as possible. The time required for fully charging/discharging the SC is generally 10 to 20 seconds; generally different depending on SCs. For example, if the SC capacitance is 3400/56(F), the maximum voltage is 2.7×56(V) and the minimum voltage is $0.5 \times 2.7 \times 56$(V), the available energy stored in the SC

is computed by

$$E_{avail} = \frac{1}{2}C\left(V_{\max}^2 - V_{\min}^2\right) = \frac{1}{2}\frac{3400}{56}\left((2.7 \cdot 56)^2 - (0.5 \cdot 2.7 \cdot 56)^2\right) \approx 520kWs. \tag{2.1}$$

If the maximum load power is 30kW, the discharging time is about 17 second. Therefore, the prediction interval of future load power is set to about 10 to 20 seconds according to the load and SC characteristics.

2.3.2 Minimization of Magnitude/Fluctuation of Battery Power

When controlling the power flow in the HESS, the magnitude and fluctuation of the power flowing in/out of the battery must be minimized because they cause an increase in the internal resistance of the battery which may diminish the battery life-time. In this section, we formulate the original problem as an optimization problem (denoted as $\mathbf{P}_1$) that minimizes the magnitude/fluctuation of the power flowing in/out of the battery.

The magnitude of the battery power and the power fluctuation of the battery can be denoted as $|p_B(t)|$ and $|p_B(t) - p_B(t-\Delta)|$, respectively. The cumulated values of these two variables for the operation time T, $\left(\sum_{t\in T}|p_B(t)|\right.$ and $\left.\sum_{t\in T}|p_B(t) - p_B(t-\Delta)|\right)$ can then be chosen as an objective function in the formulation of $\mathbf{P}_1$. However, generally, the damage to the battery is exponentially proportional to the increase of the magnitude/fluctuation of the battery power. Therefore, the objective function of $\mathbf{P}_1$ needs to be generalized in order to reflect the possible exponential damages. In order to define the objective function, the penalty function ψ can be used. The representative penalty functions are described as [20]:

- l_p-**norm function**: $\psi(u,\sigma) = |u|^p$, where p > 1. $\sum_{i=1}^{m}\psi(r_i,\sigma) = \max(r_1,\ \ldots,\ r_m)$ if p is infinite. When the l_∞-norm function is applied to the objective function

of $p_B(t)$, the optimization problem is formulated as a min-max optimization problem that minimizes the peak power of the battery $\max_{t\in T} i_B(t)$.

- **Deadzone-linear penalty function**:

$$\psi(u,\sigma) = \begin{cases} 0 & |u| \le \sigma \\ |u| - \sigma & |u| > \sigma \end{cases}$$

where $\sigma > 0$ is a given parameter that determines the width of the penalty free zone. The deadzone-linear penalty function imposes its linear penalty when $|u| > \sigma$. When σ is large, u tends to be widely spread. Contrarily, u tends to be zero when σ is zero. The penalty function values increase as the amount of power violation over a certain threshold value increases. However, the deadzone-linear penalty function does not provide a specific limit for the magnitude/fluctuation of the battery power.

- **Log barrier penalty function**:

$$\psi(u,\sigma) = \begin{cases} -\sigma^2 \log(1-(u/\sigma)^2) & |u| < \sigma \\ \infty & |u| \ge \sigma \end{cases}$$

where $\sigma > 0$ is a given parameter that decides the distribution range of u. Due to the infinite penalty for $|u| \ge \sigma$, it is hard for u to be larger than σ or smaller than $-\sigma$. The magnitude/fluctuation of the battery power can be limited within a certain boundary by applying the log barrier function to the objective function.

Among these penalty functions, we can choose one for the objective function of $\mathbf{P}_1$ according to the battery characteristics. Using the penalty functions, $\mathbf{P}_1$ is formulated as a penalty function approximation problem [20]. The objective function for the battery power magnitude is defined by $\sum_{t\in T} \psi(p_B(t), \sigma_1)$, and that for the

battery power fluctuation is defined by $\sum_{t\in T}\psi\big(p_B(t)-p_B(t-\Delta),\sigma_2\big)$ where σ_1 and σ_2 are adjustable. The formulation of $\mathbf{P}_1$ can be represented as:

$$
\begin{aligned}
\mathbf{P}_1: \quad & \text{minimize} \quad \varepsilon_{\text{mag}}\sum_{t\in T}\psi\big(p_B(t),\ \sigma_1\big)+\varepsilon_{\text{var}}\sum_{t\in T}\psi\big(p_B(t)-p_B(t-\Delta),\ \sigma_2\big) \\
& \text{subject to} \\
& p_B(t)+\sum_{k\in K}p_{S_k}(t)-\sum_{n\in N}p_{M_n}(t)=0, \\
& E_{S_k}(t)=-\sum_{\tau=1}^{t}\left(\Delta\left(p_{S_k}(\tau)-\eta_{S_k}\left|p_{S_k}(\tau)\right|\right)\right), \\
& E_{S_k}(0)=E_{S_k}(T), \\
& 0\le E_{S_k}(t)\le E_{S_k}^{\max}, \\
& k\in K,\quad t\in T,
\end{aligned}
\tag{2.2}
$$

where T is the considered time period. The decision variables are $p_B(t)$, $p_{S_k}(t)$, and $E_{S_k}(t)$. Note that $\sigma_1 \gg \sigma_2$ because the scale of $p_B(t)$ is relatively large compared to that of $p_B(t)-p_B(t-\Delta)$. The parameter ε_{mag} is the cost per the battery damage induced by the peak power and ε_{var} is the cost per the battery damage induced by the power fluctuation. When $\varepsilon_{\text{mag}}=0$ (or $\varepsilon_{\text{var}}=0$), $\mathbf{P}_1$ becomes the problem that minimizes the power fluctuation of battery (or the magnitude of the battery power).

In $\mathbf{P}_1$, the first constraint is in that the sum of the power flowing into the DC bus is equal to the sum of power flowing out of the DC bus. The second constraint shows the relationship between the energy and power in a SC. Note that the term $-\eta_{S_k}\left|p_{S_k}(\tau)\right|$ is a power loss induced by the SC. The third constraint indicates that the initial capacitor charge is fixed to be equal to the final capacitor charge so that the net energy change is zero during the operation. The inequality constraint sets the $E_{S_k}(t)$ limit.

Note that the formulation shown in (2.2) is not in the form of a convex optimization problem because there is an absolute term, i.e., $|p_{S_k}(t)|$, in the constraints.

In order to remove the absolute term for formulating $\mathbf{P}_1$ as a convex optimization problem, $p_{S_k}(t)$ is changed into the sum of two terms $p^{\text{in}}_{S_k}(t)$ and $p^{\text{out}}_{S_k}(t)$ as $p_{S_k}(t) = p^{\text{out}}_{S_k}(t) - p^{\text{in}}_{S_k}(t)$ where $p^{\text{in}}_{S_k}(t) \geq 0$ is the power following into the S_k, and $p^{\text{out}}_{S_k}(t) \geq 0$ is the power flowing out of the S_k. As a result, $\mathbf{P}_1$ can be rewritten in the following matrix form of a convex optimization problem:

$$
\begin{aligned}
\mathbf{P}_1: \quad & \text{minimize} \;\; \varepsilon_{\text{mag}}\Psi(P_B, \sigma_1) + \varepsilon_{\text{var}}\Psi(FP_B, \sigma_2) \\
& \text{subject to} \\
& P_B + \sum_{k\in K}(P^{\text{out}}_{S_k} - P^{\text{in}}_{S_k}) - \sum_{n\in N} P_{M_n} = \mathbf{0}, \\
& (A-I)E_{S_k} - D^{\text{out}}_k P^{\text{out}}_{S_k} - D^{\text{in}}_k P^{\text{in}}_{S_k} = \mathbf{0}, \\
& GE_{S_k} = \mathbf{0}, \\
& \mathbf{0} \preceq E_{S_k} \preceq E^{\max}_{S_k}\mathbf{1}, \quad P^{\text{out}}_{S_k} \succeq \mathbf{0}, \quad P^{\text{in}}_{S_k} \succeq \mathbf{0}, \\
& k \in K,
\end{aligned}
\tag{2.3}
$$

where

$$
\begin{aligned}
\Psi(\widetilde{x}, \sigma) &= \textstyle\sum_t \psi(x(t), \sigma), \\
P_B &= [p_B(1), \; \cdots, \; p_B(T)]^{\text{T}}, \\
P_{M_n} &= [p_{M_n}(1), \; \cdots, \; p_{M_n}(T)]^{\text{T}}, \\
P^{\text{out}}_{S_k} &= \left[p^{\text{out}}_{S_k}(1), \; \cdots, \; p^{\text{out}}_{S_k}(T)\right]^{\text{T}}, \\
P^{\text{in}}_{S_k} &= \left[p^{\text{in}}_{S_k}(1), \; \cdots, \; p^{\text{in}}_{S_k}(T)\right]^{\text{T}}, \\
E_{S_k} &= [E_{S_k}(0), \; \cdots, \; E_{S_k}(T)]^{\text{T}}, \\
\mathbf{0} &= [0, \; \cdots, \; 0]^{\text{T}}, \quad \mathbf{1} = [1, \; \cdots, \; 1]^{\text{T}}, \\
A &= \begin{bmatrix} [1, \; 0, \; \cdots, \; 0] & 0_{1\times 1} \\ I_{T\times T} & 0_{T\times 1} \end{bmatrix}, \\
D^{\text{out}}_k &= (\eta_{S_k} + 1)\,\Delta \begin{bmatrix} 0_{1\times T} \\ I_{T\times T} \end{bmatrix}, \\
D^{\text{in}}_k &= (1 + \eta_{S_k})\,\Delta \begin{bmatrix} 0_{1\times T} \\ I_{T\times T} \end{bmatrix}, \\
G &= (1, \; 0, \; \cdots, \; 0, \; -1) \in \mathbf{R}^{(T+1)},
\end{aligned}
$$

$$F = \begin{bmatrix} 1 & -1 & 0 & \cdots & 0 & 0 \\ 0 & 1 & -1 & 0 & \cdots & 0 \\ \vdots & & \ddots & \ddots & & \vdots \\ 0 & \cdots & 0 & 1 & -1 & 0 \\ 0 & 0 & \cdots & 0 & 1 & -1 \end{bmatrix}.$$

The meaning of the constraints in (2.3) is equivalent to that found in (2.2); and FP_B means the power fluctuation of the battery. The derivation of the second constraint is shown in Appendix 2.7. Now that $\mathbf{P}_1$ has become a convex optimization problem, it can be solved by existing solvers that find if an optimal solution for $\mathbf{P}_1$ is feasible.

2.3.3 Minimization of the Power Loss

The power loss in the HESS, which is induced by the SC ESR, results in the reduction of the battery discharge duration. Therefore the power loss in the HESS needs to be minimized in order to increase the battery discharge duration. The power loss in the HESS is proportional to the sum of the power loss induced by all of the SCs during the operation $\sum_{k\in K}\sum_t \eta_{S_k}|p_{S_k}(t)|$. Therefore, the objective function in the optimization problem (denoted as $\mathbf{P}_2$) that minimizes the power loss in HESS can be represented as

$$\text{minimize} \quad \sum_{k\in K} \eta_{S_k} \left\| P_{S_k}^{\text{out}} - P_{S_k}^{\text{in}} \right\|_1$$

where $\| \cdot \|_1$ is a function of the l_1- norm. The objective function can be cast as an LP:

$$\begin{aligned} &\text{minimize} \quad \textstyle\sum_{k\in K} \eta_{S_k} \|L_k\|_1 \\ &\text{subject to} \quad -L_k \preceq (P_{S_k}^{\text{out}} - P_{S_k}^{\text{in}}) \preceq L_k, \qquad k \in K \end{aligned}$$

with variables $P_{S_k}^{\text{out}}$, $P_{S_k}^{\text{in}}$, and $L_k = [l_k(1), \ \cdots, \ l_k(T)]$. Using these objective functions and constraints, $\mathbf{P}_2$ can be represented in the following matrix form:

$$
\begin{aligned}
\mathbf{P}_2: \quad & \text{minimize} \quad \sum_{k\in K} \eta_{S_k} \|L_k\|_1 \\
& \text{subject to} \\
& P_B + \sum_{k\in K} (P_{S_k}^{\text{out}} - P_{S_k}^{\text{in}}) - \sum_{n\in N} P_{M_n} = \mathbf{0}, \\
& (A - I)E_{S_k} - D_k^{\text{out}} P_{S_k}^{\text{out}} - D_k^{\text{in}} P_{S_k}^{\text{in}} = \mathbf{0}, k \in K \\
& GE_{S_k} = \mathbf{0}, \\
& \mathbf{0} \preceq E_{S_k} \preceq E_{S_k}^{\max}\mathbf{1}, \quad P_{S_k}^{\text{out}} \succeq \mathbf{0}, \quad P_{S_k}^{\text{in}} \succeq \mathbf{0}, \\
& -L_k \preceq P_{S_k}^{\text{out}} - P_{S_k}^{\text{in}} \preceq L_k, \\
& -\sigma_1\mathbf{1} \preceq P_B \preceq \sigma_1\mathbf{1}, \\
& -\sigma_2\mathbf{1} \preceq FP_B \preceq \sigma_2\mathbf{1}, \\
& k \in K,
\end{aligned}
$$

where the decision variables are P_B, $P_{S_k}^{\text{out}}$, $P_{S_k}^{\text{in}}$, E_{S_k}, and L_k, and the given parameters are $E_{S_k}^{\max}$, σ_1, and $\sigma_2 > 0$. The constraints are equivalent to the constraints of $\mathbf{P}_1$ except for the last three inequality constraints. The last two inequality constraints indicate the range of the magnitude/fluctuation of the power passing through the battery. $\mathbf{P}_2$ can be solved by existing LP solvers if it is feasible because it is formulated in an LP form.

2.3.4 Minimization of the Dual Objective Functions

In controlling the power flow in the HESS, two objectives need to be considered at the same time, i.e., the minimization of the magnitude/fluctuation of the battery power and the reduction of the power loss. In order to satisfy these objectives, we formulate the optimization problem (denoted as $\mathbf{P}_3$) by combining $\mathbf{P}_1$ and $\mathbf{P}_2$ as

follows:

$$
\begin{aligned}
\mathbf{P}_3: \quad & \text{minimize} \\
& \gamma\left(\varepsilon_{\text{mag}}\Psi(P_B,\sigma_1)+\varepsilon_{\text{var}}\Psi(FP_B,\sigma_2)\right)+\delta\sum_{k\in K}\eta_{S_k}\left\|L_k\right\|_1 \\
& \text{subject to} \\
& P_B+\sum_{k\in K}\left(P_{S_k}^{\text{out}}-P_{S_k}^{\text{in}}\right)-\sum_{n\in N}P_{M_n}=\mathbf{0}, \\
& (A-I)E_{S_k}-D_k^{\text{out}}P_{S_k}^{\text{out}}-D_k^{\text{in}}P_{S_k}^{\text{in}}=\mathbf{0}, \\
& GE_{S_k}=\mathbf{0}, \\
& \mathbf{0}\preceq E_{S_k}\preceq E_{S_k}^{\max}\mathbf{1}, \quad P_{S_k}^{\text{out}}\succeq\mathbf{0}, \quad P_{S_k}^{\text{in}}\succeq\mathbf{0}, \\
& -L_k\preceq P_{S_k}^{\text{out}}-P_{S_k}^{\text{in}}\preceq L_k, \\
& k\in K,
\end{aligned}
$$

where γ and δ are trade-off weighting factors that can be properly chosen according to the optimization policy. The decision variables are P_B, $P_{S_k}^{\text{out}}$, $P_{S_k}^{\text{in}}$, E_{S_k}, and L_k. The objective function of $\mathbf{P}_3$ is also convex because it is an affine convex function combination. Therefore, it can be solved if it has a feasible solution.

2.4 Algorithm

In this section, we propose an algorithm to obtain the feasible optimal solution of the optimization problem $\mathbf{P}$ ($=\mathbf{P}_1$, $\mathbf{P}_2$, or $\mathbf{P}_3$). Since the feasibility of $\mathbf{P}$ is up to the boundary parameters, i.e., σ_1, and σ_2, it is important to adjust these values in an effective manner. The algorithm is based on the multiplicative-increase -additive-decrease (MIAD) policy, which allows σ_1 and σ_2 to be increased quickly if $\mathbf{P}$ is infeasible and the parameters to be decreased slowly if $\mathbf{P}$ is feasible. As a result, the proposed algorithm permits an infeasible $\mathbf{P}$ to quickly become feasible and for the obtained solution of $\mathbf{P}$ to be optimal during the HESS operation. The detailed procedure of our algorithm will be explained after reviewing an existing solver.

2.4.1 Computation by Solver

A solver is a software tool which is used to solve the general optimization problem described as follows:

$$\begin{array}{rll} \text{minimize} & f_0(x) & \\ \text{subject to} & f_i(x) \leq 0, & i = 1, \cdots, m \\ & Ax = b. & \end{array} \tag{2.4}$$

If (2.4) is a convex optimization problem, a barrier method can solve (2.4) in a polynomial time [20]. Problem **P** can be solved by the barrier method because the formulation of **P** is basically equivalent to the canonical form of (2.4). In our approach, we rely on the barrier method to solve the energy management problem **P** under the MIAD policy.

A simple version of the barrier method is described in Algorithm 3 where ϵ is the tolerance for guaranteeing the sub-optimality, m is the number of inequality constraints in the problem, μ is the size of Newton step, and $\phi(x) = -\sum_{i=1}^{m} \log(f_i(x))$. At each iteration, the x^* is computed by Newton's method [20]. The iteration terminates when $t \geq m/\epsilon$.

Algorithm 1 The barrier method.

1: **given** feasible x, $t \leftarrow t^{(0)} > 0$, $\mu > 1$, tolerance $\epsilon > 0$.
2: **repeat**
3: Compute x^* by minimizing $tf_0 + \phi$, subject to $Ax = b$, starting at x
4: $x \leftarrow x^*$
5: $t \leftarrow \mu t$
6: **until** $m/t < \epsilon$

2.4.2 Parameter Adjustment Algorithm

Although the barrier method can solve convex optimization problems in a polynomial time, it cannot provide a proper solution if the problem has no feasible solution. Specifically, **P** cannot be optimally solved if **P** has no feasible set of solutions, in

which case, it is impossible for the HESS to deliver enough power to the loads. In this case, severe faults may occur in the entire electric system as a result.

The feasibility of $\mathbf{P}$ is up to the boundary parameters, i.e., σ_1 and σ_2, because the size of the set of feasible solutions depends on these parameters. $\mathbf{P}$ becomes feasible if σ_1 and σ_2 are large enough while it may not be feasible if σ_1 and σ_2 have too small of a value. However, very large values of σ_1 and σ_2 result in less optimal solutions of $\mathbf{P}$. Therefore, σ_1 and σ_2 need to be effectively adjusted in order to guarantee both the feasibility and optimality of $\mathbf{P}$.

To satisfy both considerations, we propose a MIAD policy for adjusting σ_1 and σ_2 efficiently. If $\mathbf{P}$ is infeasible, σ_1 and σ_2 need to be increased multiplicatively in order to quickly change an infeasible $\mathbf{P}$ to be feasible. Otherwise, σ_1 and σ_2 need to be decreased to enable $\mathbf{P}$ to have optimal solutions during the HESS operation. The parameters decrease in an additive manner in order to prevent $\mathbf{P}$ from being infeasible as long as possible.

The algorithm for obtaining a feasible optimal solution of $\mathbf{P}$ is illustrated in Algorithm 2. The algorithm is iteratively executed until the operation of the HESS stops. The algorithm consists of two parts: computation and parameter adjustment. The optimal solutions are obtained by the barrier method in the computation part, and σ_1 and σ_2 are adjusted by the MIAD policy in the parameter adjustment part. The detailed procedure is described as follows: Whenever optimal solutions, i.e., ${P_B}^*$, $P_{S_k}^{\text{out}*}$, $P_{S_k}^{\text{out}*}$, ${E_{S_k}}^*$, and ${L_k}^*$, are computed by the barrier method (in line 4), σ_1 and σ_2 decrease alternately and additively ($\sigma_1 \leftarrow \sigma_1 - \beta_1$ or $\sigma_2 \leftarrow \sigma_2 - \beta_2$). The load profiles P_{M_n} can then be updated. When $\mathbf{P}$ has no feasible solutions, σ_1 and σ_2 are adjusted as follows: 1) $\sigma_1 \leftarrow \sigma_1 + \beta_1$ (or $\sigma_2 \leftarrow \sigma_2 + \beta_2$) if $\mathbf{P}$ became infeasible due to the additive decrease of σ_1 (or σ_2) in the right previous iteration. This mechanism prevents an unnecessary increase of the boundary parameters, otherwise

2) $\sigma_1 \leftarrow \alpha\sigma_1$ and $\sigma_2 \leftarrow \alpha\sigma_2$. Fig. 2.7 shows an example of the σ_1 and σ_2 variation during the execution of Algorithm 2. A detailed explanation is given in Section V.

The initial value of σ_1 and σ_2 can be arbitrarily chosen because these values are rapidly adjusted by the proposed algorithm. For a more effective choice, the history of the magnitude/fluctuation of the battery power can be used; for example, the average magnitude/fluctuation of the battery power can be chosen for the initial value. The impact of the initial choice of σ_1 and σ_2 on the computation time will be explained in the next subsection.

2.4.3 Analysis of the Total Number of Iterations in the Algorithm

Let us consider the barrier function described in Algorithm 3. We refer to the iteration during one execution of the barrier method as the barrier iteration, and the repeated execution of barrier method as the outer iteration. The total number of iterations of the barrier method (N_{bf}) are known by:

$$\begin{aligned} N_{bf} = & \left\lceil \frac{\log(m/t^{(0)}\epsilon)}{\log\mu} \right\rceil \left(\frac{m(\mu - 1 - \log\mu)}{\mu} + c \right) \\ \approx & \; O(m \log m) \end{aligned}$$

where $c = \log_2 \log_2(1/\epsilon_{\mathrm{nt}})$. ϵ_{nt} is a tolerance in Newton's method. The N_{bf} was derived by multiplying two large terms [20]. The first term is the number of executions of line 3, and the second term is the number of iterations at each execution of line 3. The total iteration number N_{total} at each update of load profile P_{M_n} in the proposed algorithms can be represented by

$$N_{total} = N_{out} N_{bf} \tag{2.5}$$

where N_{out} is the number of outer iterations required to provide the feasible solution. If $\mathbf{P}$ is always feasible, $N_{out} = 1$ because no boundary parameters need to be

Algorithm 2 The algorithm for solving **P**.

given σ_1, σ_2, $E_{S_k}^{\max}$, η_{S_k},
$n = 1$, $m = 1$, $\alpha > 1$, $0 < \beta_1 < \sigma_1$, $0 < \beta_2 < \sigma_2$.
repeat
  update P_{M_n}, $n \in N$
  Compute ${P_B}^*$, $P_{S_k}^{\text{out}*}$, $P_{S_k}^{\text{out}*}$, ${E_{S_k}}^*$ and ${L_k}^*$ by solving the problem **P** using a solver.
  if the problem **P** is feasible **then**
    if $\sigma_1 \geq \beta_1$ and $\sigma_2 \geq \beta_2$ **then**
      if n $= 1$ **then**
        $temp_1 \leftarrow \sigma_1$
        $\sigma_1 \leftarrow \sigma_1 - \beta_1$
        $n \leftarrow 2$
      else
        $temp_2 \leftarrow \sigma_2$
        $\sigma_2 \leftarrow \sigma_2 - \beta_2$
        $n \leftarrow 1$
      end if
      Update I_{M_n}, $n \in N$
    end if
  else
    if $temp_1 - \sigma_1 = \beta_1$ **then**
      $\sigma_1 \leftarrow \sigma_1 + \beta_1$
    end if
    if $temp_2 - \sigma_2 = \beta_2$ **then**
      $\sigma_2 \leftarrow \sigma_2 + \beta_2$
    end if
    if $temp_1 - \sigma_1 \neq \beta_1$ and $temp_2 - \sigma_2 \neq \beta_2$ **then**
      if $m = 1$ **then**
        $\sigma_1 \leftarrow \alpha\sigma_1$
        $m \leftarrow 2$
      else
        $\sigma_2 \leftarrow \alpha\sigma_2$
        $m \leftarrow 1$
      end if
    end if
  end if
until the HESS is off

adjusted. In general, $N_{out} \geq 1$ because $\mathbf{P}$ can be infeasible depending on the boundary parameters or the update of the power profiles. Because N_{out} is difficult to be quantitatively estimated, we concentrate on verifying that N_{out} can be relatively small by using the MIAD policy controlling the boundary parameters.

Let us denote the boundary parameter as σ, the initial value of the parameter as σ_{int}, and the desired value of the parameter as r. The problem is feasible if condition

$$\sigma = \alpha^n \sigma_{\text{int}} \geq r$$

is satisfied where n is the number of outer iterations required for satisfying $\sigma > r$. The inequality can be rewritten as

$$n \geq \lceil \log_\alpha (r/\sigma_{int}) \rceil ,$$

which means that n is proportional to $\log r$. This characteristic makes N_{out} sufficiently small. For example, if $\alpha = 2$, $\sigma_{int} = 1$, and $r = 10000$, the number of required outer iterations is just 14. Therefore $N_{total} = N_{out} N_{bf} \approx N_{bf} \approx O(m \log m)$.

The size of β does not affect the computation time of the algorithm because it is used to update σ after the feasible solution is obtained. However, it affects how fast σ approaches an optimal value over a long period. If β is too small, the optimality of the solution will be slowly satisfied but the feasibility of the solution will be maintained over a long time. In contrast, the solution can quickly approach the optimal, but $\mathbf{P}$ will be infeasible frequently during the operation.

2.5 Simulation Results

Simulations were carried out using MATLAB in order to verify the proposed optimization formulations and algorithm. We considered the HESS topology with $K = 4$ and $N = 6$ as represented in Fig. 2.3 and the load profiles M_1-M_6 shown

Table 2.1: The SC Characteristics

num	name of SC	C_k (F)	$v_{S_k}^{\max}$ (V)	R_{S_k} (mΩ)
1	BCAP0050	50	2.7	20
2	BCAP0150	150	2.7	14
3	BCAP0310 P270 T10	310	2.7	2.2
4	BCAP0350 E270 T11	350	2.7	3.2

in Fig. 2.5. The characteristics of the considered SCs, i.e., C_k, $v_{S_k}^{\max}$, and R_{S_k}, are shown in Table I. The parameters in Table I were taken from [21]. The simulation results were obtained by the proposed algorithm solving $\mathbf{P}_3$ for minimizing the magnitude/fluctuation of the battery power and the power loss in the HESS.

2.5.1 Review of Previous Approach

In this subsection, we review Napoli's approach [9] that proposed the control strategy for the HESS where the battery, SC, and a fuel cell (FC) are connected to a DC bus through a DC/DC converter having multiple inputs. The strategy proposed by Napoli's approach can be described as follows:

$$|p_B(t)| \le p_B^{\max}, |p_{SC}(t)| \le p_{SC}^{\max}, 0 \le p_{FC}(t) \le p_{FC}^{\max},$$
$$\left|\frac{\partial p_B(t)}{\partial t}\right| \le dp_B^{\max}, \left|\frac{\partial p_{SC}(t)}{\partial t}\right| \le dp_{SC}^{\max}, \left|\frac{\partial p_{FC}(t)}{\partial t}\right| \le dp_{FC}^{\max},$$
$$p_B(t) + p_{SC}(t) + p_{FC}(t) = p_L(t),$$

where $p_B(t)$, $p_{SC}(t)$, $p_{FC}(t)$, and $p_L(t)$ are the battery/SC/FC power and power required by a load, respectively. The three constraints in the first line set the maximum power flow, and the three constraints in the second line set the maximum power fluctuation. The last constraint represents law of power conservation. Although Napoli considered the FC for the HESS, we focused on the parameters related to only the battery and SC. In their strategy, however, there are just constraints and no objective function to minimize the magnitude/fluctuation of the power flowing in/out

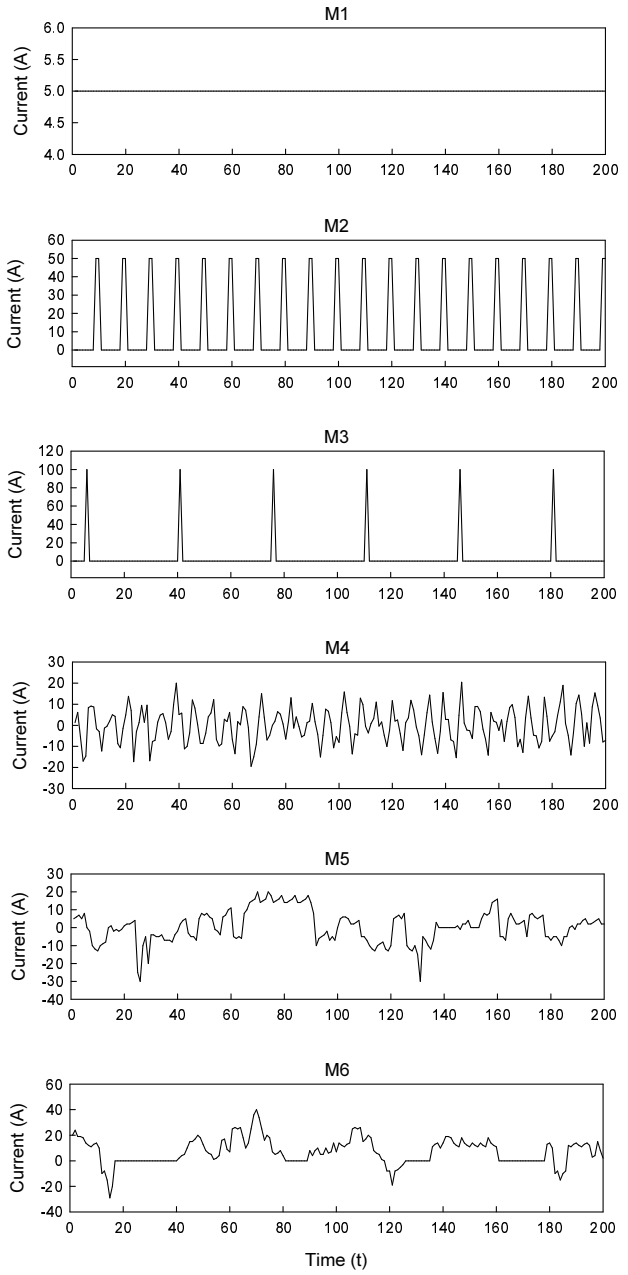

Figure 2.5: The load profiles M1-M6. Time unit: seconds

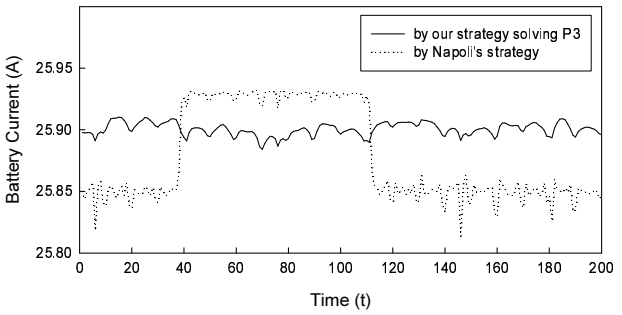

(a)

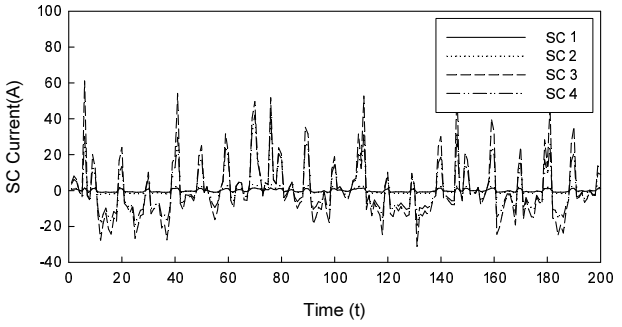

(b)

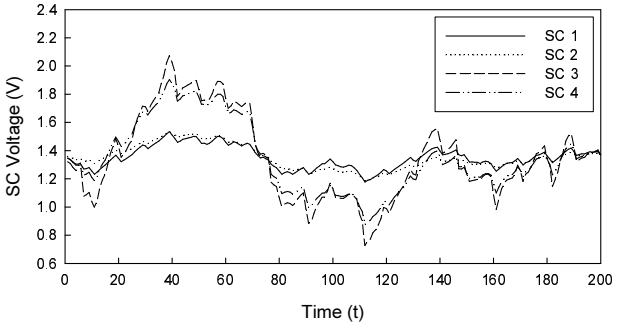

(c)

Figure 2.6: The simulation results from solving the problem of energy management in the HESS at $\varepsilon_{\text{mag}} = 0.7$, $\varepsilon_{\text{var}} = 0.3$, $\sigma_1 = 26$, $\sigma_2 = 0.8$, $\gamma = 0.001$, and $\delta = 1$. A log barrier penalty function was applied in our algorithm. (a) The battery power obtained by our algorithm and Napoli's strategy, (b) the SC power obtained by our algorithm, (c) the SC energy obtained by our algorithm.

of the battery. Therefore, it is difficult for the power flow controlled by Napoli's strategy to be optimized. The simulation results obtained by Napoli's strategy are shown in Fig. 2.6(a).

2.5.2 Simulation Results

In Fig. 2.6, we confirm that our optimization scheme for energy management in HESS can guarantee the two main objectives; the minimization of the magnitude/fluctuation of the battery power and the power loss in the HESS.

Fig. 2.6(a) shows the changing pattern of the battery power controlled by our algorithm solving $\mathbf{P}_3$ and that obtained through Napoli's strategy. The penalty function applied to $\mathbf{P}_3$ is the log barrier penalty function of σ_1 and σ_2. The result of our algorithm was obtained at $\sigma_1 = 26$, $\sigma_2 = 0.8$, $\gamma = 0.001$, $\delta = 1$, $\varepsilon_{\text{mag}} = 0.7$, and $\varepsilon_{\text{var}} = 0.3$ and that of Napoli's scheme was obtained at $p_B^{\max} = 26$ and $dp_B^{\max} = 0.8$. The battery power controlled by our strategy was maintained constantly. In contrast, the battery power controlled by Napoli's strategy had large power values and fluctuations compared to the result obtained by our strategy. If the initial values of $p_B^{\max}$ and σ_1 (or $dp_B^{\max}$ and σ_2) are much larger than 26 (or 0.8), the performance gap between the two methods increases during the operation because $p_B^{\max}$ (or $dp_B^{\max}$) is not controllable whereas σ_1 (or σ_2) is controllable.

Fig. 2.6(b) shows the changing pattern of the SC powers controlled by our algorithm solving $\mathbf{P}_3$. The SCs tend to be charged before the loads require large amounts of power and to be discharged before the regenerative power is delivered to the energy storage devices. It means that previewing the future profiles of the load power helps in obtaining a more effective energy management in the HESS. The SC powers were changed more dynamically than the battery power. This result is in agreement with the characteristics of SC in that SCs are good at supplying

high peak power and extremely fluctuated power. We can also see that the SCs, having a higher capacitance, can provide relatively large amounts of power for a short duration. Note that the amount of power flowing through S_3 is larger than that through the other SCs even though $C_4 > C_3$ because S_3 has the smallest ESR among the SCs; it means that the power loss induced by the SCs was minimized.

Fig. 2.6(c) shows the SC energies changing over the operation time. We can see that the net energy change of the SCs is equal to zero over the operation time. It means that the SoC of the SC can be maintained as constantly as possible by our optimization method; the SCs can be stably operated as a result.

2.5.3 Adjustment of the Boundary Parameters in the Algorithm

Fig. 2.7 shows the history of σ_1 and σ_2 during the execution of the algorithm solving $\mathbf{P}_3$. The initial values given in our simulation were $\sigma_1 = 2$, $\sigma_2 = 0.5$, $\alpha = 2$, $\beta_1 = 2$, and $\beta_2 = 0.5$. In the area of (A), σ_1 and σ_2 increase alternately and exponentially because $\mathbf{P}_3$ is infeasible. After $\mathbf{P}_3$ became feasible, in (B), the boundary parameters started to decrease additively in order to find a optimal solution. In (C), σ_1 was converged near the value of 26 but σ_2 still decreased. Finally, σ_1 and σ_2 were converged to 26 and 0.8 respectively in (D). The number of outer iterations required until $\mathbf{P}_3$ became feasible was 7 as we can see in Fig. 2.7.

From these results, we can confirm that the boundary parameters were effectively controlled by the MIAD policy. The feasibility of $\mathbf{P}$ was satisfied by the multiplicative increase of the parameters within a small number of iterations. The optimality of the $\mathbf{P}$ solutions was also guaranteed during the operation time with little additional overhead.

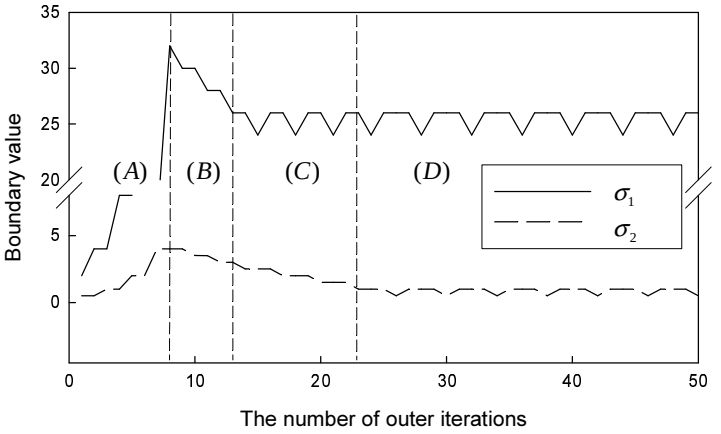

Figure 2.7: The adjustment of the boundary parameters σ_1 and σ_2 in Algorithm 2. Their initial values were $\sigma_1 = 2$, $\sigma_2 = 0.5$, $\alpha = 2$, $\beta_1 = 2$, and $\beta_2 = 0.5$. Average time of each inner iteration is 0.15 seconds.

2.6 Conclusion

In this chapter, the optimization of the energy management in battery/SC hybrid energy storage systems has been investigated. We described optimization approaches to achieve two objectives: the minimization of the magnitude/fluctuation of the battery power and the power loss in the HESS. We proposed an algorithm to adjust the boundary parameters based on the multiplicative-increase -additive-decrease (MIAD) principle. The proposed algorithm can guarantee a feasible optimal solution within a few iterations. As a result, the power flow in the HESS can be optimally controlled. The life of the battery can be extended and the size of battery can be reduced through our scheme because it effectively minimizes the magnitude/fluctuation of the battery power. Therefore, the proposed optimization scheme is suitable to be deployed in state-of-the-art applications, e.g., EVs or smart home energy systems, where a small size and a longer life of battery has been strongly required.

2.7 Proof of 2^{nd} constraint in $\mathbf{P}_2$

The second constraint in $\mathbf{P}_1$ can be rewritten as follows:

$$\begin{aligned}
&E_{S_k}(t) \\
&= -\sum_{\tau=1}^{t} \Delta \left(p_{S_k}(\tau) - \eta_{S_k} \left|p_{S_k}(\tau)\right|\right) \\
&= E_{S_k}(t-\Delta) - \Delta \left(p_{S_k}(t) - \eta_{S_k} \left|p_{S_k}(t)\right|\right) \\
&= E_{S_k}(t-\Delta) - \Delta \left(\left(p^{\text{out}}_{S_k}(t) - p^{\text{in}}_{S_k}(t)\right) - \eta_{S_k} \left|p^{\text{out}}_{S_k}(t) - p^{\text{in}}_{S_k}(t)\right|\right) \\
&= E_{S_k}(t-\Delta) - \Delta \left(\left(p^{\text{out}}_{S_k}(t) - p^{\text{in}}_{S_k}(t)\right) - \eta_{S_k} \left(p^{\text{out}}_{S_k}(t) + p^{\text{in}}_{S_k}(t)\right)\right) \\
&= E_{S_k}(t-\Delta) - \Delta \left(1 - \eta_{S_k}\right) p^{\text{out}}_{S_k}(t) - \Delta \left(1 + \eta_{S_k}\right) p^{\text{in}}_{S_k}(t).
\end{aligned}$$

Using the matrices A, D^{out}_k, and D^{in}_k, the previous equation can be represented as

$$E_{S_k} = AE_{S_k} - D^{\text{out}}_k P^{\text{out}}_{S_k} - D^{\text{in}}_k P^{\text{in}}_{S_k}.$$

Therefore,

$$(A - I)E_{S_k} - D^{\text{out}}_k P^{\text{out}}_{S_k} - D^{\text{in}}_k P^{\text{in}}_{S_k} = \mathbf{0}.$$

Chapter 3

Real-time Optimization for Power Management Systems of a Battery/Supercapacitor Hybrid Energy Storage System in Electric Vehicles

3.1 Introduction

Batteries in Electric Vehicles (EVs) can be easily damaged by the peak power or fluctuated power when the vehicles accelerate or decelerate. To prevent the battery from being damaged, battery/super-capacitor (SC) hybrid energy storage systems (HESS) can be utilized for the EVs.

When controlling the power flowing through the HESS, the following objectives have mainly been considered. As described in Chapter 2, the magnitude/variation of the battery power and the power loss should be minimized. In addition, the SoC of the SC should be adjusted according to future driving profiles [29][35][37].

Although these objectives should be accomplished at the same time when the HESS power is controlled, the previous approaches have not achieved these objectives

simultaneously. Moreover, while the real-time load dynamics should be considered when computing the reference voltage of the SC, it has not been considered in all of the previous works. Carter *et al* [29] propose a rule-based strategy for HESS power control. In this approach, described in Section IV, the HESS power is controlled based on several state parameters, i.e., the motor power, maximum battery power, reference voltage of the SC and the SC voltage. Zandi *et al* [33] propose a power control algorithm based on a Fuzzy Logic Control (FLC). The input variables considered in this approach are the battery SoC, the SC SoC, and the load power. The power split ratio between the battery and the SC can be computed by using the membership functions and the rule-bases, which are previously defined based on the input variables. These rule-based control strategy [29][33] are easily implemented in the HESS for real-time operation. Schaltz *et al* [43] investigate the influence of the battery/SC HESS sizing on the battery life time in a fuelcell HEV. In this approach, they show a power control strategy in which the power of the battery/FC should be lower than such threshold values. However, these approaches cannot provide an optimal HESS power minimizing the magnitude/variation of the battery power.

In order to compute the optimal HESS power for EVs, several researchers have designed the problem of HESS power control as an optimization problem. Moreno *et al* [30] formulate an optimization problem which minimizes the power loss in a DC/DC converter. In order to solve this problem, the authors apply their idea to a neural network in which the HESS power can be controlled in real time. Nevertheless, they do not try to minimize the magnitude/variation of the battery power. Wang *et al* [31][32] propose a methodology for sizing the HESS and controlling the HESS power. In this approach, the objective is also to minimize the power loss. When computing the power loss, however, the loss caused by the DC/DC converter is not considered despite the fact that it is relatively large compared to the loss caused by

the battery/SC. Moreover, it is not attempted to minimize the magnitude/variation of the battery power. Choi *et al* [34][35] formulate the HESS power control problem as a convex optimization problem in an effort to provide an optimal solution. The objective of the optimization problem is to minimize the magnitude/variation of the battery current. However, this approach is based on assumptions that are too ideal, i.e., the future operating profile is previously given, and the power loss caused by the DC/DC converters is zero. Bauman *et al* [36] propose an optimization method of which objective is to maximize the efficiency and to minimize the mass and the cost for determining the optimal battery/SC size for the fuelcell/battery/SC HESS. However, they do not attempt to compute the optimal HESS power under dynamic load situations. Romaus *et al* [37] attempt to optimize the power flowing through the battery/SC HESS using Stochastic Dynamic Programming (SDP). In this optimization problem, two objectives are considered; 1) the power loss induced by the battery/SC HESS, and 2) the gap between the SC voltage and the reference voltage of the SC, which is determined experimentally based on typical driving situations. The algorithm of the SDP consists of four steps: the initial guess, an evaluation of the strategy, improving the strategy, and exiting the iteration if costs converge. The strategy based on the SDP algorithm has the following weaknesses: 1) the SDP requires large computational overhead due to the two-stage optimization process, i.e., the second and third step, in a single iteration, and 2) the performance of the HESS power control scheme can be worsen when the vehicle is driven in unpredictable situations. In addition, they do not try to minimize the magnitude/fluctuation of the battery power. Hredzak *et al* [38] and Torreglosa *et al* [39] propose a strategy based on the Model Predictive Control (MPC) algorithm. The MPC algorithms show good performance if the motor power changes with predictable patterns. Laldin *et al* [40] propose the predictive algorithm of which objective is to minimize the power loss.

The authors present a Markov process with nine states, which is defined from the speed/acceleration of the driving cycle known previously. However, the accuracy of the predicted value of the motor power decreases when the speed of the vehicle sharply increases or decreases. In other words, the SC cannot be used effectively when the motor provides or requires an extremely high level of power.

In this chapter, we investigate the real-time optimization of the power management scheme for the battery/SC HESS in EVs. Our contributions can be summarized as follows:

1) We design a new control framework for the real-time control of the power flowing through the battery/SC HESS in EVs. The framework consists of two parts: one for computing the SC reference voltage based on the load dynamics, and the other for optimizing the power flowing through the HESS.

2) We propose a methodology for computing the reference voltage of the SC considering real-time load dynamics, i.e., the vehicle dynamics, characteristics of the motor, the driving conditions, and the regenerative braking systems. With the proposed method, the SC can handle the future power required by the traction motor even when a future operation profile is not given beforehand.

3) We formulate a convex optimization problem that minimizes the magnitude/variation of the battery power and the power loss simultaneously. The formulated optimization problem is shown to become an equality constrained problem which can repeatedly be computed by general solvers in polynomial time. The reference voltage of the SC computed by the proposed method is used as a given parameter in the constraints of the formulated problem.

The remainder of this chapter is organized as follows: Section II describes the system architecture considered in this chapter. Section III proposes the power control framework for the HESS in EVs and explains how the reference voltage of the SC

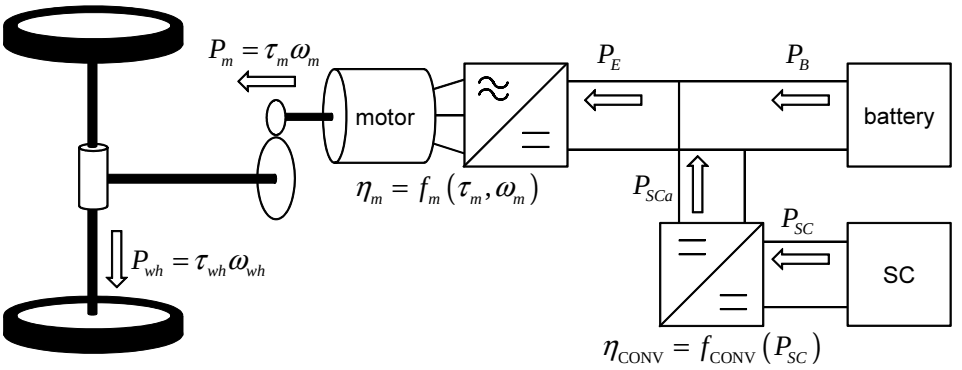

Figure 3.1: Schematic of the system architecture.

is computed considering previously mentioned factors. In addition, the proposed optimization problem for controlling the HESS power is presented. Simulation results and the conclusion are given in Sections IV and V, respectively.

3.2 System Description

The system architecture considered in this chapter is presented in Fig. 3.1. The vehicle has a front-wheel driven powertrain with an electric motor that yields a maximum power of 50 kW, and a gearbox of which the gear ratio assumed to be fixed. The braking system of the EV consists of a mechanical braking system and a regenerative braking system; the mechanical/electrical braking torque is determined by the braking strategy designed beforehand. The motor is connected to the HESS through an inverter. In the HESS, the battery and the SC are connected through a DC/DC converter which is controlled by the proposed optimization strategy. Details will be explained in the following subsections.

3.2.1 Powertrain Model

The resistance force at speed $v(t)$ can be calculated by the following equation [41]:

$$F_v(v(t)) = \frac{1}{2}\rho_a c_D A_f v(t)^2 + F_R(v(t)) + g m_t \sin\vartheta(t), \tag{3.1}$$

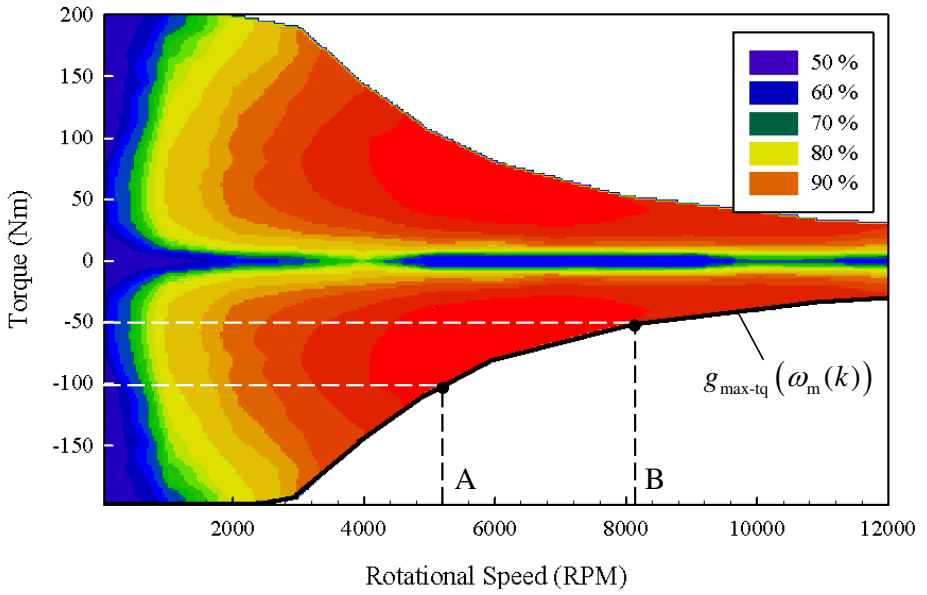

Figure 3.2: Motor efficiency map. According to the torque and rotational speed, the power efficiency is determined. For example, at -50(Nm) and 6000(RPM), the power efficiency is about 95%.

where ρ_a, c_D, and A_f are the air density, drag coefficient, and frontal area, respectively. Note that the force $F_v(v(t))$ is obtained by the summation of the aerodynamic drag, the rolling resistance, and the grading resistance. The rolling resistance $F_R(v(t))$ can be derived by a fifth-order polynomial function of the vehicle speed $v(t)$

$$F_R(v(t)) = gm_{\mathrm{t}} \cos\vartheta(t)\{a_0 + a_1 v(t) + a_2 v(t)^2 + a_3 v(t)^3 + a_4 v(t)^4 + a_5 v(t)^5\}, \quad (3.2)$$

where $a_0, a_1, \ldots, a_5$ are obtained from actual experimental results. In this work, we refer to the coefficients from Sciarretta's work [41].

The torque at the wheels required to accelerate the vehicle is equal to the sum of the resistance torque and the dynamic torque for acceleration. It is computed as

$$\tau_{\mathrm{wh}}(t) = r_{\mathrm{wh}} F_v(t) + \frac{\theta_v}{r_{\mathrm{wh}}} \frac{dv(t)}{dt}, \quad (3.3)$$

where r_{wh} is the radius of the wheels and θ_v is the total inertia of the vehicle. The rotational speed of the wheels can be intuitively calculated as follows:

$$\omega_{\mathrm{wh}}(t) = v(t)/r_{\mathrm{wh}}. \quad (3.4)$$

The force at the wheels is delivered from/to the driving motor through a gearbox as described in Fig. 3.1. According to the gear ratio G_r, the torque and rotational speed at the motor are determined as

$$\tau_{\mathrm{m}}(t) = \tau_{\mathrm{wh}}(t)/G_r, \quad (3.5)$$

$$\omega_{\mathrm{m}}(t) = \omega_{\mathrm{wh}}(t) G_r. \quad (3.6)$$

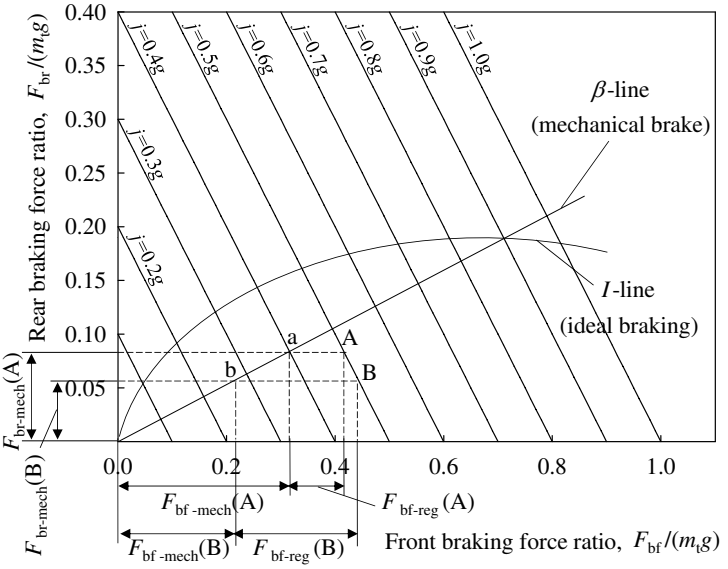

Figure 3.3: Braking forces varying with deceleration rate [48].

Using the values of $\tau_{\mathrm{m}}(t)$ and $\omega_{\mathrm{m}}(t)$, the input power of the motor-inverter can be calculated as

$$P_E(t) = \begin{cases} \tau_{\mathrm{m}}(t)\omega_{\mathrm{m}}(t)/\eta_{\mathrm{m}}(t) & \text{if } \tau_{\mathrm{m}}(t) \geq 0 \\ \tau_{\mathrm{m}}(t)\omega_{\mathrm{m}}(t)\eta_{\mathrm{m}}(t) & \text{otherwise} \end{cases} \tag{3.7}$$

where $0 < \eta_{\mathrm{m}}(t) < 1$ is the motor-inverter efficiency, which is computed as a function of $\tau_{\mathrm{m}}(t)$ and $\omega_{\mathrm{m}}(t)$:

$$\eta_{\mathrm{m}}(t) = f_{\mathrm{m}}\left(\omega_{\mathrm{m}}(t), \tau_{\mathrm{m}}(t)\right). \tag{3.8}$$

The function f_{m} can be experimentally obtained from a bench test [47]; f_{m} considered in this chapter is presented in Fig.3.2.

3.2.2 Regenerative Braking System

One of the most important features of EVs is their ability to convert significant amounts of braking energy into electric energy that can be stored in the energy storage and then reused. Because the braking torque required is generally much larger

than the torque that an electric motor can produce, mechanical braking systems should coexist with the regenerative braking system.

The braking force distribution strategy is shown in Fig. 3.3 [48]. Here, β-line represents a fixed ratio of the mechanical braking force between the front and rear wheels, and I-line is the ideal braking force of the EV. If the braking force required by the stroke of the brake pedal is $0.5m_{\mathrm{t}}g$, for example, the operating points of the braking force should be placed on the line of $j = 0.5g$; the point A and B in Fig. 3.3 are candidates for the braking force with $0.5m_{\mathrm{t}}g$. When point A is chosen as the braking point, the regenerative braking force $F_{\mathrm{bf-reg}}(\mathrm{A})$ is determined by segment A-a because the EV considered here has a front-wheel-driven powertrain. The rest of the braking force is supplied by the mechanical braking force of the front and rear wheels, denoted as $F_{\mathrm{bf-mech}}(\mathrm{A})$ and $F_{\mathrm{br-mech}}(\mathrm{A})$, respectively. In other words, $F_{\mathrm{bf-reg}}(\mathrm{A}) + F_{\mathrm{bf-mech}}(\mathrm{A}) + F_{\mathrm{br-mech}}(\mathrm{A})$ is equal to the total braking force of $0.5m_{\mathrm{t}}g$. In a similar way, we can compute the braking force $F_{\mathrm{bf-reg}}(\mathrm{B})$, $F_{\mathrm{bf-mech}}(\mathrm{B})$, and $F_{\mathrm{br-mech}}(\mathrm{B})$. As shown in Fig. 3.3, $F_{\mathrm{bf-reg}}(\mathrm{B})$ is larger than $F_{\mathrm{bf-reg}}(\mathrm{A})$, meaning that the regenerative energy at point B is larger than that at point A. Note that $F_{\mathrm{bf-reg}}(\mathrm{B})$ should be smaller or equal to the maximum force that can be produced by the motor $F_{\mathrm{m}}^{\max}$. In other words, if $F_{\mathrm{bf-reg}}(\mathrm{B})$ is equal to $F_{\mathrm{m}}^{\max}$, we can say that point B is an optimal operating point for obtaining the regenerative braking energy. Therefore, we compute the regenerative braking force $F_{\mathrm{bf-reg}}$ as follows:

$$F_{\mathrm{bf-reg}}(t) = \begin{cases} 0 & \text{if } v(t) < v_0 \\ F_{\mathrm{b}}(t) & \text{else if } F_{\mathrm{b}}(t) < F_{\mathrm{m}}^{\max} \\ F_{\mathrm{m}}^{\max} & \text{otherwise} \end{cases} \tag{3.9}$$

where $F_{\mathrm{b}}(t)$ is the required braking force and v_0 is the low speed threshold; generally v_0 is 15km/h [48]. The regenerative energy that can be obtained at less than 15km/h is too low because electromotive force is scarcely generated by the motor

at low rotational speeds. Therefore, $F_{\mathrm{bf-reg}}(t)$ is set to zero when $v(t) < v_0$. The regenerative braking system described in this section will be applied to compute a suitable SoC for the SC.

3.2.3 Battery/SC Hybrid Energy Storage Systems

Fig. 3.1 presents the battery/SC HESS providing power ($P_E(t)$) to the motor through an inverter. In the HESS, the battery and the SC are connected through active DC/DC converters. The HESS can be constructed with several types of topologies, as explained in earlier work [28][34]. Generally, the SC is connected through a DC/DC converter because a DC/DC converter permits the voltage of the SC to differ from that of the DC bus. Among all HESS topologies, the specific topology in which only-the SC is connected through the DC/DC converter, as described in Fig. 3.1, has mainly been studied due to the fact that it has good controllability in that the HESS power can effectively be controlled by the DC/DC converter connected to the SC. Moreover, it is possible for the battery in this topology to be damaged by too large peak power over a very short time. However, the peak power flowing through the battery can be reduced rapidly by the DC/DC converter in real-time. The low configuration cost is another factor. Only one DC/DC converter is used to construct the HESS. We assume that the net power flowing in and out of the DC bus is equal to zero; that is, $P_B(t) + P_{SCa}(t) - P_E(t) = 0$, where $P_B(t)$, $P_{SCa}(t)$, and $P_E(t)$ are the SC power converted by the DC/DC converter, the battery power and the power delivered to the motor.

Battery/SC model

The battery has a finite level of energy which is denoted as $\sum_t P_B(t)\Delta = E_B^{\max}$, where $E_B^{\max}$ is the maximum energy which can be stored in the battery. The internal

Table 3.1: The Battery Parameters

V_{B0}	battery constant voltage (V)	312.44
R_B	internal resistance (Ω)	7.2
K_B	polarisation voltage (V)	1.1307
A_B	exponential zone amplitude (V)	37.44
D_B	exponential zone time constant inverse ($(\mathrm{Ws})^{-1}$)	9.4328e-08

voltage is modeled as in [45]:

$$V_{B,\mathrm{int}}(t) = V_{B0} - K_B\left(\frac{E_B^{\max}}{-E_B(t)}\right) + A_B \exp\left(-D_B\left(E_B^{\max} - E_B(t)\right)\right),$$
$$V_B(t) = V_{B,\mathrm{int}}(t) - R_B i_B(t),$$

where $i_B(t)$, $V_B(t)$, R_B, and $E_B(t)$ denote the battery current, the battery voltage, the internal resistance of the battery, and the energy stored in the battery respectively. The parameters V_{B0}, K_B, A_B, and D_B, which are shown in TABLE 3.1, can be calculated using the discharge curve of the considered battery (see [45]). The power loss induced by the battery can be derived as follows:

$$P_{\mathrm{B,Loss}}(t) = \left(\frac{P_B(t)}{V_B(t)}\right)^2 R_B. \tag{3.10}$$

The energy stored in the SC, denoted as $E_{SC}(t)$, can be calculated using $V_{SC}(t)$ as follows:

$$E_{SC}(t) = \frac{1}{2} C_{SC} V_{SC}^2(t), \tag{3.11}$$

where C_{SC} is the capacitance of the SC. The minimum voltage of the SC ($V_{SC}^{\min}$) is limited to half of the maximum voltage of the SC ($V_{SC}^{\max}$) because the efficiency of the DC/DC converter connected to the SC becomes too low when the voltage of the SC ($V_{SC}(t)$) is lower than $V_{SC}^{\max}/2$ as shown in Fig. 3.4.

DC/DC converter model

The DC/DC converter controls the SC power denoted as $P_{SC}(t)$ and the output power of the DC/DC converter denoted as $P_{SCa}(t)$. The relationship between $P_{SC}(t)$ and $P_{SCa}(t)$ can be expressed as

$$P_{SCa}(t) = P_{SC}(t) - |P_{\text{conv,Loss}}(t)|\,, \tag{3.12}$$

where $P_{\text{conv,Loss}}(t)$ is the power loss induced by the DC/DC converter, the determination of which depends on the SC current and the SC voltage. The value of $P_{\text{conv,Loss}}(t)$ is computed as [46]:

$$P_{\text{conv,Loss}}(t) = \left(\frac{P_{SCa}(t)}{V_B(t)(1-D)}\right)^2 DR_{on}, \tag{3.13}$$

where D is shown at the bottom of this page.

The R_{on} is the drain-source resistance of the switch which is included in the DC/DC converter. The efficiency map of the DC/DC converter is shown in Fig. 3.4. The detailed architecture of the battery/SC HESS will be described in the next section.

3.3 Power Control System for HESS

In this section, we propose the power control framework for the battery/SC HESS in EVs. The proposed power control framework consists of two parts, as described in Fig. 3.5; $\mathbf{P}_1$, which computes the SC reference voltage (V_{SC}^{ref}) based on the vehicle dynamics; and $\mathbf{P}_2$, which optimizes the power flowing through the HESS. The details of $\mathbf{P}_1$ and $\mathbf{P}_2$ are explained in the following subsections.

$$D = \frac{V_B + V_{SC}\left(2 - R_{on}P_{SCa}/V_B^2\right) \pm \sqrt{\left\{V_B + V_{SC}\left(2 - R_{on}P_{SCa}/V_B^2\right)\right\}^2 - 4\left(V_B + V_{SC}\right)V_{SC}}}{2\left(V_B + V_{SC}\right)}.$$

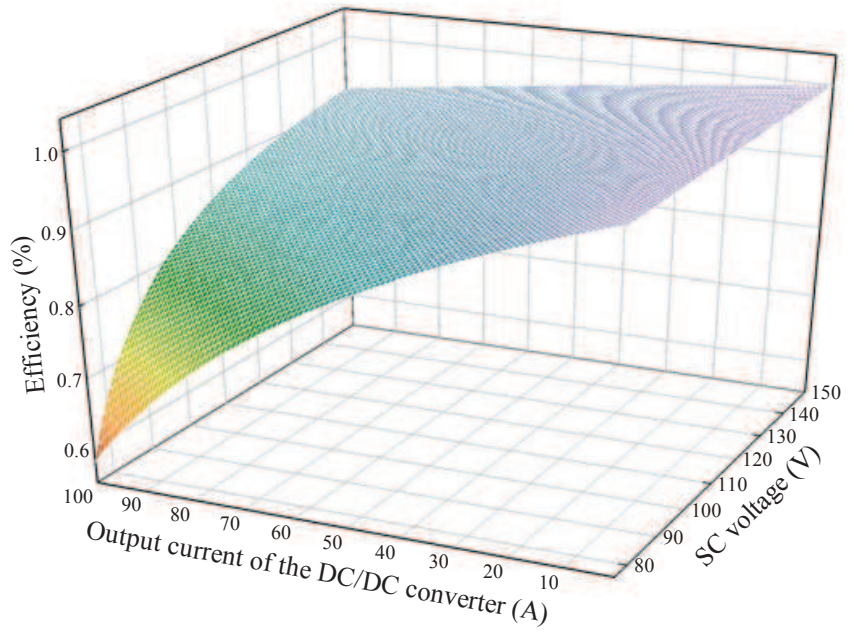

Figure 3.4: DC/DC converter efficiency map.

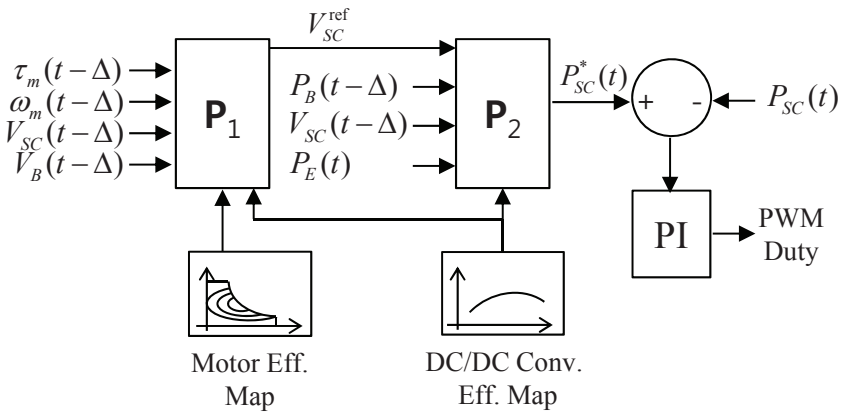

Figure 3.5: Flowchart of the proposed power control strategy

3.3.1 Computation of SC Reference Voltage

As mentioned in the introduction, the reference voltage of the SC (V_{SC}^{ref}) needs to be adjusted in order to maximize the SC's ability to support the peak power. If the future operation of the motor can be known in advance, it is easy to control V_{SC}^{ref} efficiently. However, it is difficult to obtain the future operation of the motor in advance. In this subsection, we present a method for computing a suitable value of V_{SC}^{ref} without knowledge of the future operating profile of the motor.

Before the motor requires a large amount of power, the SC should previously be charged up to $V_{SC}^{\max}$ in order to provide sufficient power to the motor whenever needed. In many experiments, it was observed that the motor requires a large amount of power, typically when the vehicle starts. Therefore, V_{SC}^{ref} is set to $V_{SC}^{\max}$ when the vehicle speed is zero. This basic strategy allows us to control V_{SC}^{ref} by considering only the energy generated from regenerative braking.

As described in Fig. 3.5, $\mathbf{P}_1$ computes V_{SC}^{ref} via $\tau_{\text{m}}(t-\Delta)$ and $\omega_{\text{m}}(t-\Delta)$, which can be considered as the given parameters at time t. From these two parameters, the future speed and torque at the wheels can be calculated as iteratively follows:

$$\begin{aligned} v_{\text{wh}}^{\text{fut}}(k) = & \, v_{\text{wh}}^{\text{fut}}(k-1) \\ & + \Delta \left(\frac{r_{\text{wh}}}{\theta_v} \right) \left(\tau_{\text{wh}}^{\text{fut}}(k-1) - r_{\text{wh}} F_v \left(v_{\text{wh}}^{\text{fut}}(k-1) \right) \right) \end{aligned} \tag{3.14}$$

$$\tau_{\text{wh}}^{\text{fut}}(k) = a_d \left(\frac{\theta_v}{r_{\text{wh}}} \right) + r_{\text{wh}} F_v \left(v_{\text{wh}}^{\text{fut}}(k-1) \right), \tag{3.15}$$

where

$$\begin{aligned} v_{\text{wh}}^{\text{fut}}(0) = & r_{\text{wh}} \omega_{\text{m}} \left(t - \Delta \right) / G_r \\ \tau_{\text{wh}}^{\text{fut}}(0) = & G_r \tau_{\text{m}} \left(t - \Delta \right). \end{aligned}$$

Eq. (3.15) is equivalent to (3.3), and Eq. (3.14) can be derived from (3.15). Here, $k \in [1, K]$ where $K = T/\Delta$ is the time of the near future. If $v_{\text{wh}}^{\text{fut}}(k) \leq 0$, then

$v_{\mathrm{wh}}^{\mathrm{fut}}(k) = 0$. The force $F_v(\cdot)$ in (3.14) and (3.15) can be calculated using (3.1). The parameter a_d in (3.15) is the minimum acceleration (maximum deceleration), which can be provided by the ego-vehicle; that is,

$$a_d = \min_{\forall \tau} \frac{dv(\tau)}{d\tau}. \tag{3.16}$$

The calculated value of $\tau_{\mathrm{wh}}^{\mathrm{fut}}(k)$ is provided by the mechanical braking and the regenerative braking systems. As presented in the previous section, $\tau_{\mathrm{wh}}^{\mathrm{fut}}(k)$ should be converted into regenerative braking energy to the greatest extent possible. Therefore, $\tau_{\mathrm{wh}}^{\mathrm{fut}}(k)$ is provided by the motor only if $\left|\tau_{\mathrm{wh}}^{\mathrm{fut}}(k)\right|$ is not larger than the maximum torque that can be provided by the motor ($\tau_{\mathrm{m}}^{\max}(k)$). If $\left|\tau_{\mathrm{wh}}^{\mathrm{fut}}(k)\right|$ is larger than $\tau_{\mathrm{m}}^{\max}(k)$, the rest of the braking torque is supported by mechanical braking. Therefore, the future rotational speed and torque of the motor can be calculated as follows:

$$\omega_{\mathrm{m}}^{\mathrm{fut}}(k) = G_r v_{\mathrm{wh}}^{\mathrm{fut}}(k)/r_{\mathrm{wh}} \tag{3.17}$$

$$\tau_{\mathrm{m}}^{\mathrm{fut}}(k) = \begin{cases} 0 & \text{if } \; v_{\mathrm{wh}}^{\mathrm{fut}}(k) < v_0 \\ \tau_{\mathrm{wh}}^{\mathrm{fut}}(k)/G_r & \text{else if } \; \left|\tau_{\mathrm{wh}}^{\mathrm{fut}}(k)/G_r\right| < \tau_{\mathrm{m}}^{\max}(k) \\ -\tau_{\mathrm{m}}^{\max}(k) & \text{otherwise,} \end{cases} \tag{3.18}$$

where r_{wh} is the radius of the wheels and G_r is the gear ratio. Here, $\tau_{\mathrm{m}}^{\max}(k)$ can be determined by the maximum torque function, denoted as $g_{\max-\mathrm{tq}}$, which is a function of $\omega_{\mathrm{m}}(k)$, as described in Fig. 3.2. For example, a motor operating at rotational speed A can provide braking torque up to 100Nm. Similarly, $\tau_{\mathrm{m}}^{\max}(k) = 50\mathrm{Nm}$ if the motor operates at point B.

Using $\omega_{\mathrm{m}}^{\mathrm{fut}}(k)$ and $\tau_{\mathrm{m}}^{\mathrm{fut}}(k)$, the power delivered from the motor-inverter can be calculated as

$$p_{\mathrm{E}}^{\mathrm{fut}}(k) = \omega_{\mathrm{m}}^{\mathrm{fut}}(k)\tau_{\mathrm{m}}^{\mathrm{fut}}(k)\eta_{\mathrm{m}}(k), \tag{3.19}$$

where $\eta_{\mathrm{m}}(k)$ is the motor-inverter efficiency as computed by (3.8). Note that $p_{\mathrm{E}}^{\mathrm{fut}}(k) \leq 0$.

Although the regenerative braking energy delivered from the motor is charged to not only the SC but also the battery, we set the energy charged to the SC equal to the regenerative braking energy in order to minimize the peak power delivered to the battery. The energy charged to the SC in the near future with duration T can be computed by

$$E_{SC}^{\text{fut}} = \sum_{k=1}^{K} \left(p_{\text{E}}^{\text{fut}}(k) + |P_{\text{conv,Loss}}(k)| \right) \Delta, \tag{3.20}$$

where $|P_{\text{conv,Loss}}(k)|$ is the power loss of the DC/DC converter as computed by (3.13). From the computed value of E_{SC}^{fut}, the reference voltage of the SC can be calculated using (3.11) as follows:

$$V_{SC}^{\text{ref}} = \sqrt{2\frac{E_{SC}^{\text{fut}}}{C_{SC}} + (V_{SC}^{\max})^2}. \tag{3.21}$$

Note that $E_{SC}^{\text{fut}} \leq 0$ because only the regenerative braking energy is considered when computating V_{SC}^{ref}. Nevertheless, the SC can deliver the required future motor power sufficiently because the stored energy in the SC, i.e., $E_{SC}^{\text{ref}} - E_{SC}^{\min}$, can be used for $p_E^{\text{fut}} > 0$. If the vehicle speed is zero, for example, the SC needs to be fully charged in order to provide enough power to the motor in near future.

3.3.2 Computation of the optimal SC power

In this subsection, we formulate a convex optimization problem to optimize the power flow in the HESS. The objective of the optimization problem is to minimize the magnitude/variation of the battery power and the energy loss. The formulated problem is solved in $\mathbf{P}_2$, as described in Fig. 3.5. By solving the proposed optimization problem, the optimal power flowing through the HESS can be obtained.

Objective function

In order to design the objective function of the optimization problem, penalty functions $\psi(\cdot)$ can be applied. A common characteristic of penalty functions is that the

function value increases as the absolute input value increases. The representative penalty functions are described in Chapter 2.

Using penalty functions which are convex and denoted by $\psi(\cdot)$, the power control problem can be formulated as a penalty function approximation problem [20]. The objective function can be formulated as the sum of the penalty functions, i.e.,

$$\begin{aligned}\alpha_1\psi_1\left(P_B(t)\right) + \alpha_2\psi_2\left(P_B(t) - P_B(t-\Delta)\right) \\ + \alpha_3\psi_3\left(P_B(t), V_B(t)\right) + \alpha_4\psi_4\left(P_{SCa}(t), V_{SC}(t), V_B(t)\right) \\ + \alpha_5\psi_5\left(E_{SC}(t), E_{SC}^{\text{ref}}\right), \quad (3.22)\end{aligned}$$

where $E_{SC}(t)$ is the energy stored in the SC. It can be calculated from $V_{SC}(t)$ using (3.11). Similarly, E_{SC}^{ref}, which is the reference energy of the SC, can be derived from V_{SC}^{ref}. The values of α_1, ..., α_5 are trade-off parameters. The terms ψ_1 and ψ_2 are a function of the magnitude and the variation of the battery power. The terms ψ_3 and ψ_4 correspondingly refer to the power loss caused by the battery and the DC/DC converter respectively. The final term ψ_5 is added to adjust the energy stored in the SC based on E_{SC}^{ref}, which is computed by $\mathbf{P}_1$.

Design of the penalty functions

It is important to design penalty functions that minimize the objectives efficiently. A large $P_B(t)$, especially $P_B(t) > P_B^{\text{thre}}$ where P_B^{thre} is a threshold of the battery power which can shorten the battery's life. Therefore, the function ψ_1 should have more of a handicap when $P_B(t) > P_B^{\text{thre}}$, as expressed by

$$\psi_1 = \max\left(0, |u_1| - 1\right), \quad (3.23)$$

where $u_1 = P_B(t)/P_B^{\text{thre}}$. Similarly, the function ψ_2 can also be represented as

$$\psi_2 = \max\left(0, |u_2| - 1\right), \quad (3.24)$$

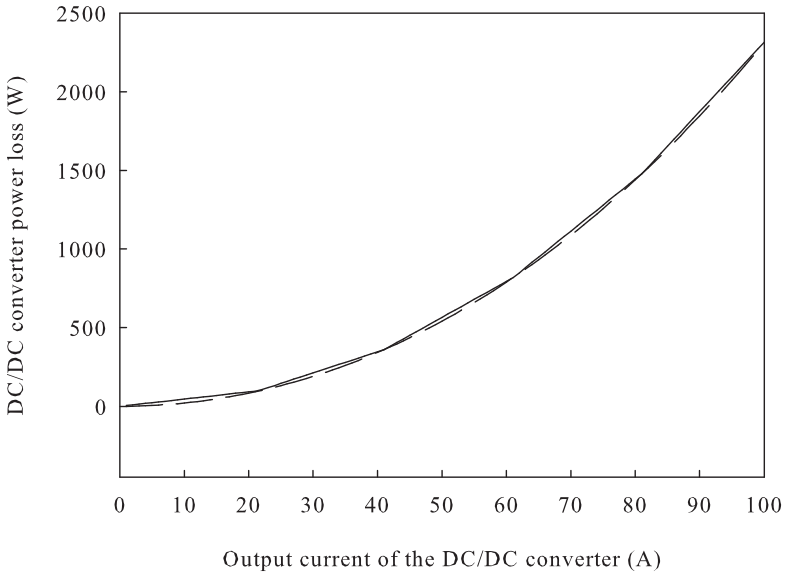

Figure 3.6: The power loss of DC/DC converter when $V_B = 300(V)$ and $V_{SC} = 150(V)$. The dashed line is obtained by (3.13) and the solid line is its approximated piecewise linear function.

.

where $u_2 = (P_B(t) - P_B(t-\Delta))/P_{B,\mathrm{var}}^{\mathrm{thre}}$. The threshold values, i.e., P_B^{thre} and $P_{B,\mathrm{var}}^{\mathrm{thre}}$, can be determined arbitrarily or experimentally. The function ψ_5, which needs to be as close to zero as possible to minimize the gap between $E_{SC}(t)$ and E_{SC}^{ref}, can be expressed as

$$\psi_5 = |u_5|\,, \tag{3.25}$$

where $u_5 = \left(E_{SC}(t) - E_{SC}^{\mathrm{ref}}\right)/\left(E_{SC}^{\max} - E_{SC}^{\min}\right)$. Note that $|u_5| \leq 1$ because $E_{SC}(t)$ and E_{SC}^{ref} are in $\left[E_{SC}^{\max}, E_{SC}^{\min}\right]$.

The ψ_3 and ψ_4 are a function of the power loss induced by the battery and the DC/DC converter respectively. Therefore, these penalty functions can be designed as follows:

$$\psi_3 = \left(\frac{P_B(t)}{V_B(t)}\right)^2 R_B, \tag{3.26}$$

$$\psi_4 = R_{on}\left(\frac{P_{SCa}(t)}{V_B(t)}\right)^2 \frac{D}{(1-D)^2}, \tag{3.27}$$

where ψ_4 is equal to (3.13). Because ψ_3 and ψ_4 are not convex, we need to make these penalty functions convex. In (3.26), $V_B(t)$ can be replaced with $V_B(t-\Delta)$, which can be known at time t, in order to make ψ_3 convex. This is acceptable because the difference between $V_B(t)$ and $V_B(t-\Delta)$ is sufficiently small. In (3.27), similarly, $V_B(t)$ and $V_{SC}(t)$ can be replaced with $V_B(t-\Delta)$ and $V_{SC}(t-\Delta)$. Because $V_B(t)$ and $V_{SC}(t)$ were replaced by the known parameters, the power loss equation (3.27) becomes a function of $P_{SCa}(t)$. This function can be designed as a piecewise linear function which is a convex function as shown in Fig. 3.6. Note that the shape of the piecewise linear function is determined depending on $V_B(t-\Delta)$ and $V_{SC}(t-\Delta)$.

Adjustment of tradeoff factors

The tradeoff factors, i.e., $\alpha_1, \ldots, \alpha_5 \geq 0$, affect the weight of the functions included in the objective function. Generally, the weight of the penalty function becomes

larger as the corresponding tradeoff factor increases. If $\psi(u) = |u|$, for example, $\alpha_i\psi(u) > \alpha_j\psi(u)$ for all u, where $\alpha_i > \alpha_j$. If $\psi(u)$ is designed as the deadzone linear function, $\alpha_i\psi(u) > \alpha_j\psi(u)$ for $|u| > \sigma$ and $\alpha_i\psi(u) = \alpha_j\psi(u) = 0$ for $|u| \leq \sigma$, where $\alpha_i > \alpha_j$. Note that the function has no penalty when $|u| \leq \sigma$.

Here, α_1, which is the cost of the battery damage caused by $|P_B(t)| - P_B^{\text{thre}}$, can be derived approximately from

$$\text{cost}_B \times \frac{N_{\text{reduced}}}{N_{\text{normal}}} = \alpha_1 \times \frac{P_{\text{B}}^{\text{max}}}{P_{\text{B}}^{\text{thre}}} \times T \times (N_{\text{normal}} - N_{\text{reduced}}), \quad (3.28)$$

where cost_B is the price of the battery, N_{normal} is the initial cycle life of the battery, N_{reduced} is the battery cycle life reduced by P_B^{max} which is a maximum available power of the battery, and T is the time of battery use with P_B^{max}. In (3.28), the term $\text{cost}_B \times N_{\text{reduced}}/N_{\text{normal}}$ means the battery cost lost by P_B^{max}, and the term $T \times (N_{\text{normal}} - N_{\text{reduced}})$ is total hours of battery use. The factor α_2 can similarly be designed with the cost of the battery damage caused by $|P_B(t) - P_B(t-\Delta)| - P_{B,\text{var}}^{\text{thre}}$. We assume that the tradeoff factor α_1 and α_2 can experimentally be determined. In addition, α_3 and α_4 can simply be designed with the cost per unit power because the functions ψ_3 and ψ_4 are functions of the power.

The function $0 \leq \psi_5 \leq 1$ can be considered as representing the potential damage of the battery; for example, $P_B(t)$ increases when ψ_5 increases. Therefore, the last tradeoff factor α_5 can be defined as

$$\alpha_5 = \alpha_1. \quad (3.29)$$

Optimization problem

The problem concerning the control of the power flow in the HESS can be formulated as a convex optimization problem which is solved using $\mathbf{P}_2$, as follows:

$$\begin{aligned} \text{min.} \quad & \text{Eq.(3.22)} \\ \text{s.t.} \quad & P_B(t) + P_{SCa}(t) - P_E(t) = 0, \\ & P_{SCa}(t) = P_{SC}(t) - \left|P_{\text{conv,Loss}}(t)\right|, \\ & E_{SC}(t) - E_{SC}(t-\Delta) = -P_{SC}(t)\Delta, \\ & E_{SC}^{\min} \leq E_{SC}(t) \leq E_{SC}^{\max}. \end{aligned} \tag{3.30}$$

In this formulation, the control variables are $P_B(t)$, $P_{SC}(t)$, $P_{SCa}(t)$, and $E_{SC}(t)$. The voltage of the SC can easily be computed from $E_{SC}(t)$ using (3.11). However, this formulation is not a convex optimization problem because the second constraint function regarding $P_{SC}(t)$ is not an affine function; the equality constraint functions of a convex problem must be affine. In order to make the second constraint affine, we replace $P_{\text{conv,Loss}}(t)$ with $P_{\text{conv,Loss}}(t-\Delta)$, which can be determined at time t. Because the time gap Δ is sufficiently small, it is acceptable to assume that the difference between the DC/DC converter efficiencies at time $t-\Delta$ and t are negligible. Moreover, the accumulated error caused by the negligible difference between $P_{\text{conv,Loss}}(t-\Delta)$ and $P_{\text{conv,Loss}}(t)$ does not diverge because the given parameters included in the formulated problem are updated at each instant. Therefore, the problem regarding the control of the power flow in the HESS can be expressed as a convex optimization problem, as follows:

$$\begin{aligned} \text{min.} \quad & \text{Eq.(3.22)} \\ \text{s.t.} \quad & \text{The constraints of Eq.(3.30) where} \\ & \text{second equality is substituted with} \\ & P_{SCa}(t) = P_{SC}(t) - \left|P_{\text{conv,Loss}}(t-\Delta)\right|. \end{aligned}$$

Algorithm 3 The barrier method.

1: **given** feasible x, $t \leftarrow t^{(0)} > 0$, $\mu > 1$, tolerance $\epsilon > 0$.
2: **repeat**
3: Compute x^* by minimizing $tf_0 + \phi$, subject to $Ax = b$, starting at x
4: $x \leftarrow x^*$
5: $t \leftarrow \mu t$
6: **until** $m/t < \epsilon$

In order to obtain the optimal power of the SC denoted as $P^*_{SCa}(t)$, the formulated problem needs to be solved by a solver.

Computation by solver

A general form of the convex problem can be described as follows:

$$\begin{array}{rll} \text{minimize} & f_0(x) & \\ \text{subject to} & f_i(x) \leq 0, & i = 1, \cdots, m \\ & Ax = b, & \end{array}$$

where $f_0, \ldots, f_m : \mathbf{R}^n \rightarrow \mathbf{R}$ are convex and twice continuously differentiable, and $A \in \mathbf{R}^{p \times n}$ with **rank** $A = p < n$. In order to solve the problem with a guaranteed specified accuracy level of ϵ, the general form needs to be changed to an equality constrained problem

$$\begin{array}{rl} \text{minimize} & (m/\epsilon) f_0(x) + \phi(x) \\ \text{subject to} & Ax = b, \end{array}$$

where ϵ is the tolerance to guarantee the sub-optimality, m is the number of inequality constraints in the problem, and $\phi(x) = -\sum_{i=1}^{m} \log(f_i(x))$.

The barrier method, a typical solver, can solve the equality constrained problem in polynomial time [20]. A simple version of the barrier method is described by Algorithm 3, where μ is the size of the Newton step. At each iteration, x^* is computed by Newton's method. The iteration terminates when $t \geq m/\epsilon$.

Table 3.2: The Vehicle Parameters

ρ_a	air density (kg/m^3)	1.205
c_D	drag coefficient	0.32
A_f	frontal area (m^2)	2.31
m_t	vehicle mass (kg)	1680
θ_v	vehicle total inertia (kg·m^2)	145
r_{wh}	wheel radius (m)	0.29
G_r	gear ratio	6.45
a_0	rolling resistance coefficient	$8.80{\cdot}10^{-3}$
a_1	rolling resistance coefficient	$-6.42{\cdot}10^{-5}$
a_2	rolling resistance coefficient	$9.27{\cdot}10^{-6}$
a_3	rolling resistance coefficient	$-3.30{\cdot}10^{-7}$
a_4	rolling resistance coefficient	$6.68{\cdot}10^{-9}$
a_5	rolling resistance coefficient	$-4.46{\cdot}10^{-11}$
C_{SC}	SC capacitance (F)	3400/56
$V_{SC}^{\max}$	maximum voltage of SC (V)	2.7·56
P_B^{thre}	the threshold of the power causing damage to the battery (kW)	15
$P_{B,\text{var}}^{\text{thre}}$	the threshold of the power variation causing damage to the battery (kW/s)	1.5
$P_{\text{conv}}^{\max}$	maximum power of DC/DC converter (kW)	50

The proposed formulation shown in the previous subsection can be presented with the equality constraint problem. The total number of iterations of the barrier method is

$$\begin{aligned} N_{bf} = & \left\lceil \frac{\log(m/t^{(0)}\epsilon)}{\log\mu} \right\rceil \left(\frac{m(\mu - 1 - \log\mu)}{\mu} + c \right) \\ \approx & \; O(m \log m), \end{aligned}$$

where $c = \log_2 \log_2(1/\epsilon_{\text{nt}})$ [20]. Here, ϵ_{nt} denotes the tolerance in Newton's method. In the results, the optimal power $P_B^*(t)$ and $P_{SCa}^*(t)$ can directly be derived from $x^*(t)$ provided by the barrier method. Based on the value of $P_{SCa}^*(t)$, the PI controller described in Fig. 3.5 adjusts the PWM duty cycle of the DC/DC converter to keep the SC power close to $P_{SCa}^*(t)$.

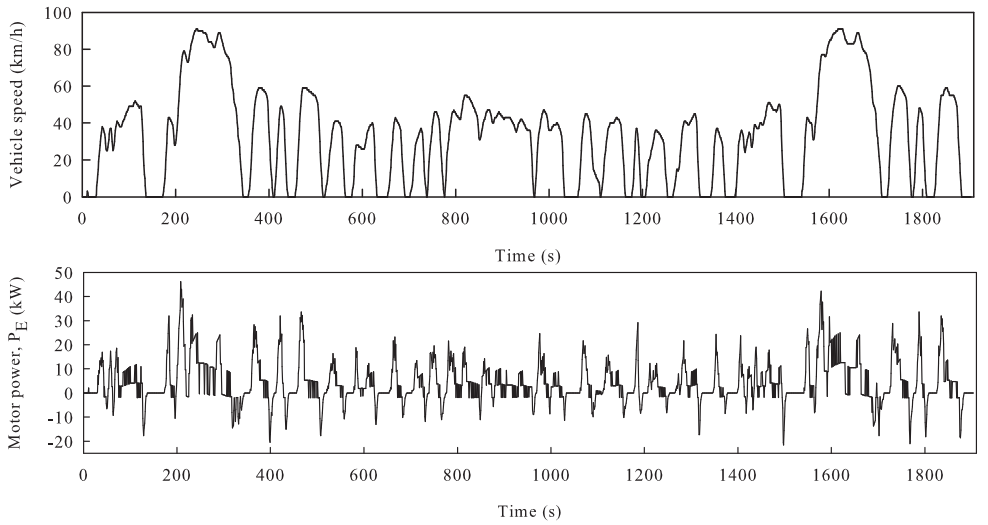

Figure 3.7: The operating profile: the speed profile (FTP75) and the power required by the motor. The required power is computed by using the dynamic model described in Section II-A.

.

3.4 Simulation Result

A simulation program was implemented in MATLAB in order to validate the aforementioned HESS system architecture and the optimization problem. In the simulation, we considered the HESS topology presented in Fig. 3.1. The considered driving cycle, which is a speed profile termed FTP75, is shown in Fig. 3.7. Using this speed profile, the power required by the electric motor can be derived using the power train model described in Section II-A. Because we assume that the future operating profile cannot be known in advance, the optimal power of a battery/SC is computed at each instant. The vehicle parameters applied in the simulation are shown in Table 3.2 [41]. The simulation results were obtained by solving the proposed optimization problem, which minimizes the magnitude/variation of the battery power and the power loss. The solver implemented in the simulation is SeDuMi [20] which is a

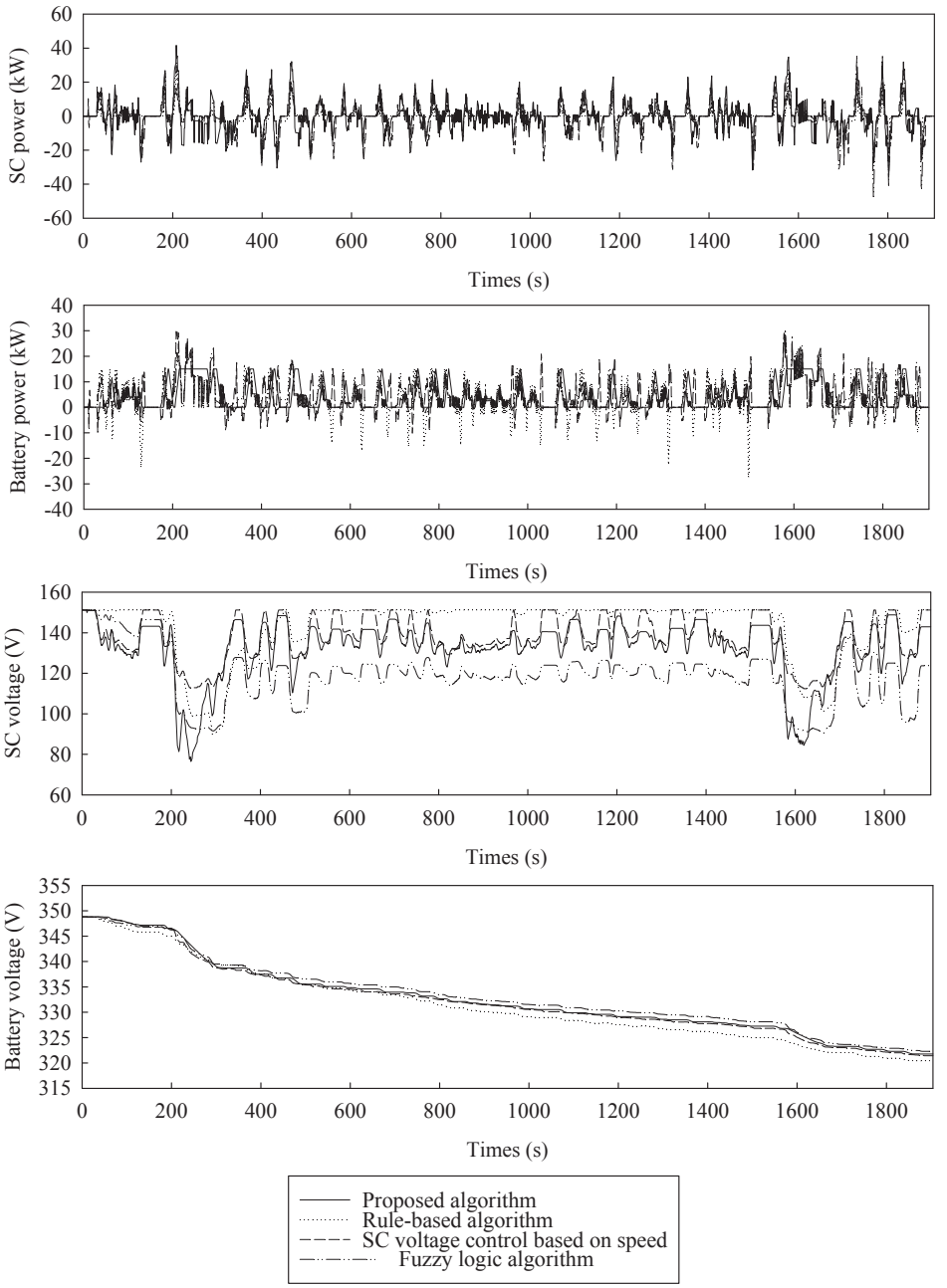

Figure 3.8: The simulation results: the SC power, the battery power, the SC voltage, and the battery voltage.

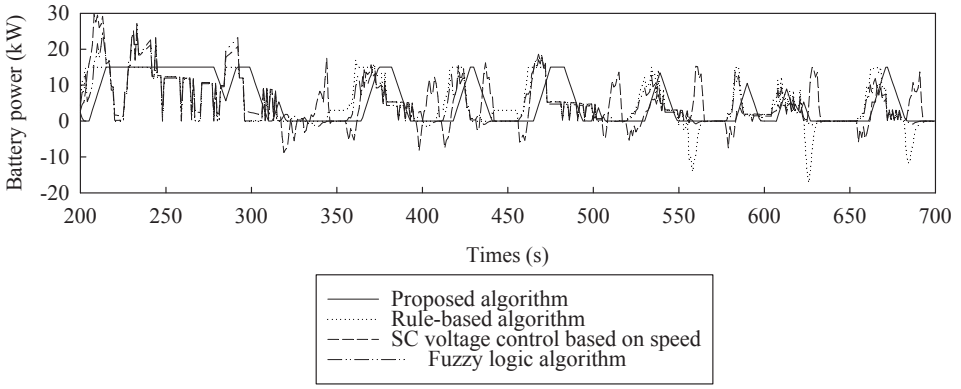

Figure 3.9: The battery power from $t = 200$ to 700 computed by the proposed strategy and the other strategies, i.e., the rule-based strategy, the SC voltage control based on the vehicle speed, and the fuzzy logic strategy.

MATLAB-based solver for solving convex optimization problems.

For a performance comparison, the rule-based strategy [29], the SC voltage control based on the vehicle speed [30], and a fuzzy logic strategy [33] were considered in the simulation. In the rule-based algorithm, the HESS power is controlled based on several states, i.e., the motor power ($P_M^{\mathbf{req}}$), the threshold of the power causing damage to the battery ($P_B^{\mathbf{thre}}$), the reference voltage of the SC ($V_{SC}^{\mathbf{ref}}$), and the voltage of the SC (V_{SC}), as follows:

- $P_M^{\mathbf{req}} > P_B^{\mathbf{thre}}$: the SC supplies $P_M^{\mathbf{req}} - P_B^{\mathbf{thre}}$. If the SC does not have sufficient energy to supply $P_M^{\mathbf{req}} - P_B^{\mathbf{thre}}$, the SC supplies as much power as possible and the battery supplies the rest.

- $P_M^{\mathbf{req}} \leq P_B^{\mathbf{thre}}$: the battery provides $P_M^{\mathbf{req}}$. If $V_{SC} \leq V_{SC}^{\mathbf{ref}}$, the battery supplies power to both the motor and the SC.

- $P_M^{\mathbf{req}} < 0$ (regenerative braking): the SC receives as much power as possible and the battery receives the rest.

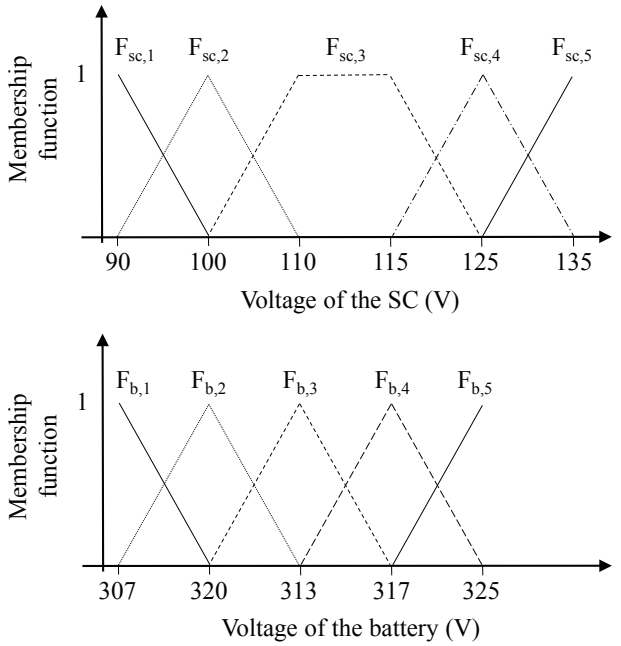

Figure 3.10: The membership function used in the fuzzy logic strategy for comparison.

In this simulation, $P_B^{\mathbf{thre}} = 15kW$.

In the SC voltage control strategy based on the vehicle speed, the SC voltage is determined by $V_{SC}^{\max}\sqrt{1-\omega/\omega_{\max}}$, where v is the speed of the vehicle and ω is the rotational speed of the motor. In this simulation, $\omega_{\max} = 2\pi \times 12k(\text{RPM})/60(\text{sec})$.

In the fuzzy logic strategy, the input variables considered are the battery voltage, the SC voltage, and the load power. The membership functions for the battery voltage and the SC voltage are listed as the following five categories: very negative, negative, zero, positive, and very positive. The membership functions of the load power are categorized into three types: recovery, normal, and overload. Because the HESS considered in an earlier work [33] and that in this chapter are different with regard to the maximum voltage of the energy storage devices, we modified the scale of the input of the membership functions and the values used for the rule bases.

	$F_{b,1}$	$F_{b,2}$	$F_{b,3}$	$F_{b,4}$	$F_{b,5}$
$F_{sc,1}$	0.2	0.1	0.1	0.0	0.0
$F_{sc,2}$	0.3	0.3	0.2	0.2	0.1
$F_{sc,3}$	0.4	0.4	0.3	0.3	0.2
$F_{sc,4}$	0.5	0.4	0.4	0.3	0.3
$F_{sc,5}$	0.6	0.5	0.5	0.4	0.3

Discharging case ($p_E \leq 20kW$)

	$F_{b,1}$	$F_{b,2}$	$F_{b,3}$	$F_{b,4}$	$F_{b,5}$
$F_{sc,1}$	0.3	0.3	0.2	0.1	0.0
$F_{sc,2}$	0.4	0.4	0.3	0.3	0.2
$F_{sc,3}$	0.7	0.7	0.7	0.6	0.5
$F_{sc,4}$	1.0	0.9	0.8	0.8	0.7
$F_{sc,5}$	1.0	0.9	0.9	0.8	0.8

Discharging case ($p_E > 20kW$)

	$F_{b,1}$	$F_{b,2}$	$F_{b,3}$	$F_{b,4}$	$F_{b,5}$
$F_{sc,1}$	0.1	0.3	0.8	0.9	1.0
$F_{sc,2}$	0.1	0.3	0.6	0.8	1.0
$F_{sc,3}$	0.0	0.2	0.5	0.7	0.9
$F_{sc,4}$	0.0	0.1	0.2	0.4	0.5
$F_{sc,5}$	0.0	0.0	0.0	0.1	0.4

Charging case

Figure 3.11: The look-up (rule bases) table used in the fuzzy logic strategy for comparison.

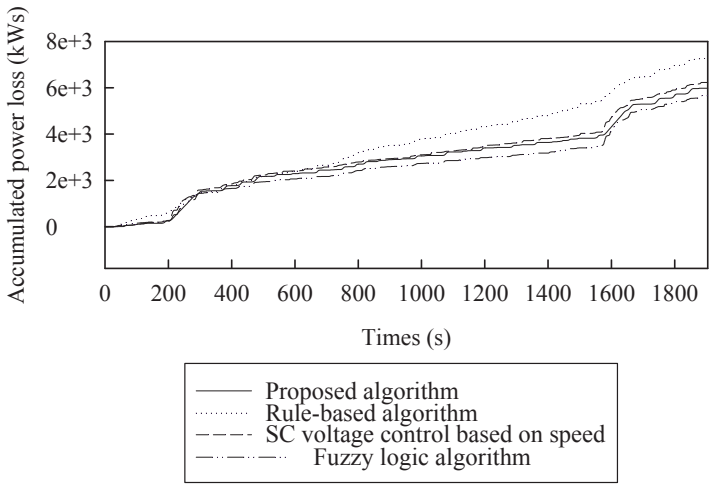

Figure 3.12: The accumulated power loss computed by the proposed strategy and the other strategies, i.e., the rule-based strategy, the SC voltage control based on the vehicle speed, and the fuzzy logic strategy.

(See Fig.3.10 and Fig.3.11 for the membership functions and the lookup table used in the fuzzy logic control strategy).

Simulations were carried out with several trade-off factors, $S_\alpha = (\alpha_1, \alpha_2, \alpha_3, \alpha_4, \alpha_5)$. Fig. 3.8 shows the changing pattern of the SC power, the battery power, the SC voltage, and the battery voltage as computed by the proposed strategy and the other strategies, i.e., the rule-based strategy, the strategy with SC voltage control based on the vehicle speed, and the fuzzy logic strategy. In Fig. 3.9, the battery power from $t = 200$ to 700 is shown in detail. The black line in Fig. 3.8 was obtained by the proposed strategy with $S_\alpha = (0.1481, 0.01481, 1/3000, 1/3000, 0.1481)$. The average computation time for a single iteration of the proposed algorithm is 42.8 ms and the maximum time is 78.1 ms. This value can change depending on the solver used.

As shown in Fig. 3.8, the battery controlled by the rule-based strategy tends to be discharged when the motor power increases strongly, indicating that the rule-

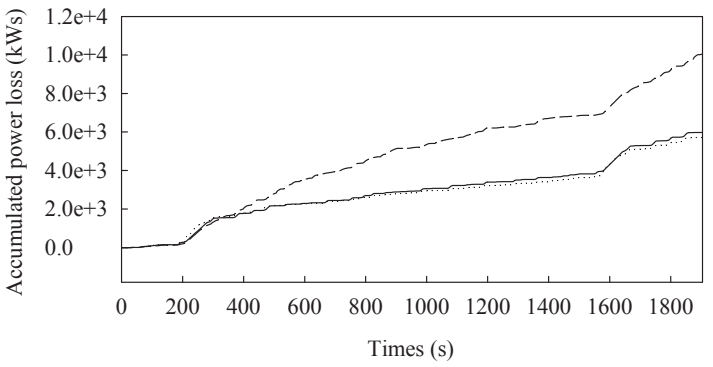

Figure 3.13: The accumulated power loss computed by the proposed strategy with S_α =(0.1481, 0.01481, 1/3000, 1/3000, 0.1481) (solid line), S_α =(0, 0, 1/3000, 1/3000, 0.1481) (dotted line), and S_α =(0.1481, 0.01481, 0, 0, 0.1481) (broken line).

Table 3.3: Simulation results

	Proposed	Rule-based.	Speed based.	Fuzzy logic.
Max. mag. of P_b (W)	15000	32641	27432	29677
Ave. mag. of P_b (W)	4065.14	3929.95	5264.55	4729.66
Standard dev.	5243.81	5358.79	5435.77	5050.26
Max. var. of P_b (W/s)	1500.2	16323.8	18320.9	16485.26
Ave. var. of P_b (W/s)	616.22	1706.88	2049.86	1974.80
Standard dev.	690.29	2320.84	2884.14	2435.74

based strategy can effectively keep the battery power within P_B^{thre}. However, it is not discharged in general urban driving situations. This indicates that the rule-based control method is not appropriate for urban situations, in which the motor frequently requires considerable and fluctuating power due to the repeated stop-and-go driving patterns used in such situations. The battery power controlled by the rule-based strategy is relatively large compared to the other values when $P_B(t) < 0$, as the SC cannot absorb the large amount of the power provided by the motor. The speed-based SC voltage control strategy and the fuzzy logic strategy can reduce the battery power more effectively than the rule-based strategy in urban driving situations as presented from the cases when $t = 400$ to 700 in Fig. 3.9. However, these strategies cannot prevent the battery power from exceeding the threshold which causes damage to the battery when the motor requires an extremely large amount of power, as shown from the cases when $t = 200$ to 300. It is observed that the proposed strategy can restrict the battery power below P_B^{thre} with variation below $P_{B,\text{var}}^{\text{thre}}$. In other words, the proposed method can reduce the magnitude/fluctuation of the battery power effectively and make the SC receive more regenerative energy from the motor. Thus, the life of the battery can be extended by the proposed optimization method.

Fig. 3.12 shows the comparison of the accumulated power losses as computed by the four strategies. As shown in Fig. 3.12, the lowest power loss is obtained by the fuzzy logic strategy, not our proposed strategy. However, the difference between the amount of the power loss provided by the fuzzy logic strategy and that provided by our strategy is small. The reasons why the proposed strategy does not show the best performance in terms of the power loss are as follows: 1) our strategy minimizes not only the power loss but also the magnitude/fluctuation of

the battery power, and 2) the SC voltage is influenced by the SC reference voltage, which depends on the load dynamics. Note that the SC reference voltage is not considered in the fuzzy logic strategy. Fig. 3.13 shows the effect of the trade-off factors when using the proposed strategy. The dotted line was obtained with $S_\alpha = (0, 0, 1/3000, 1/3000, 0.1481)$ which means that the magnitude/fluctuation of the battery power was not considered in the simulation. In contrast, the broken line was obtained with $S_\alpha = (0.1481, 0.01481, 0, 0, 0.1481)$ which means that the power loss was not considered in the simulation. As shown in Fig. 3.13, the power loss computed with $S_\alpha = (0, 0, 1/3000, 1/3000, 0.1481)$ is lower than that computed with $S_\alpha = (0.1481, 0.01481, 0, 0, 0.1481)$ because the objective function formulated with $S_\alpha = (0, 0, 1/3000, 1/3000, 0.1481)$ imposes more of a penalty to the power loss function. In other words, it is clear that the power loss term of the objective function in the proposed strategy, i.e., ψ_3 and ψ_4, can effectively reduce the power loss induced by the battery/SC HESS.

Table III shows the statistics of the battery power computed by four strategies, which can be obtained from Fig. 3.8. As shown in Table III, the maximum magnitude/variation of the battery power calculated by our strategy, i.e., 15000 (W) and 1500.2 (W/s) respectively, are much smaller than that computed by the other strategies. This simulation result means that the proposed method can be used for increasing the life of the battery effectively because the damage of the battery is exponentially increased as the magnitude/variation of the battery power increase. Although the average battery power computed by our strategy is slightly larger than that controlled by the rule-based strategy, the difference between these two values is not large.

3.5 Conclusion

In this chapter, real-time optimization for the power management systems for the battery/SC HESS in EVs was investigated. We described a power control framework to control the power flowing through the HESS and proposed a methodology for computing the reference voltage of the SC in order to adjust the SoC of the SC without a future operating profile. Finally, we formulated a convex optimization problem to achieve the following goals: minimizing the magnitude/fluctuation of the battery power, minimizing the energy loss, and minimizing the gap between the SC voltage and its reference value. We reformulated the problem of the HESS power control into an equality constrained problem, which can be solved by a general solver such as the barrier method within a few iterations in a polynomial time. As a result, the life of the battery can be extended and the size of the battery can be reduced through our scheme because it effectively minimizes the magnitude/fluctuation of the battery power. In addition, the proposed scheme can be applied for sizing the SC because the amount of charging/discharging energy can be analyzed by a function which computes the SC reference voltage and by a function which computes the optimal SC power.

Chapter 4

Robust Multi-Target Tracking Scheme based on Gaussian Mixture Probability Hypothesis Density Filter

4.1 Introduction

In the previous chapters, it was explained that the future driving profiles (speed, acceleration) is required for improving the power control of the battery/supercapacitor (SC) hybrid energy storage system (HESS) in electric vehicles (EVs). To predict the future speed/acceleration, the driving environments such as traffic lights, lanes, surrounding vehicles, or pedestrians should be accurately recognized from the measurements obtained from on-board sensors. The multi-target tracking is one of the fundamental technologies required for recognizing the driving environments.

For tracking multi-targets, the Multiple Hypotheses Tracking (MHT) [49]-[51] algorithm has traditionally been used, in which the multiple hypothesis are generated and evaluated through associating tracks with measurements. For example, let's assume that there are two predicted states (T_1, T_2) and three measurements

(O_1, O_2, O_3). The possible hypotheses are generated as follows:

$$
\begin{aligned}
H(1) &= \{T_1, T_2, NT(O_1), NT(O_2), NT(O_3)\}, \\
H(2) &= \{T(T_1; O_1), T_2, NT(O_2), NT(O_3)\}, \\
H(3) &= \{T(T_2; O_2), T_1, NT(O_1), NT(O_3)\}, \\
H(4) &= \{T(T_2; O_3), T_1, NT(O_1), NT(O_2)\}, \\
H(5) &= \{T(T_1; O_1), T(T_2; O_2), NT(O_3)\}, \\
H(6) &= \{T(T_1; O_1), T(T_2; O_3), NT(O_2)\}, \\
H(7) &= \{T(T_1; O_2), T(T_2; O_1), NT(O_3)\}, \\
H(8) &= \{T(T_1; O_2), T(T_2; O_3), NT(O_1)\}, \\
H(9) &= \{T(T_1; O_3), T(T_2; O_1), NT(O_2)\}, \\
H(10) &= \{T(T_1; O_3), T(T_2; O_2), NT(O_1)\},
\end{aligned}
$$

where $T(T_i; O_j)$ is the state estimated from the prediction T_i and the measurement O_j, and $NT(O_j)$ is the state newly generated from O_j. All generated hypothesis are evaluated by the likelihood ratio (LR) for a given combination of data. (See [50] for more detail of LR). However, the MHT scheme is not suitable for tracking multi-targets since it requires large computational overhead for the track-to-measurement data association process. As we can see in the previous example, the number of track-measurement combination increases exponentially as the number of track/measurement increases. Recently, the Probability Hypotheses Density (PHD) filter [52]-[54] has come into the spotlight, because it can effectively handle target birth/death without the track-to-measurement data association process. The PHD filter computes the first-order moment of the posterior density recursively, from which the multiple estimates can be extracted [53]. To provide a closed form solution for the PHD recursion, the Gaussian Mixture Probability Hypotheses Density (GM-PHD) filter, based on the Kalman filter, was proposed and widely applied to efficiently update posterior density [54]. Since the GM-PHD filter estimates the cardinality with a high covariance when the number of targets is large, the Gaussian Mixture Cardinalized PHD (GM-CPHD) filter [55] was proposed, in which not only the posterior intensity but also the probability distribution of the number of targets are propagated.

However, several issues arise with the GM-PHD (or GM-CPHD) filter. These inaccuracies are related to the birth intensity generation [56][57]. Since it is assumed that the birth targets appear over small specific areas defined with the mean and covariance known a priori as in [54][55], the birth targets that appear in the non-predefined region cannot be estimated properly. To cover these birth targets, it is required to generate the birth intensity with random positions, but the random birth intensity may cause short-lived false tracks. Although the short-lived false tracks can be reduced if the number of the birth states is small, it normally needs more time to confirm the states.

The inaccuracies are related to not only the birth intensity generation but also the target tractability [58]-[61]. Since the GM-PHD filter does not provide the identity for individual targets, the estimated states can be merged or deleted by the merging/pruning process [54] as described in Alg.5. Consequentially, the states may be removed if the corresponding measurements are missed. Even if the lost measurements are recovered later, it requires several iterations to confirm the states. With these problems, if the GM-PHD filter is applied to track the surrounding vehicles, for example, it can result in serious false estimation especially when some measurements are missing. In addition, there could appear another problem which we call as the weight under/over-estimation problem. The weight under-estimation and over-estimation problem arises when there are missed detections and clutters, respectively, and may result in the improper weight update that causes inaccurate estimates. The weight under/over-estimation problem will be explained in detail in the next section.

Although the previous approaches have tried to overcome the problems related to the birth intensity generation [56][57] and target tractability [58]-[61], they have not provided an effective method to solve these problems simultaneously. Moreover,

they cannot provide an accurate result if there are many clutters (false positive detections) and lost detections (false negative detections) since they do not consider the weight under/over estimation problem. In real applications, however, because there could appear many false positive/negative detections when detecting multi-targets, the described problems should be resolved in order to increase the estimation accuracy.

In this chapter, we propose a robust multi-target tracking scheme based on the GM-PHD filter in order to overcome the aforementioned problems. The scheme can provide relatively accurate estimations even if there are numerous false positive/negative detections. The proposed robust GM-PHD filter consists of five steps, as shown in Fig.4.2: 1) Target prediction and PHD update component construction, 2) State and measurement evaluation, 3) PHD updating and merging, 4) Duplication check, and 5) Birth intensity generation for the next iteration.

We propose a method to evaluate the multiple states/measurements. In the proposed scheme, all states are tagged with the confirmation scores which are updated according to whether or not there are any measurements in the corresponding observation gates. The weights of the states are adaptively determined in different ways based on the updated confirmation score to solve the problems related to weight update. In addition, the measurements not associated with any tracked states are classified and utilized to generate the Gaussian birth intensity.

The states are tracked using the corresponding identities in the proposed robust GM-PHD filter. Accordingly, the states that have different identities do not merge with each other. As a result, the duplicated states may exist depending on the target estimation. For this problem, we also propose a method that finds and removes the duplicated states. In this chapter, we do not consider the cardinalized PHD filter that requires large computational overhead for estimating the cardinality because

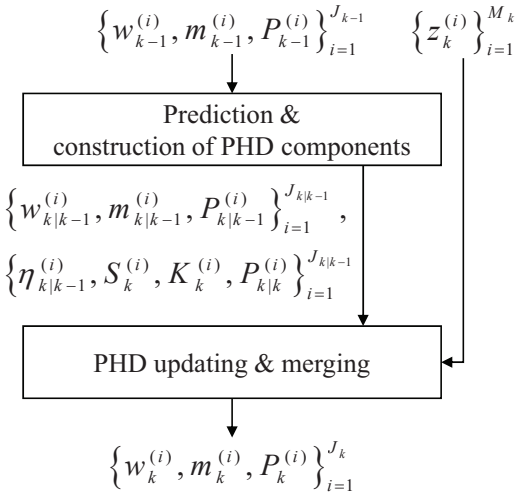

Figure 4.1: Overall procedure of the conventional GM-PHD filter [54].

the number of states are managed by the steps of target evaluation and duplication check, not estimated using the weight parameters.

The remainder of this chapter is organized as follows. Section II explains the GM-PHD filter and the problems shown when implementing the GM-PHD filter for the multi-target tracking. We describe the proposed multi-target tracking scheme based on the GM-PHD filter in Section III. Section IV examines the proposed approaches to nonlinear Gaussian models. Section V shows the simulation results for the proposed robust GM-PHD filter scheme and the other implementations based on the GM-PHD filter. The conclusion is given in Section VI.

4.2 Background and Motivation

4.2.1 Prediction of Future Driving Profile

As described in the abstract, the energy stored in the SC (Super-Capacitor) can be effectively adjusted if the future driving profile (speed/acceleration) can be predicted. Because the future speed/acceleration is strongly affected by the surround-

ing objects, especially vehicles, the chapter 4 focuses on the accurate estimation for multi-targets. In this section, we present how the reference voltage of the SC is calculated based on the surrounding vehicle information that can be estimated by the multi-target tracking scheme.

From the estimated states of surrounding vehicles, the future driving profile can be roughly predicted using the car following model [66]. In this section, we consider the Gazis-Herman-Rothery (GHR) model defined by

$$a_i(t) = cv_i^m(t)\frac{v_{i+1}(t-d\Delta) - v_i(t-d\Delta)}{(x_{i+1}(t-d\Delta) - x_i(t-d\Delta))^l}, \tag{4.1}$$

where $a_i(t)$, $v_i(t)$, and $x_i(t)$ are the acceleration, speed, and position of the i-th vehicle at time t. The $(i+1)$-th vehicle is a front vehicle of the i-th vehicle. The c, m, and l are the model parameters to be determined and d is the driver reaction time. Using (4.1), the future driving profile is obtained by

$$a_i(t+k\Delta) = cv_i^m(t+k\Delta)\frac{v_{i+1}(t+(k-d)\Delta) - v_i(t+(k-d)\Delta)}{(x_{i+1}(t+(k-d)\Delta) - x_i(t+(k-d)\Delta))^l}, \tag{4.2}$$

$$v_i(t+k\Delta) = v_i(t+(k-1)\Delta) + \Delta a_i(t+(k-1)\Delta), \tag{4.3}$$

$$x_i(t+k\Delta) = x_i(t+(k-1)\Delta) + \Delta v_i(t+(k-1)\Delta), \tag{4.4}$$

for $k = 1, \ldots, K$. Based on the predicted future acceleration/speed/position, the reference voltage of the SC in the HESS can be computed by the computing procedure described in Sec 3.3.1.

4.2.2 Brief Overview of The Conventional GM-PHD Filter

In this section, we introduce the GM-PHD filter [54]. The basic architecture of the GM-PHD filter is shown in Fig.4.1. The state transition and measurement are modelled by a linear Gaussian model, i.e.,

$$x_{k|k-1} = F_{k-1}x_{k-1} + \omega_{k-1}, \tag{4.5}$$

$$z_k = H_k x_{k|k-1} + \varepsilon_k, \tag{4.6}$$

where F_{k-1} is the state transition matrix, H_k is the observation matrix, ω_{k-1} is the process noise with covariance Q_{k-1}, and ε_k is the measurement noise with covariance R_k. In the GM-PHD filter, the state at time $k-1$ is presented with an density function as

$$\mathcal{N}\left(x; m_{k-1}^{(i)}, P_{k-1}^{(i)}\right), \text{ for } i = 1, \ldots, J_{k-1}, \tag{4.7}$$

where $\mathcal{N}(\cdot; m, P)$ denotes a Gaussian density with mean m and covariance P.

The multi-states at time $k-1$ can be presented with the Gaussian mixture as

$$v_{k-1}(x) = \sum_{i=1}^{J_{k-1}} w_{k-1}^{(i)} \mathcal{N}\left(x; m_{k-1}^{(i)}, P_{k-1}^{(i)}\right), \tag{4.8}$$

where $w_{k-1}^{(i)}$ is the weight parameter that adjusts the Gaussian density height. The mean $m_{k-1}^{(i)}$ can be considered as the i-th state estimation. All states can be described by the weight, mean, and covariance.

The prediction intensity for the existing targets and birth targets are calculated as

$$v_{k|k-1}(x) = \sum_{i=1}^{J_{k|k-1}} w_{k|k-1}^{(i)} \mathcal{N}\left(x; m_{k|k-1}^{(i)}, P_{k|k-1}^{(i)}\right), \tag{4.9}$$

where

$$\begin{aligned} w_{k|k-1}^{(i)} &= p_{S,k} w_{k-1}^{(i)}, \quad m_{k|k-1}^{(i)} = F_{k-1} m_{k-1}^{(i)}, \\ P_{k|k-1}^{(i)} &= Q_{k-1} + F_{k-1} P_{k-1}^{(i)} F_{k-1}^T, \end{aligned} \tag{4.10}$$

for $i = 1, \ldots, J_{k-1}$ (existing states) and

$$\begin{aligned} w_{k|k-1}^{(J_{k-1}+j)} &= w_{\gamma,k}^{(j)}, \quad m_{k|k-1}^{(J_{k-1}+j)} = m_{\gamma,k}^{(j)}, \\ P_{k|k-1}^{(J_{k-1}+j)} &= P_{\gamma,k}^{(j)}, \end{aligned} \tag{4.11}$$

for $j = 1, \ldots, J_{\gamma,k}$ (birth states). $w_{\gamma,k}^{(j)}$, $m_{\gamma,k}^{(j)}$, and $P_{\gamma,k}^{(j)}$ are given. The state survival probability $p_{S,k}$ is also given. The number of predictions is $J_{k|k-1} = J_{k-1} + J_{\gamma,k}$. In this chapter, we do not consider the prediction model related to spawned targets in [54].

Using the predicted state parameters $w_{k|k-1}^{(i)}$, $m_{k|k-1}^{(i)}$, and $P_{k|k-1}^{(i)}$, the PHD update components can be computed as

$$\begin{aligned}
&\eta_{k|k-1}^{(i)} = H_k m_{k|k-1}^{(i)}, \quad S_k^{(i)} = R_k + H_k P_{k|k-1}^{(i)} H_k^T, \\
&K_k^{(i)} = P_{k|k-1}^{(i)} H_k^T \left[S_k^{(i)}\right]^{-1}, \\
&P_{k|k}^{(i)} = \left[I - K_k^{(i)} H_k\right] P_{k|k-1}^{(i)}.
\end{aligned} \tag{4.12}$$

The posterior intensity at time k is also presented by the Gaussian mixture and updated using

$$\begin{aligned}
v_k(x) = &\left(1 - p_{D,k}\right) v_{k|k-1}(x) \\
&+ \sum_{z \in Z_k} \sum_{i=1}^{J_{k|k-1}} w_k^{(i)}(z) \mathcal{N}\left(x; m_k^{(i)}(z), P_k^{(i)}\right),
\end{aligned} \tag{4.13}$$

where

$$\begin{aligned}
w_k^{(i)}(z) &= \frac{p_{D,k} w_{k|k-1}^{(i)} \mathcal{N}\left(z; \eta_{k|k-1}^{(i)}, S_k^{(i)}\right)}{\kappa_k(z) + \sum_{l=1}^{J_{k|k-1}} p_{D,k} w_{k|k-1}^{(l)} \mathcal{N}\left(z; \eta_{k|k-1}^{(l)}, S_k^{(l)}\right)}, \\
m_k^{(i)}(z) &= m_{k|k-1}^{(i)} + K_k^{(i)}\left(z - \eta_{k|k-1}^{(i)}\right), \\
P_k^{(i)} &= P_{k|k}^{(i)}.
\end{aligned}$$

The detection probability $p_{D,k}$ is given. The recursive form of the PHD update part is shown in Alg.4. The number of Gaussian terms in $v_k(x)$ is $J_{k|k-1} + J_{k|k-1} M_k$, where M_k is the number of measurements. Because the number of Gaussian terms increases exponentially as the PHD filter is iteratively processed, the weak weight Gaussian terms are removed and some close ones being too close are merged through the pruning process. After pruning, the posterior intensity is

$$v_k(x) = \sum_{i=1}^{J_k} w_k^{(i)} \mathcal{N}\left(x; m_k^{(i)}, P_k^{(i)}\right), \tag{4.14}$$

which presents the multi-target state estimates by the GM-PHD filter. The recursive form for the GM-PHD filter is shown in [54].

Algorithm 4 Procedure of the PHD Component Update [54].

for $j = 1$ **to** $J_{k|k-1}$ **do**
  $\widetilde{w}_k^{(j)} = (1 - p_{D,k})\, w_{k|k-1}^{(j)}, \quad \widetilde{m}_k^{(j)} = m_{k|k-1}^{(j)}, \quad \widetilde{P}_k^{(j)} = P_{k|k-1}^{(j)}.$
end for
$l = 0$
for each $z \in Z_k$ **do**
  $l := l + 1.$
  for $j = 1$ **to** $J_{k|k-1}$ **do**
    $\widetilde{w}_k^{(lJ_{k|k-1}+j)} = p_{D,k} w_{k|k-1}^{(j)} \mathcal{N}\left(z; \eta_{k|k-1}^{(j)}, S_k^{(j)}\right),$
    $\widetilde{m}_k^{(lJ_{k|k-1}+j)} = m_{k|k-1}^{(j)} + K_k^{(j)}\left(z - \eta_{k|k-1}^{(j)}\right),$
    $\widetilde{P}_k^{(lJ_{k|k-1}+j)} = P_{k|k}^{(j)}.$
  end for
  $\text{WeightSum} = \sum_{i=1}^{J_{k|k-1}} \widetilde{w}_{k|k-1}^{(lJ_{k|k-1}+i)}.$
  for $j = 1$ **to** $J_{k|k-1}$ **do**
    $\widetilde{w}_k^{(lJ_{k|k-1}+j)} := \widetilde{w}_k^{(lJ_{k|k-1}+j)} / (\kappa_k + \text{WeightSum})$
  end for
end for
$\widetilde{J}_k = J_{k|k-1} + lJ_{k|k-1}.$
output $\left\{\widetilde{w}_k^{(i)}, \widetilde{m}_k^{(i)}, \widetilde{P}_k^{(i)}\right\}_{i=1}^{\widetilde{J}_k}.$

4.2.3 Problems of the GM-PHD Filter

There are several problems of the GM-PHD Filter that may lead to inaccurate estimation results. In the following subsections, we present the problems of the GM-PHD filter. The first and second problems, which are related to the birth intensity generation and target tractability, have been investigated by the previous researches, and the weight under/over-estimation problem are newly discovered in this chapter. These problems can lead to inaccurate estimation results when there are many lost detections or clutters.

Birth Intensity Generation

In the original GM-PHD filter, the birth targets are assumed to appear over small specific areas defined with the mean and covariance known a priori [52]-[55]. However, this assumption is not suitable for general cases, because the birth targets may appear in a region that is not covered in the predefined birth intensity. It results in

Algorithm 5 Procedure of Pruning for the Gaussian Mixture PHD Filter [54].

given

$\Omega_{k-1} = \left\{w_k^{(i)}, m_k^{(i)}, P_k^{(i)}\right\}_{i=1}^{J_k}$, a truncation threshold T, and a merging threshold U. Set $l = 0$, and $I = \left\{i = 1, \ldots, J_k | w_k^{(i)} > T\right\}$.

repeat

$l := l + 1$.

$j := \arg\max_{i \in I} w_k^{(i)}$.

$L := \left\{i \in I | \left(m_k^{(i)} - m_k^{(j)}\right)^T \left(P_k^{(i)}\right)^{-1} \left(m_k^{(i)} - m_k^{(j)}\right) \leq U\right\}$.

$\tilde{w}_k^{(l)} = \sum_{i \in L} w_k^{(i)}$.

$\tilde{m}_k^{(l)} = \frac{1}{\tilde{w}_k^{(l)}} \sum_{i \in L} w_k^{(i)} m_k^{(i)}$.

$\tilde{P}_k^{(l)} = \frac{1}{\tilde{w}_k^{(l)}} \sum_{i \in L} w_k^{(i)} \left(P_k^{(i)} + \left(\tilde{m}_k^{(l)} - m_k^{(i)}\right)\left(\tilde{m}_k^{(l)} - m_k^{(i)}\right)^T\right)$.

$I := I \backslash L$.

until $I = \emptyset$

a higher incidence of short-lived false tracks to generate the birth intensities with a random position [56].

To overcome the problems introduced by predefined birth intensity, the birth intensity can be generated based on the measurements from newborn targets [56][57].

Target Tractability

In the GM-PHD filter, the weight parameters are updated as described in Alg.4. Since the GM-PHD filter does not provide identities for targets, it is difficult to construct the tracks for individual targets [58]-[61].

To solve this problem, The PHD with the Multiple-Hypothesis Tracking (MHT) method has been proposed [58]. However, it requires large computational overhead due to the following reasons: 1) a prediction process exists in both PHD and MHT, and 2) solving a track-measurement association problem is a complex multidimensional assignment problem that is NP hard [60].

In order to construct the tracks for individual targets without the MHT algorithm, Lin *et al.* [60] proposed attaching labels to the states. For example, the

n-th track label at time $k-1$ can be denoted by a state estimate and its covariance (i.e., $\mathcal{T}_{k-1}^{n} = \left\{\widehat{x}_{k-1}^{n}, P_{k-1}^{n}\right\}$). In addition, they proposed associating the tracks with the state estimations; not measurements. Once the tracks are associated with the state estimations at time k, the position at the next time $k+1$ can be predicted. If the measurements at time $k+1$ are within the validation gates for any tracks, more particles with a relatively large weight are generated around the measurements. Otherwise, the particles are still generated around the measurements, but the number of particles does not have to be large.

Panta *et al* [61] proposed the tag-based GM-PHD filter scheme. In the tag-based PHD filter, the state estimates can be tracked by using individual tags. For example, the states at time $k-1$ and at time k can be considered as a same target if they have the same tag. The $J_{k|k-1}(1+M_k)$ states computed by Alg.4 can be classified into $J_{k|k-1}$ groups using the tags (identities). For each group, the state with the largest weight is picked as a representative state.

Weight Under-estimation

When the tracked states are not associated with any measurements, the state weights become small, specially if there is no clutter measurement. For example, let's assume that the prediction weights are $w_{k|k-1}^{(i)} = 1$ where $i = 1, 2, 3$. From the predictions, the updated weights are calculated by Alg.4 as

$$\widetilde{w}_{k}^{(i)} = \frac{p_{D,k} w_{k|k-1}^{(i)} \mathcal{N}\left(z;\cdot\right)}{\sum_{j=1}^{3} p_{D,k} w_{k|k-1}^{(j)} \mathcal{N}\left(z;\cdot\right)}, \tag{4.15}$$

where $\mathcal{N}\left(z;\cdot\right) = 0.2$ if the measurement z is associated with the i-th state prediction, and $\mathcal{N}\left(z;\cdot\right) = 0.001$ otherwise. The detection probability $P_{D,k} = 0.9$. If the measurements $z_{k}^{(i)}$ where $i = 1, 2, 3$ are detected and they are associated with the

corresponding predictions, the weights are calculated using (4.15) as

$$\begin{aligned}\widetilde{w}_k^{(1)} &= \tfrac{1\times 0.2}{1\times 0.2+1\times 0.001+1\times 0.001} = 0.99,\\ \widetilde{w}_k^{(2)} &= \tfrac{1\times 0.001}{1\times 0.2+1\times 0.001+1\times 0.001} = 0.005,\\ \widetilde{w}_k^{(3)} &= \tfrac{1\times 0.001}{1\times 0.2+1\times 0.001+1\times 0.001} = 0.005,\end{aligned}$$

for $z_k^{(1)}$. In the same manner, the other weights can be updated as

$$\widetilde{w}_k^{(4)} = 0.005, \widetilde{w}_k^{(5)} = 0.99, \widetilde{w}_k^{(6)} = 0.005,$$

for $z_k^{(2)}$ and

$$\widetilde{w}_k^{(7)} = 0.005, \widetilde{w}_k^{(8)} = 0.005, \widetilde{w}_k^{(9)} = 0.99,$$

for $z_k^{(3)}$. As a result, the weights of the posterior intensities are obtained through the merging process as

$$\begin{aligned}w_k^{(1)} &= (1-P_{D,k})w_{k|k-1}^{(1)} + \widetilde{w}_k^{(1)} + \widetilde{w}_k^{(4)} + \widetilde{w}_k^{(7)} = 1.1,\\ w_k^{(2)} &= (1-P_{D,k})w_{k|k-1}^{(2)} + \widetilde{w}_k^{(2)} + \widetilde{w}_k^{(5)} + \widetilde{w}_k^{(8)} = 1.1,\\ w_k^{(3)} &= (1-P_{D,k})w_{k|k-1}^{(3)} + \widetilde{w}_k^{(3)} + \widetilde{w}_k^{(6)} + \widetilde{w}_k^{(9)} = 1.1.\end{aligned}$$

This means that the weights are updated properly if the state predictions do not lose their detections.

On the other hand, if the $z_k^{(1)}$ and $z_k^{(2)}$ are detected and associated with the corresponding predictions, while $z_k^{(3)}$ is missed, the weights are updated using (4.15) as

$$\widetilde{w}_k^{(1)} = 0.99, \widetilde{w}_k^{(2)} = 0.005, \widetilde{w}_k^{(3)} = 0.005,$$

for $z_k^{(1)}$ and

$$\widetilde{w}_k^{(4)} = 0.005, \widetilde{w}_k^{(5)} = 0.99, \widetilde{w}_k^{(6)} = 0.005,$$

for $z_k^{(2)}$. The weights of the posterior intensities are obtained through the merging process as

$$\begin{aligned}w_k^{(1)} &= (1-P_{D,k})w_{k|k-1}^{(1)} + \widetilde{w}_k^{(1)} + \widetilde{w}_k^{(4)} = 1.095,\\ w_k^{(2)} &= (1-P_{D,k})w_{k|k-1}^{(1)} + \widetilde{w}_k^{(2)} + \widetilde{w}_k^{(5)} = 1.095,\\ w_k^{(3)} &= (1-P_{D,k})w_{k|k-1}^{(1)} + \widetilde{w}_k^{(3)} + \widetilde{w}_k^{(6)} = 0.11.\end{aligned}$$

Due to the small weight $w_k^{(3)}$, the corresponding state is deleted by the pruning process if $w_k^{(3)}$ is smaller than the threshold w_{th}. To prevent the states missing detections (but being still alive) from being deleted, Panta *et al* [61] proposed deleting the states if the corresponding weights $w_k^{\cdot} < w_{\text{th}}$ consecutively. However, the tiny weights cannot easily be restored to normal even if the states are associated with some measurements, because the weights are propagated from time $k-1$ to k. In other words, if the propagated weight $w_{k|k-1}^{(\cdot)}$ is too small, it is difficult for $w_k^{(\cdot)}$ to be large even though the Gaussian term $\mathcal{N}(z;\cdot)$ is large. Moreover, the estimation accuracy degrades due to the small weight. For example, if the third state obtains its measurement after missing measurements consecutively ($w_{k|k-1}^{(1,2)} = 1$ and $w_{k|k-1}^{(3)} = 10^{-6}$), the weight are updated as

$$\begin{aligned} \widetilde{w}_k^{(1)} &= 0.995, \widetilde{w}_k^{(2)} = 0.0049, \widetilde{w}_k^{(3)} = 4.9 \times 10^{-9}, \\ \widetilde{w}_k^{(4)} &= 0.0049, \widetilde{w}_k^{(5)} = 0.995, \widetilde{w}_k^{(6)} = 4.9 \times 10^{-9}, \end{aligned}$$

for $z_k^{(1)}$, $z_k^{(2)}$, and

$$\begin{aligned} \widetilde{w}_k^{(7)} &= \tfrac{1\times 0.001}{1\times 0.001+1\times 0.001+10^{-6}\times 0.2} = 0.49995, \\ \widetilde{w}_k^{(8)} &= \tfrac{1\times 0.001}{1\times 0.001+1\times 0.001+10^{-6}\times 0.2} = 0.49995, \\ \widetilde{w}_k^{(9)} &= \tfrac{10^{-6}\times 0.2}{1\times 0.001+1\times 0.001+10^{-6}\times 0.2} = 0.0001, \end{aligned}$$

for $z_k^{(3)}$. From the updated weights, the first estimate is computed through the merging process as

$$\begin{aligned} m_k^{(1)} &= \frac{(1-p_{D,k}) w_{k|k-1}^{(1)} m_{k|k-1}^{(1)} + \sum_{i=1,4,7} \tilde{w}_k^{(i)} \tilde{m}_k^{(i)}}{(1-p_{D,k}) w_{k|k-1}^{(1)} + \sum_{i=1,4,7} \tilde{w}_k^{(i)}} \\ &= \frac{0.1 m_{k|k-1}^{(1)} + 0.995 \tilde{m}_k^{(1)} + 0.0049 \tilde{m}_k^{(4)} + 0.4999 \tilde{m}_k^{(7)}}{0.1 + 0.995 + 0.0049 + 0.4999} \\ &= 0.062 m_{k|k-1}^{(1)} + 0.622 \tilde{m}_k^{(1)} + 0.003 \tilde{m}_k^{(4)} + 0.312 \tilde{m}_k^{(7)}. \end{aligned}$$

Since the weight $\widetilde{w}_k^{(7)}$ is too large, the estimate of the first target is significantly affected by the measurement $z_k^{(3)}$ although the first state is not associated with $z_k^{(3)}$.

(The mean $\widetilde{m}_k^{(1)}$, $\widetilde{m}_k^{(4)}$, and $\widetilde{m}_k^{(7)}$ are computed using the measurement $z_k^{(1)}$, $z_k^{(2)}$, and $z_k^{(3)}$ respectively as shown in Alg.4). In the same manner, the estimate of the second target is also affected by the measurement $z_k^{(3)}$. It means that the inaccurate estimates may exist due to the weights decreased by the missed detections. In the merging process, the weights of the posterior intensities are computed as

$$
\begin{aligned}
w_k^{(1)} &= (1 - P_{D,k}) w_{k|k-1}^{(1)} + \widetilde{w}_k^{(1)} + \widetilde{w}_k^{(4)} + \widetilde{w}_k^{(7)} = 1.4998, \\
w_k^{(2)} &= (1 - P_{D,k}) w_{k|k-1}^{(2)} + \widetilde{w}_k^{(2)} + \widetilde{w}_k^{(5)} + \widetilde{w}_k^{(8)} = 1.4998, \\
w_k^{(3)} &= (1 - P_{D,k}) w_{k|k-1}^{(3)} + \widetilde{w}_k^{(3)} + \widetilde{w}_k^{(6)} + \widetilde{w}_k^{(9)} = 0.0003.
\end{aligned}
$$

This result means that the tiny weights cannot easily be restored to normal even though the states are associated with some measurements.

Weight Over-estimation

The weights $\widetilde{w}_k^{(\cdot)}$ become too large if they are updated using the measurements not associated with any states. For example, let's assume that there are the state predictions with $w_{k|k-1}^{(i)} = 1$ where $i = 1, 2, 3$ and the measurements $z_k^{(j)}$ where $j = 1, 2, 3, 4$. The $z_k^{(1,2,3)}$ are associated with the corresponding states and $z_k^{(4)}$ is the clutter not associated with the states. The weights are updated by (4.15) where $\mathcal{N}(z; \cdot) = 0.2$ if the measurement z is associated with the i-th state prediction, and $\mathcal{N}(z; \cdot) = 0.001$ otherwise. The detection probability $P_{D,k} = 0.9$. Using the measurements $z_k^{(j)}$, the weights are computed by

$$
\begin{aligned}
&\widetilde{w}_k^{(1)} = 0.99, \widetilde{w}_k^{(2)} = 0.005, \widetilde{w}_k^{(3)} = 0.005, \\
&\widetilde{w}_k^{(4)} = 0.005, \widetilde{w}_k^{(5)} = 0.99, \widetilde{w}_k^{(6)} = 0.005, \\
&\widetilde{w}_k^{(7)} = 0.005, \widetilde{w}_k^{(8)} = 0.005, \widetilde{w}_k^{(9)} = 0.99,
\end{aligned}
$$

for the $z_k^{(1,2,3)}$ associated with the states, and

$$
\begin{aligned}
\widetilde{w}_k^{(10)} &= \tfrac{1 \times 0.001}{1 \times 0.001 + 1 \times 0.001 + 1 \times 0.001} = 0.333, \\
\widetilde{w}_k^{(11)} &= \tfrac{1 \times 0.001}{1 \times 0.001 + 1 \times 0.001 + 1 \times 0.001} = 0.333, \\
\widetilde{w}_k^{(12)} &= \tfrac{1 \times 0.001}{1 \times 0.001 + 1 \times 0.001 + 1 \times 0.001} = 0.333,
\end{aligned}
$$

for the $z_k^{(4)}$ not associated with any states. In the merging process, the first estimate is computed by

$$\begin{aligned} m_k^{(1)} &= \frac{(1-p_{D,k})w_{k|k-1}^{(1)} m_{k|k-1}^{(1)} + \sum_{i=1,4,7,10} \tilde{w}_k^{(i)} \tilde{m}_k^{(i)}}{(1-p_{D,k})w_{k|k-1}^{(1)} + \sum_{i=1,4,7,10} \tilde{w}_k^{(i)}} \\ &\approx \frac{0.1 m_{k|k-1}^{(1)} + 0.99\tilde{m}_k^{(1)} + 0.333\tilde{m}_k^{(10)}}{0.1 + 0.99 + 0.005 + 0.005 + 0.333} \\ &\approx 0.07 m_{k|k-1}^{(1)} + 0.69\tilde{m}_k^{(1)} + 0.23\tilde{m}_k^{(10)}. \end{aligned}$$

Since the weight $\widetilde{w}_k^{(10)}$ is too large, the estimate of the first target is significantly affected by the measurement $z_k^{(4)}$ although the first state is not associated with $z_k^{(4)}$. (The mean $\widetilde{m}_k^{(10)}$ is computed using the measurement $z_k^{(4)}$ as shown in Alg.4). In the same manner, the second/third estimates are also affected by the measurements $z_k^{(4)}$ which is a clutter.

Because the $p_{D,k} w_{k|k-1}^{(i)} \mathcal{N}(z;\cdot)$ term in (4.15), which causes the weight under/over estimation, is included in the GM-CPHD filter [55], these problems can occur when implementing the GM-CPHD.

4.3 The Proposed Robust GM-PHD Filter

As explained in the previous section, the estimated states at time k can be presented by $w_k^{(i)}$, $m_k^{(i)}$, and $P_k^{(i)}$. In the proposed robust GM-PHD filter, the following additional parameters are used to manage the states: 1) the track label identities $\mathrm{Id}_k^{(i)}$, 2) the confirmation scores $\mu_k^{(i)}$, which indicate whether the corresponding states are confirmed or not, 3) the duplication time $\rho_k^{(i)}$, and 4) the survival time $\tau_k^{(i)}$. In other words, the targets at time k can be presented by the state parameters,

$$\Omega_k = \left\{ w_k^{(i)}, m_k^{(i)}, P_k^{(i)}, \mathrm{Id}_k^{(i)}, \mu_k^{(i)}, \rho_k^{(i)}, \tau_k^{(i)} \right\}_{i=1}^{J_k}, \tag{4.16}$$

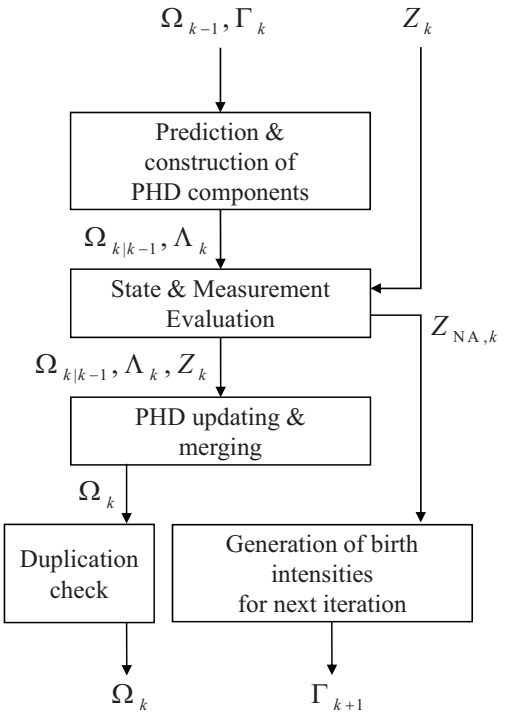

Figure 4.2: Overall procedure of the proposed robust GM-PHD filter. The steps marked with * are newly proposed in this chapter.

where Ω_k is a set of state parameters at time k. The additional parameters $\mu_k^{(i)}$, $\rho_k^{(i)}$, and $\tau_k^{(i)}$, will be explained in the following subsections.

The estimated states are categorized into three states:

- Unconfirmed states: The birth states are evaluated for several iterations in order to confirm if they are from true targets or clutters. We call these states the unconfirmed states with the confirmation score $\mu_k^{(i)} > 0$.
- Confirmed states: The states from the true targets are confirmed states with confirmation score $\mu_k^{(i)} = 0$.
- Lost states: The states missing detections should not be removed before confirming if the corresponding targets exist or not. We call these states the lost states with the confirmation score $\mu_k^{(i)} < 0$.

The posterior intensity $v_k(x)$ is updated through the five steps as described in Fig.4.2. The pseudo code of the overall procedure of the proposed robust GM-PHD filter is shown in Alg.6. The characteristics of the five steps will be explained in the following subsections.

4.3.1 Target Prediction and PHD Update Component Construction

The state parameters of the predictions are

$$\Omega_{k|k-1} = \left\{ w_{k|k-1}^{(i)}, m_{k|k-1}^{(i)}, P_{k|k-1}^{(i)} , \right. \\ \left. \mathrm{Id}_{k|k-1}^{(i)}, \mu_{k|k-1}^{(i)}, \rho_{k|k-1}^{(i)}, \tau_{k|k-1}^{(i)} \right\}_{i=1}^{J_{k|k-1}} . \tag{4.17}$$

In the first step, the parameters in $\Omega_{k|k-1}$ are determined. The w, m, and P of the predictions are computed by (4.10) and (4.11) using the existing target state parameters Ω_{k-1} and birth state parameters for

$$\Gamma_k = \left\{ w_{\gamma,k}^{(i)}, m_{\gamma,k}^{(i)}, P_{\gamma,k}^{(i)}, \mathrm{Id}_{\gamma,k}^{(i)} \right\}_{i=1}^{J_{\gamma,k}} . \tag{4.18}$$

The parameter set Γ_k is previously determined at time $k-1$. The identity Id, confirmation score μ, duplication time ρ, and survival time τ for predictions are determined by

$$\begin{aligned} \mathrm{Id}_{k|k-1}^{(i)} &= \mathrm{Id}_{k-1}^{(i)}, & \mu_{k|k-1}^{(i)} &= \mu_{k-1}^{(i)}, \\ \rho_{k|k-1}^{(i)} &= \rho_{k-1}^{(i)}, & \tau_{k|k-1}^{(i)} &= \tau_{k-1}^{(i)} + 1, \end{aligned}$$

where $i = 1, \ldots, J_{k-1}$ (existing states), and

$$\begin{aligned} \mathrm{Id}_{k|k-1}^{(J_{k|k-1}+j)} &= \mathrm{Id}_{k-1}^{(j)}, & \mu_{k|k-1}^{(J_{k|k-1}+j)} &= \mu_{\max}, \\ \rho_{k|k-1}^{(J_{k|k-1}+j)} &= 0, & \tau_{k|k-1}^{(J_{k|k-1}+j)} &= 1, \end{aligned}$$

where $j = 1, \ldots, J_{\gamma,k}$ (birth states). The survival time τ of the existing target states are increased as $\tau_{k|k-1}^{(i)} = \tau_{k-1}^{(i)} + 1$ and the τ of birth target states are set to one. The reason of $\mu_{k|k-1}^{(\cdot)} = \mu_{\max}$ for birth targets will be explained in the subsection of the state/measurement evaluation. From the predicted m and P in (4.17), the PHD update components are

$$\Lambda_k = \left\{ \eta_{k|k-1}^{(i)}, S_k^{(i)}, K_k^{(i)}, P_{k|k}^{(i)} \right\}_{i=1}^{J_{k|k-1}}, \tag{4.19}$$

and computed by (4.12).

The pseudo code of the algorithm described in this subsection is shown in Alg.7.

4.3.2 State and Measurement Evaluation

For the measurement evaluation, the measurements $z_k^{(j)}$, where $j = 1, \ldots, M_k$, are checked to determine if they are in the observation gates of the predicted estimations $\eta_{k|k-1}^{(i)}$, where $i = 1, \ldots, J_{k|k-1}$.

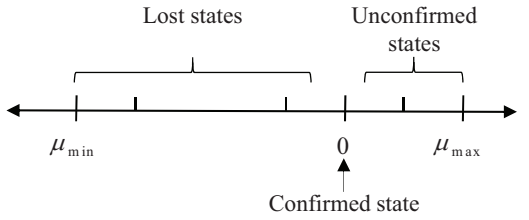

Figure 4.3: The confirmation score system μ. According to the confirmation score, the corresponding states are categorized into the following states: unconfirmed, confirmed, and lost states.

The evaluation matrix denoted by $A = \{a_{ij}\}$ is determined by

$$a_{ij} = \begin{cases} 1, & \text{if } z_k^{(j)} \text{ is in the validation gate of } \eta_{k|k-1}^{(i)}, \\ 0, & \text{otherwise.} \end{cases}$$

In other words, $a_{ij} = 1$ if

$$(\eta_{k|k-1}^{(i)} - z_k^{(j)})^T [S_k^{(i)}]^{-1} (\eta_{k|k-1}^{(i)} - z_k^{(j)}) \leq G_{\text{th}},$$

and $a_{ij} = 0$, otherwise. The measurements which are not in any observation gate of $\eta_{k|k-1}^{(i)}$ are classified as non-associated measurements. In other words, the measurement $z_k^{(j)}$ satisfying $\sum_{i=1}^{J_{k|k-1}} a_{ij} = 0$ is moved from the measurement set Z_k to the non-associated measurement set $Z_{\text{NA,k}}$. As a result, the components in Z_k can be considered as the measurements associated with some tracked targets. Through categorizing the measurements into Z_k and $Z_{\text{NA},k}$, the weight over-estimation problem explained in Section II can be overcome because the measurements not associated with any states are not used for updating the PHD weights. The pseudo code of the measurement evaluation is presented in Alg.8.

As described in Fig.4.3, the states are categorized into confirmed states ($\mu = 0$), the unconfirmed states ($\mu > 0$), and the lost states ($\mu < 0$). Using the evaluation matrix $A = \{a_{ij}\}$ that is already determined when evaluating the measurements,

the confirmation scores $\mu_{k|k-1}^{(i)}$ are updated by

$$\mu_{k|k-1}^{(i)} := \begin{cases} 0, & \text{if } \sum_{j=1}^{M_k} a_{ij} > 0, \mu_{k|k-1}^{(i)} \leq 0, \\ \mu_{k|k-1}^{(i)} - 1, & \text{if } \sum_{j=1}^{M_k} a_{ij} = 0, \mu_{k|k-1}^{(i)} \leq 0, \\ \mu_{k|k-1}^{(i)} - 1, & \text{if } \sum_{j=1}^{M_k} a_{ij} > 0, \mu_{k|k-1}^{(i)} > 0, \\ \mu_{\max} + 1, & \text{if } \sum_{j=1}^{M_k} a_{ij} = 0, \mu_{k|k-1}^{(i)} > 0, \end{cases} \tag{4.20}$$

where $i = 1, \ldots, J_k$. The inequality $\sum_{j=1}^{M_k} a_{ij} > 0$ means that the i-th state is associated with some measurements. The first case of (4.20) means that the lost states and confirmed states become the confirmed states if the states are associated with some measurements. Otherwise, they become the lost states with decreased confirmation scores. The third case of (4.20) means that the unconfirmed states approach the confirmed states if the states are associated with some measurements. Otherwise, their confirmation scores become larger than the maximum confirmation score $\mu_{\max}$. After updating the confirmation scores, the state parameters with $\mu_k^{(i)} < \mu_{\min}$ or $\mu_k^{(i)} > \mu_{\max}$ are removed from $\Omega_{k|k-1}$.

If the unconfirmed and lost states become the confirmed states, their weights are updated by

$$w_{k|k-1}^{(i)} := w_{\text{confirm}}, \tag{4.21}$$

where w_{confirm} is an average weight of the confirmed states at time $k-1$ to overcome the weight under-estimation problem described in Section II. Because the weights decreased by the consecutive missed detection cannot be easily restored to normal in the step of PHD updating, the update of (4.21) is essential.

The absolute value of the minimum confirmation score $|\mu_{\min}|$ is the maximum number of consecutively missed detections. The probability that one state loses its measurement consecutively should be much smaller such as

$$(1 - p_{D,k})^{|\mu_{\min}|} < \varepsilon, \tag{4.22}$$

where $P_{D,k}$ is the detection probability and ε is an extremely small value. From (4.22), the minimum confirmation score can be obtained by

$$\mu_{\min} = -\max\left(\left\lfloor \frac{\varepsilon}{1-p_{D,k}} \right\rfloor, n_{\text{missed}}\right), \tag{4.23}$$

where $\lfloor x \rfloor$ is the maximum integer smaller than x and n_{missed} is the minimum waiting time before lost state deletion. In the simulation, $n_{\text{missed}} = 4$.

The absolute value of the maximum confirmation score $|\mu_{\max}|$ is the time required to confirm the birth states. The probability that one clutter is consecutively considered as a correct measurement should be much smaller such as

$$(p_{C,k})^{|\mu_{\max}|} < \varepsilon, \tag{4.24}$$

where $p_{C,k}$ is the probability that a clutter is classified incorrectly as correct. From (4.24), the maximum confirmation score can be determined as

$$\mu_{\max} = \max\left(\left\lfloor \frac{\varepsilon}{p_{C,k}} \right\rfloor, n_{\text{unconfirmed}}\right) \tag{4.25}$$

where $n_{\text{unconfirmed}}$ is the minimum time required to confirm birth states. In the simulation, $n_{\text{unconfirmed}} = 2$. The pseudo code of the state evaluation is shown in Alg.9.

4.3.3 PHD Updating and Merging

The posterior intensity $v_k(x)$ is computed by (4.13). The state parameters shown in (4.16) that represent $v_k(x)$ can be calculated in the PHD updating process. The weights and means that are updated, but not merged, are denoted as $\widetilde{w}_k^{(i)}$ and $\widetilde{m}_k^{(i)}$. The $\widetilde{w}_k^{(i)}$ and $\widetilde{m}_k^{(i)}$ are updated from the predicted parameters $\Omega_{k|k-1}$ and the PHD update components Λ_k as described in Alg.10. The Gaussian terms represented by the $\widetilde{w}_k^{(i)}$ and $\widetilde{m}_k^{(i)}$ are shown in Fig.4.4.

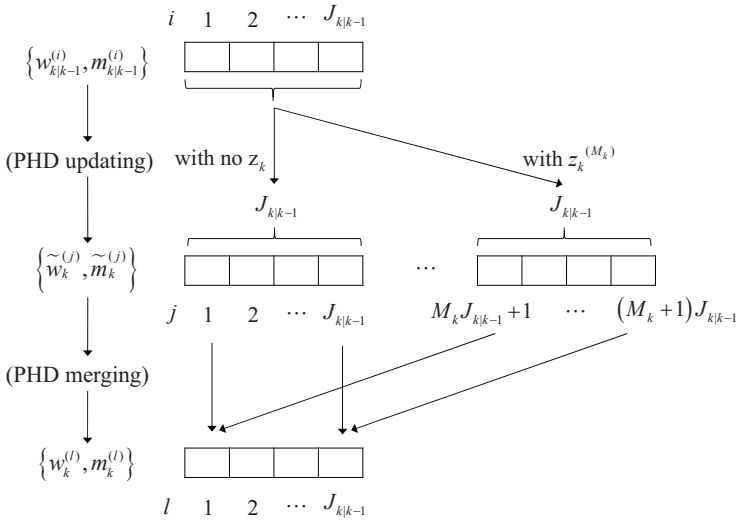

Figure 4.4: The PHD updating and merging process. Each cell means the Gaussian term represented by w and m. In the merging process, the Gaussian terms originating from the same target are merged into a single Gaussian term.

Because the number of state parameters increases exponentially as the PHD filter is iteratively processed, the PHD should be merged effectively. Therefore, the updated state parameters $\widetilde{w}_k$ and $\widetilde{m}_k$ generated from the same target are merged into a single state parameter using

$$w_k^{(i)} = \sum_{j=1}^{J_{k|k-1}} \widetilde{w}_k^{(lJ_{k|k-1}+j)},$$
$$m_k^{(i)} = \frac{1}{w_k^{(i)}} \sum_{j=1}^{J_{k|k-1}} \widetilde{w}_k^{(lJ_{k|k-1}+j)} \widetilde{m}_k^{(lJ_{k|k-1}+j)},$$

where $i = 1, \ldots, J_{k|k-1}$ and $l = 0, \ldots, M_k$. Fig.4.4 shows how to merge the $\widetilde{w}_k^{(j)}$, $\widetilde{m}_k^{(j)}$ into $w_k^{(l)}$, $m_k^{(l)}$, where $j = 1, \ldots, J_{k|k-1} + M_k J_{k|k-1}$ and $l = 1, \ldots, J_{k|k-1}$. The covariances $P_k^{(i)}$ is equal to $P_{k|k-1}^{(i)}$, where $i = 1, \ldots, J_{k|k-1}$. To overcome the underestimation problem and improve the estimation accuracy, the w, m, and P of the lost states ($\mu < 0$) are determined by

$$w_k^{(i)} = w_{k|k-1}^{(i)}, \quad m_k^{(i)} = m_{k|k-1}^{(i)}, \quad P_k^{(i)} = P_{k|k-1}^{(i)},$$

where $i = 1, \ldots, J_{k|k-1}$.

The identities $\mathrm{Id}_k^{(i)}$, confirmation scores $\mu_k^{(i)}$, duplication times $\rho_k^{(i)}$, and survival times $\tau_k^{(i)}$ are equal to the $\mathrm{Id}_{k|k-1}^{(i)}$, $\mu_{k|k-1}^{(i)}$, $\rho_{k|k-1}^{(i)}$, and $\tau_{k|k-1}^{(i)}$ where $i = 1, \ldots, J_{k|k-1}$. Note that $J_k = J_{k|k-1}$ because the disappeared or duplicated states are not be removed in the PHD updating and merging process. Finally, the targets at time k can be presented using the Gaussian mixture with state parameters (4.16). The pseudo code of the algorithm explained in this subsection is shown in Alg.10.

4.3.4 Duplication Check

The duplication times $\rho_k^{(i)}$ are updated in this step. If some states are too close to the i-th state, the $\rho_k^{(i)}$ increases and the $\rho_k^{(i)}$ decreases otherwise. After updating the duplication times, the states with $\rho_k^{(i)} > \rho_{\max}$ are removed except for the representing state that is the oldest state with the maximum survival time τ among the duplicated states. Because the states with different IDs are not merged in the PHD merging process, the duplicated states should be checked and deleted by the duplication check process. The pseudo code of the algorithm described in this subsection is shown in Alg.11.

4.3.5 Birth Intensity Generation for the Next Iteration

In this process, the birth intensities at time $k+1$ are generated by using the measurements $\in Z_{\mathrm{NA},k}$ not associated with any predictions at time k. The measurements $\in Z_{\mathrm{NA},k}$ are determined in the measurement evaluation. The w and P of the birth intensities are determined by $w_{\gamma,k+1}^{(i)} = w_b$ and $P_{\gamma,k+1}^{(i)} = P_b$, respectively. The m of the birth intensities are determined by

$$m_{\gamma,k+1}^{(i)} = \begin{bmatrix} z_{\mathrm{NA},k}^{(i)} \\ \mathcal{O} \end{bmatrix}, \text{ for } i = 1, \ldots, M_{\mathrm{NA},k}, \tag{4.26}$$

where $z_{\mathrm{NA},k}^{(i)} \in Z_{\mathrm{NA},k}$ and $\mathcal{O}$ is a zero vector. For example, if the position and velocity are estimated and the position is measured from sensors, the $m_{\gamma,k+1}$ consists of the measured position in $Z_{\mathrm{NA},k}$ and zero velocity. When the observation matrix H_k is invertible, $m_{\gamma,k+1}^{(i)}$ is equal to $H_k^{-1} z_{\mathrm{NA},k}^{(i)}$.

The $\mathrm{Id}_{\gamma,\mathrm{k+1}}^{(\mathrm{i})}$ is determined by choosing an identity from a set of the unused identities $\mathrm{ID}_{\mathrm{unused}}$. If the $\mathrm{ID}_{\mathrm{unused}}$ is empty, then the unused identities at time k are collected.

The other parameters, μ, ρ, and τ, used to manage the birth states are simply initialized at the next iteration as described in the step of the target prediction. The pseudo code of the algorithm explained in this subsection is shown in Alg.12.

4.4 Nonlinear Gaussian Model Extension

As the original GM-PHD can be extended to nonlinear target models [54], the proposed scheme can also be extended to the nonlinear Gaussian model as

$$x_{k|k-1} = f\left(x_{k-1}, \omega_{k-1}\right), \tag{4.27}$$

$$z_k = h\left(x_{k|k-1}, \varepsilon_k\right), \tag{4.28}$$

where f and h are known nonlinear functions. ω_{k-1} and ε_k are zero-mean Gaussian process noise and measurement noise with covariance Q_{k-1} and R_k, respectively. In order to compute the state parameters of the predictions $w_{k|k-1}^{(i)}$, $m_{k|k-1}^{(i)}$, and $P_{k|k-1}^{(i)}$, and to construct the PHD update components $\eta_{k|k-1}^{(i)}$, $S_k^{(i)}$, $K_k^{(i)}$, and $P_{k|k}^{(i)}$, the extended Kalman (EK) filter and the unscented Kalman (UK) filter can be utilized. The EK-PHD and UK-PHD are described in [54]. Using the computed state predictions and PHD update components, the robust GM-PHD filter scheme can be applied.

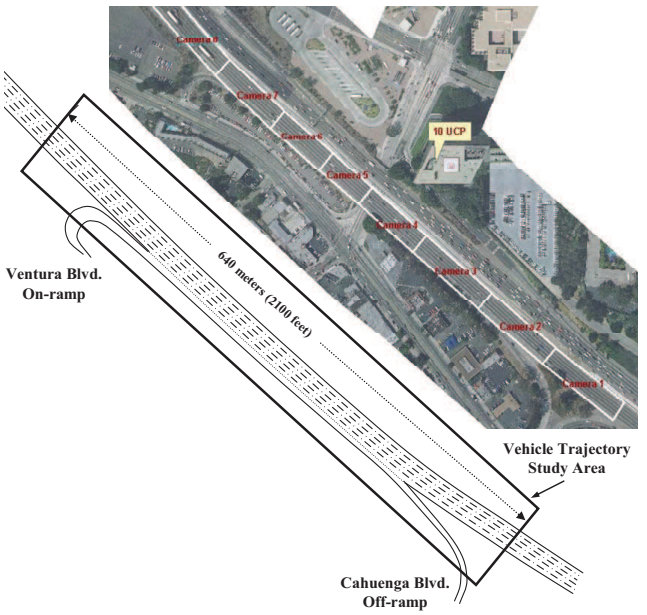

Figure 4.5: NGSIM dataset coverage: US-101 highway [65].

4.5 Simulation Results

We used the NGSIM dataset for simulation [65], which contains multiple vehicle trajectory data, e.g., vehicle ID, frame ID, vehicle position, vehicle size, vehicle class, and lane identification, needed for behavioral algorithm research. The traffic data used in the simulation was collected on a segment of the US 101 freeway (Hollywood Freeway) located in Los Angeles, California, as described in Fig.4.5 [65]. The data were collected between 8:05 a.m. and 8:20 a.m. on June 15th, 2005. The raw data for NGSIM dataset were recorded using the surveillance camera mounted on the top of buildings. The data related only to the vehicle position are used as the reference. For illustrative purposes, we consider the vehicle trajectory data for the frame ID as those between 201 and 400. We generate the measurement data through

$$z_k^{(j)} = x_{\mathrm{ref,k}}^{(i)} + \varepsilon_k^{(i)}, \quad \text{if } \delta_k^{(i)} < P_{D,k} \ ,$$

where $z_k^{(j)}$ is the j-th two-dimensional measurement at time k and $x_{\mathrm{ref,k}}^{(i)}$ is the i-th reference position at time k. If an uniform random variable $\delta_k^{(i)} \in [0,1]$ is larger than the detection probability $P_{D,k}$, the measurement that corresponds to $x_{\mathrm{ref,k}}^{(i)}$ is not generated. The measurement noise $\varepsilon_k^{(i)}$ is a zero-mean Gaussian noise with standard deviation $\sqrt{2}$. In addition, the clutters over the surveillance region [80(ft) $\times$ 500(ft)] are added to the measurement data. The state $x_k = [x, y, \dot{x}, \dot{y}]^T$ consists of position $[x, y]^T$ and velocity $[\dot{x}, \dot{y}]^T$. The unit time Δ is 0.1s. The linear Gaussian models (4.5),(4.6) considered in the simulation can be presented using

$$F_{k-1} = \begin{bmatrix} I_2 & \Delta I_2 \\ 0_2 & I_2 \end{bmatrix}, \qquad H_k = \begin{bmatrix} I_2 & 0_2 \end{bmatrix},$$
$$Q_{k-1} = \sigma_\omega^2 \begin{bmatrix} \frac{\Delta^4}{4} I_2 & \frac{\Delta^3}{2} I_2 \\ \frac{\Delta^3}{2} I_2 & \Delta^2 I_2 \end{bmatrix}, \quad R_k = \sigma_\varepsilon^2 I_2,$$

where I_2 and 0_2 denote the 2×2 identity and zero matrices, respectively. The standard deviation of the process noise σ_ω^2 is 5(ft/s^2) and that of the measurement noise σ_ε^2 is given by 2(ft). The survival probability $p_{S,k}$ is 0.99 and the weight and covariance used for generating birth intensities, denoted as w_b and P_b, are 0.01 and diag([5, 5, 20, 20]), respectively. $[\mu_{\min}, \mu_{\max}]$ is $[-4, 2]$ and the maximum duplication time $\rho_{\max}$ is 5.

The simulation was carried out with the detection probabilities $p_{D,k} = 0.75, 0.9$, and 0.9999. The number of clutters are $\lambda_c = 5, 10$, and 15. The $p_{D,k}$ and λ_c can effect the false negative/positive detection rate. The parameters $G_{\mathrm{th}} = 9$, and $D_{\mathrm{th}} = 1$ (see Table.4.1 for the parameters) are applied.

For comparison, three versions of the GM-PHD filter were applied to track the multi-targets: 1) the original GM-PHD filter [54], 2) the tag-based GM-PHD filter [61], and 3) proposed robust GM-PHD filter. The original GM-PHD filter is described in Sec. II. In the tag-based GM-PHD filter, each state has a tree with

$1 + M_k$ branches as described in Sec. II. The heaviest branch $w_k^{(i)} > w_{\text{th}}$ is picked from each tree to construct individual target tracks. If all branches on a tree are consecutively $w_k^{(i)} < w_{\text{th}}$, the corresponding state is removed. In the applied original and tag-based GM-PHD filter, the birth intensities are generated with a random position $m_{\gamma,k} = [x_{\gamma,k}, y_{\gamma,k}, 0, 0]^T$, where $x_{\gamma,k} \in [0, 80]$ and $y_{\gamma,k} \in [0, 500]$ are randomly generated with an uniform distribution.

Fig.4.6 shows the measurements obtained with the detection probability $p_{D,k} = 0.9999$ and $\lambda_c = 15$ clutters. The multi-vehicles drive on the multi-lane road and the number of observed vehicles increases with time. In Fig.4.7 we can see that the proposed robust GM-PHD filter scheme can provide accurate multi-target tracking results.

In order to evaluate the estimation performance of the robust GM-PHD filter, the OSPA distance metric [64] was adopted in the simulation. The OSPA metric between the estimated target set $\hat{X} = \{\hat{x}^{(1)}, \ldots, \hat{x}^{(m)}\}$ and the reference set $Y = \{y^{(1)}, \ldots, y^{(n)}\}$ at time k with $m \leq n$ is calculated by

$$\bar{d}_p^{(c)}\left(\hat{X}, Y\right) = \left(\frac{1}{n}\left(\min_{\pi \in \Pi_n} \sum_{i=1}^{m} d^{(c)}\left(x^{(i)}, y^{(\pi(i))}\right)^p + c^p\left(n - m\right)\right)\right)^{1/p},$$

where $d^{(c)}(x, y) = \min\left(c, ||x - y||\right)$. If $m > n$, $\bar{d}_p^{(c)}(\hat{X}, Y) := \bar{d}_p^{(c)}(Y, \hat{X})$. The parameters p and c are set to 1 and 200(ft), respectively. Before calculating the OSPA metric, the permutation sets Π_n between $\hat{X}$ and Y should be determined.

Fig.4.8(a) and 4.8(b) show the cardinality and OSPA metric of the multi-target estimations obtained by the original, tag-based and robust GM-PHD filter with $p_{D,k} = 0.9999$ and $\lambda_c = 5$ and 15. In these scenarios, the cardinality estimated by the three GM-PHD filters are not significantly different from the true cardinality and the estimated OSPA are small enough. These filter schemes can provide accurate estimates if there is few detection loss. The proposed scheme provides the

best estimates among the three GM-PHD schemes. The OSPA at early iteration is relatively large since there are a few confirmed estimates at that time, so this phenomenon is generally shown in the multi-target tracking.

The cardinality estimated by the original and tag-based GM-PHD filter oscillates up and down slightly since the birth intensities are generated using random positions in their schemes. On the other hand, the cardinality obtained by the proposed scheme do not oscillate because the birth intensities are formed based on the non-associated measurements and they are managed by using the confirmation score μ. The unconfirmed states, $\mu > 0$, are evaluated for $\mu_{\max}$.

Fig.4.9 and 4.10 show the cardinality and OSPA metric obtained by worse detection rates $p_{D,k} = 0.9$ and 0.75, respectively. At a low detection rate, the estimation accuracy also becomes also low. When $p_{D,k} = 0.9$, the original GM-PHD filter dramatically degrades because the states with low weights are removed or merged into other states. On the other hand, the tag-based and robust GM-PHD filter schemes provide relatively accurate estimates because the states are deleted if they consecutively have low weights. When $p_{D,k} = 0.75$, we can see both the original and tag-based GM-PHD filter provide inaccurate estimations. The cardinality is significantly different from the true targets and the OSPA distance is relatively large. On the other hand, we can see that the robust GM-PHD filter can provide relatively accurate estimations although $p_{D,k}$ is not large.

We can confirm that the robust GM-PHD filter can effectively estimate the multi-target states even though there are many false positives and negatives, which can negatively affect the multi-target tracking.

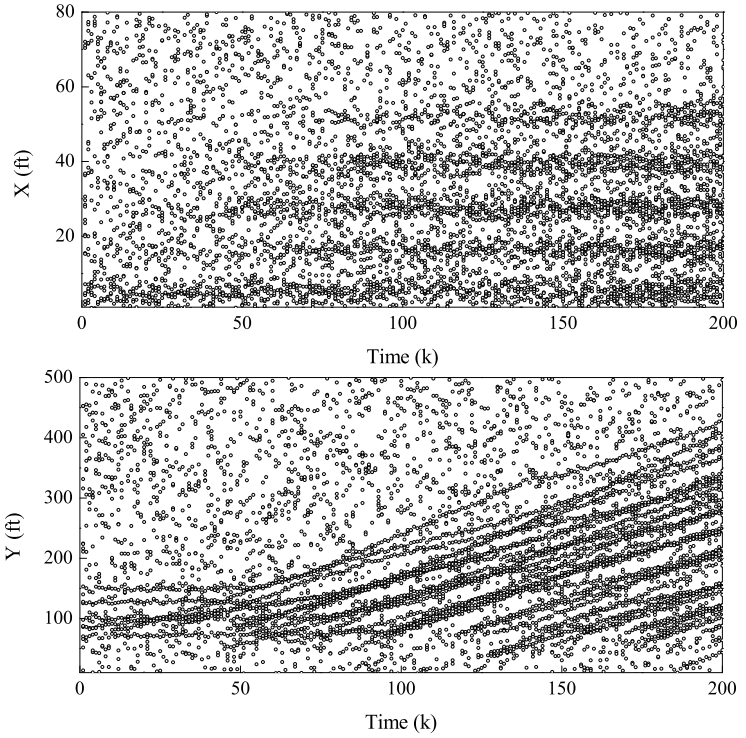

Figure 4.6: Measurements obtained with the detection probability $p_{D,k} = 0.9999$ and $\lambda_c = 15$ clutters.

4.6 Conclusion

We investigated the robust multi-target tracking scheme based on the GM-PHD filter. Through the robust GM-PHD filter, the multi-targets can be effectively estimated even if there are many false positive/negative detections. The robust GM-PHD filter scheme includes the processing step of evaluating multiple states/measurements which is designed to overcome the weight under/over-estimation problem. Furthermore, it includes the step of generating the birth intensity for the next iteration using the measurements not associated with any tracked states. In the simulation, the robust GM-PHD filter showed relatively accurate estimation results with the accurate cardinality and short OSPA distance. These achievement can be applied

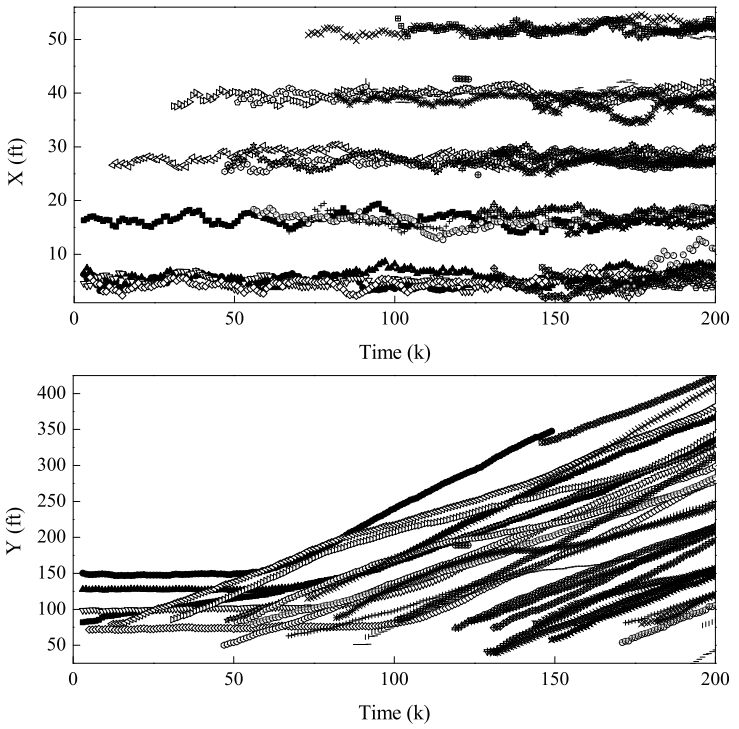

Figure 4.7: Multi-target tracks estimated by the proposed robust GM-PHD filter scheme with the detection probability $p_{D,k} = 0.9999$ and $\lambda_c = 15$ clutters.

to state-of-the-art applications such as robotics or intelligent vehicle technologies.

Table 4.1: The Notations

w	weight
m	mean (peak) of the intensity
P	covariance of the intensity
Id	Identity
μ	confirmation score
ρ	duplication time
τ	survival time
$X_k^{(i)}$	X of the i-th state at time k
$X_{\gamma,k}^{(i)}$	X of the i-th birth state
$X_{k\|k-1}^{(i)}$	X of the i-th prediction
$\eta_{k\|k-1}^{(i)}, S_k^{(i)}$ $K_k^{(i)}, P_{k\|k}^{(i)}$	PHD update components
$z_k^{(i)}$	i-th measurement at time k
$z_{\mathrm{NA},k}^{(i)}$	i-th measurement not associated with any states
Ω_k	a set of the state parameters
Γ_k	a set of the birth state parameters
$\Omega_{k\|k-1}$	a set of the prediction parameters
Λ_k	a set of the PHD components
$\mathrm{ID}_{\mathrm{unused}}$	a set of the unused IDs
Z_k	a set of $z_k^{(i)}$
$Z_{\mathrm{NA},k}$	a set of $z_{\mathrm{NA},k}^{(i)}$
$J_k, J_{\gamma,k}, J_{k\|k-1}$	the number of $X_k^{(i)}$, $X_{\gamma,k}^{(j)}$, and $X_{k\|k-1}^{(l)}$
$M_k, M_{\mathrm{NA},k}$	the number of $z_k^{(i)}$ and $z_{\mathrm{NA},k}^{(i)}$
$p_{S,k}$	the state survival probability
$p_{D,k}$	the detection probability
κ_k	the intensity of clutter at time
λ_c	the number of clutters over the surveillance region
G_{th}	a size of the observation gate of predictions
D_{th}	a distance threshold for the duplication check

Algorithm 6 Overall procedure of the proposed robust GM-PHD filter.

1: **given**

2: $\Omega_{k-1} = \left\{ w_{k-1}^{(i)}, m_{k-1}^{(i)}, P_{k-1}^{(i)}, \mathrm{Id}_{k-1}^{(i)}, \mu_{k-1}^{(i)}, \rho_{k-1}^{(i)}, \tau_{k-1}^{(i)} \right\}_{i=1}^{J_{k-1}}$,

3: $\Gamma_k = \left\{ w_{\gamma,k}^{(i)}, m_{\gamma,k}^{(i)}, P_{\gamma,k}^{(i)}, \mathrm{Id}_{\gamma,k}^{(i)} \right\}_{i=1}^{J_{\gamma,k}}$, where $w_{\gamma,k}^{(i)} = w_b$, $P_{\gamma,k}^{(i)} = P_b$,

4: $Z_k = \left\{ z_k^{(i)} \right\}_{i=1}^{M_k}$,

5: $\mathrm{ID}_{\mathrm{unused}} = \left\{ \mathrm{Id}^{(i)} \right\}_{i=1}^{N_{\max} - J_{k-1} - J_{\gamma,k}}$,
where $\mathrm{Id}^{(i)} \notin \left\{ \mathrm{Id}_{k-1}^{(j \in 1,\ldots,J_{k-1})} \cup \mathrm{Id}_{\gamma,k}^{(l \in 1,\ldots,J_{\gamma,k})} \right\}$, and

6: $w_{\mathrm{confirm}} = E\left[w_{k-1}^{(i)} \right]$ where $\left\{ i | \mu_{k-1}^{(i)} = 0 \right\}$.

Step.1 (Target prediction and PHD update component construction.)

7: $\left[\Omega_{k|k-1}, \Lambda_k \right] = f_{\mathrm{Alg.7}}\left(\Omega_{k-1}, \Gamma_k \right)$,
where
$\Omega_{k|k-1} = \left\{ w_{k|k-1}^{(i)}, m_{k|k-1}^{(i)}, P_{k|k-1}^{(i)}, \mathrm{Id}_{k|k-1}^{(i)}, \mu_{k|k-1}^{(i)}, \rho_{k|k-1}^{(i)}, \tau_{k|k-1}^{(i)} \right\}_{i=1}^{J_{k|k-1}}$,
$\Lambda_k = \left\{ \eta_{k|k-1}^{(i)}, S_k^{(i)}, K_k^{(i)}, P_{k|k}^{(i)} \right\}_{i=1}^{J_{k|k-1}}$.

Step.2 (State and measurement evaluation.)

8: $\left[\Omega_{k|k-1}, \Lambda_k, Z_k, Z_{\mathrm{NA},k} \right] = f_{\mathrm{Alg.8}}\left(\Omega_{k|k-1}, \Lambda_k, Z_k, w_{\mathrm{confirm}} \right)$,
where $Z_{\mathrm{NA},k} = \left\{ z_{\mathrm{NA},k}^{(i)} \right\}_{i=1}^{M_{\mathrm{NA},k}}$.

Step.3 (PHD updating and merging.)

9: $\left[\Omega_k \right] = f_{\mathrm{Alg.10}}\left(\Omega_{k|k-1}, \Lambda_k, Z_k \right)$,
where $\Omega_k = \left\{ w_k^{(i)}, m_k^{(i)}, P_k^{(i)}, \mathrm{Id}_k^{(i)}, \mu_k^{(i)}, \rho_k^{(i)}, \tau_k^{(i)} \right\}_{i=1}^{J_k}$.

Step.4 (Duplication check.)

10: $\left[\Omega_k \right] = f_{\mathrm{Alg.11}}\left(\Omega_k \right)$.

Step.5 (birth intensity generation for the next iteration.)

11: $\left[\Gamma_{k+1}, \mathrm{ID}_{\mathrm{unused}} \right] = f_{\mathrm{Alg.12}}\left(Z_{\mathrm{NA},k}, \mathrm{ID}_{\mathrm{unused}}, \left\{ \mathrm{Id}_k^{(i)} \right\}_{i=1}^{J_k} \right)$,
where
$\Gamma_{k+1} = \left\{ w_{\gamma,k+1}^{(i)}, m_{\gamma,k+1}^{(i)}, P_{\gamma,k+1}^{(i)}, \mathrm{Id}_{\gamma,k+1}^{(i)} \right\}_{i=1}^{J_{\gamma,k+1}}$.

12: **output** $\Omega_k, \Gamma_{k+1}, \mathrm{ID}_{\mathrm{unused}}$.

Algorithm 7 Target prediction and PHD update component construction.

given

$\Omega_{k-1} = \left\{ w_{k-1}^{(i)}, m_{k-1}^{(i)}, P_{k-1}^{(i)}, \mathrm{Id}_{k-1}^{(i)}, \mu_{k-1}^{(i)}, \rho_{k-1}^{(i)}, \tau_{k-1}^{(i)} \right\}_{i=1}^{J_{k-1}}$, and

$\Gamma_k = \left\{ w_{\gamma,k}^{(i)}, m_{\gamma,k}^{(i)}, P_{\gamma,k}^{(i)}, \mathrm{Id}_{\gamma,k}^{(i)} \right\}_{i=1}^{J_{\gamma,k}}$.

(Prediction for existing targets)

$i = 0$.

for $j = 1$ **to** J_{k-1} **do**

  $i := i + 1$.

  $w_{k|k-1}^{(i)} = p_{S,k} w_{k-1}^{(j)}, \quad m_{k|k-1}^{(i)} = F_{k-1} m_{k-1}^{(j)}$,

  $P_{k|k-1}^{(i)} = Q_{k-1} + F_{k-1} P_{k-1}^{(j)} F_{k-1}^T$,

  $\mathrm{Id}_{k|k-1}^{(i)} = \mathrm{Id}_{k-1}^{(j)}, \quad \mu_{k|k-1}^{(i)} = \mu_{k-1}^{(j)}$,

  $\rho_{k|k-1}^{(i)} = \rho_{k-1}^{(j)}, \quad \tau_{k|k-1}^{(i)} = \tau_{k-1}^{(j)} + 1$.

end for

(Prediction for birth targets)

for $j = 1$ **to** $J_{\gamma,k}$ **do**

  $i := i + 1$.

  $w_{k|k-1}^{(i)} = w_{\gamma,k}^{(j)}, \quad m_{k|k-1}^{(i)} = m_{\gamma,k}^{(j)}, \quad P_{k|k-1}^{(i)} = P_{\gamma,k}^{(j)}$,

  $\mathrm{Id}_{k|k-1}^{(i)} = \mathrm{Id}_{\gamma,k}^{(j)}, \quad \mu_{k|k-1}^{(i)} = \mu_{\max}, \quad \rho_{k|k-1}^{(i)} = 0, \quad \tau_{k|k-1}^{(i)} = 1$.

end for

$J_{k|k-1} = i$.

(Construction of PHD update components)

for $j = 1$ **to** $J_{k|k-1}$ **do**

  $\eta_{k|k-1}^{(j)} = H_k m_{k|k-1}^{(j)}, \quad S_k^{(j)} = R_k + H_k P_{k|k-1}^{(j)} H_k^T$,

  $K_k^{(j)} = P_{k|k-1}^{(j)} H_k^T [S_k^{(j)}]^{-1}, \quad P_{k|k}^{(j)} = [I - K_k^{(j)} H_k] P_{k|k-1}^{(j)}$.

end for

output

$\Omega_{k|k-1} = \left\{ w_{k|k-1}^{(i)}, m_{k|k-1}^{(i)}, P_{k|k-1}^{(i)}, \mathrm{Id}_{k|k-1}^{(i)}, \mu_{k|k-1}^{(i)}, \rho_{k|k-1}^{(i)}, \tau_{k|k-1}^{(i)} \right\}_{i=1}^{J_{k|k-1}}$,

$\Lambda_k = \left\{ \eta_{k|k-1}^{(i)}, S_k^{(i)}, K_k^{(i)}, P_{k|k}^{(i)} \right\}_{i=1}^{J_{k|k-1}}$.

Algorithm 8 State and measurement evaluation (part 1).

given

$\Omega_{k|k-1} = \left\{ w_{k|k-1}^{(i)}, m_{k|k-1}^{(i)}, P_{k|k-1}^{(i)}, \right.$
$\left. \mathrm{Id}_{k|k-1}^{(i)}, \mu_{k|k-1}^{(i)}, \rho_{k|k-1}^{(i)}, \tau_{k|k-1}^{(i)} \right\}_{i=1}^{J_{k|k-1}}$,

$\Lambda_k = \left\{ \eta_{k|k-1}^{(i)}, S_k^{(i)}, K_k^{(i)}, P_{k|k}^{(i)} \right\}_{i=1}^{J_{k|k-1}}$, and

$Z_k = \left\{ z_k^{(i)} \right\}_{i=1}^{M_k}$.

w_{confirm}.

(Make an evaluation matrix, A)

$A = \left[\left\{ a_{ij} = 0 | i \in \left(1, \ldots, J_{k|k-1}\right), j \in (1, \ldots, M_k) \right\} \right]$.

for $i = 1$ **to** $J_{k|k-1}$ **do**

  for $j = 1$ **to** M_k **do**

    if $\left(\eta_{k|k-1}^{(i)} - z_k^{(j)}\right)^T \left[S_k^{(i)}\right]^{-1} \left(\eta_{k|k-1}^{(i)} - z_k^{(j)}\right) \leq G_{\mathrm{th}}$ **then**

      $a_{ij} = 1$.

    end if

  end for

end for

(Find the measurements not associated with any tracked targets)

$l = 0, \quad L = \phi$.

for $j = 1$ **to** M_k **do**

  if $\sum_{i=1}^{J_{k|k-1}} a_{ij} = 0$ **then**

    $l := l + 1$.

    $z_{\mathrm{NA},k}^{(l)} = z_k^{(j)}, \quad L := [L, j]$.

  end if

end for

for $j \in L$ **do**

  Delete $\left\{ z_k^{(j)} \right\}$ from Z_k

end for

$M_k := M_k - \mathrm{length}(L), \quad M_{\mathrm{NA},k} := \mathrm{length}(L)$.

Go to Alg.9

Algorithm 9 State and measurement evaluation (part 2).

(Update the confirmation scores, $\mu_{k|k-1}^{(i)}$ for $i \in \{1, \ldots, J_{k|k-1}\}$)
for $i = 1$ **to** $J_{k|k-1}$ **do**
  if $\sum_{j=1}^{M_k} a_{ij} > 0$ **then**
    if $\mu_{k|k-1}^{(i)} < 0$ **then**
      $\mu_{k|k-1}^{(i)} = 0, \quad w_{k|k-1}^{(i)} = w_{\text{confirm}}$.
    else
      if $\mu_{k|k-1}^{(i)} > 0$ **then**
        $\mu_{k|k-1}^{(i)} := \mu_{k|k-1}^{(i)} - 1$
        if $\mu_{k|k-1}^{(i)} = 0$ **then**
          $w_{k|k-1}^{(i)} = w_{\text{confirm}}$.
        end if
      end if
    end if
  else
    if $\mu_{k|k-1}^{(i)} \leq 0$ **then**
      $\mu_{k|k-1}^{(i)} := \mu_{k|k-1}^{(i)} - 1$.
    else
      $\mu_{k|k-1}^{(i)} := \mu_{\max} + 1$.
    end if
  end if
end for
(Delete the useless targets)
$L = \phi$. (Empty matrix)
for $i = 1$ **to** $J_{k|k-1}$ **do**
  if $\left(\mu_{k|k-1}^{(i)} < \mu_{\min}\right)$ or $\left(\mu_{k|k-1}^{(i)} > \mu_{\max}\right)$ **then**
    $L := [L, i]$.
  end if
end for
for $i \in L$ **do**
  Delete $\left\{w_{k|k-1}^{(i)}, m_{k|k-1}^{(i)}, P_{k|k-1}^{(i)}, \text{Id}_{k|k-1}^{(i)}, \mu_{k|k-1}^{(i)}, \rho_{k|k-1}^{(i)}, \tau_{k|k-1}^{(i)}\right\}$ from $\Omega_{k|k-1}$.
  Delete $\left\{\eta_{k|k-1}^{(i)}, S_k^{(i)}, K_k^{(i)}, P_{k|k}^{(i)}\right\}$ from Λ_k.
end for
$J_{k|k-1} := J_{k|k-1} - \text{length}(L)$.
output updated $\Omega_{k|k-1}$, Λ_k, Z_k, and $Z_{\text{NA},k} = \left\{z_{\text{NA},k}^{(i)}\right\}_{i=1}^{M_{\text{NA},k}}$

Algorithm 10 PHD updating and merging

given

$\Omega_{k|k-1} = \left\{ w_{k|k-1}^{(i)}, m_{k|k-1}^{(i)}, P_{k|k-1}^{(i)}, \mathrm{Id}_{k|k-1}^{(i)}, \mu_{k|k-1}^{(i)}, \rho_{k|k-1}^{(i)}, \tau_{k|k-1}^{(i)} \right\}_{i=1}^{J_{k|k-1}}$,

$\Lambda_k = \left\{ \eta_{k|k-1}^{(i)}, S_k^{(i)}, K_k^{(i)}, P_{k|k}^{(i)} \right\}_{i=1}^{J_{k|k-1}}$, and

$Z_k = \left\{ z_k^{(i)} \right\}_{i=1}^{M_k}$.

(PHD update)

for $j = 1$ **to** $J_{k|k-1}$ **do**

  $\widetilde{w}_k^{(j)} = \left(1 - p_{D,k}\right) w_{k|k-1}^{(j)}, \quad \widetilde{m}_k^{(j)} = m_{k|k-1}^{(j)}$.

end for

$l = 0$

for each $z \in Z_k$ **do**

  $l := l + 1$.

  for $j = 1$ **to** $J_{k|k-1}$ **do**

    $\widetilde{w}_k^{(lJ_{k|k-1}+j)} = p_{D,k} w_{k|k-1}^{(j)} \mathcal{N}\left(z; \eta_{k|k-1}^{(j)}, S_k^{(j)}\right)$,

    $\widetilde{m}_k^{(lJ_{k|k-1}+j)} = m_{k|k-1}^{(j)} + K_k^{(j)}\left(z - \eta_{k|k-1}^{(j)}\right)$,

  end for

  $\mathrm{WeightSum} = \sum_{i=1}^{J_{k|k-1}} \widetilde{w}_{k|k-1}^{(lJ_{k|k-1}+i)}$.

  for $j = 1$ **to** $J_{k|k-1}$ **do**

    $\widetilde{w}_k^{(lJ_{k|k-1}+j)} := \widetilde{w}_k^{(lJ_{k|k-1}+j)} / \left(\kappa_k + \mathrm{WeightSum}\right)$

  end for

end for

$\widetilde{J}_k = J_{k|k-1} + lJ_{k|k-1}$.

$\left\{ \widetilde{w}_k^{(i)}, \widetilde{m}_k^{(i)}, \widetilde{P}_k^{(i)} \right\}_{i=1}^{\widetilde{J}_k}$.

(Merging process)

for $j = 1$ **to** $J_{k|k-1}$ **do**

  if $\mu_{k|k-1}^{(j)} < 0$ **then**

    $w_k^{(j)} := w_{k|k-1}^{(j)}, \quad m_k^{(j)} := m_{k|k-1}^{(j)}, \quad P_k^{(j)} := P_{k|k-1}^{(j)}$.

  else

    $w_k^{(j)} = 0, \quad m_k^{(j)} = [0, \ldots, 0]^T$.

    for $l = 0$ **to** M_k **do**

      $l' = lJ_{k|k-1} + j$.

      $w_k^{(j)} := w_k^{(j)} + \widetilde{w}_k^{(l')}, \quad m_k^{(j)} := m_k^{(j)} + \widetilde{w}_k^{(l')} \widetilde{m}_k^{(l')}$.

    end for

    $m_k^{(j)} := m_k^{(j)} / w_k^{(j)}$.

    $P_k^{(j)} = P_{k|k}^{(j)}$.

  end if

  $\mathrm{Id}_k^{(j)} = \mathrm{Id}_{k|k-1}^{(j)}, \quad \mu_k^{(j)} = \mu_{k|k-1}^{(j)}, \quad \rho_k^{(j)} = \rho_{k|k-1}^{(j)}, \quad \tau_k^{(j)} = \tau_{k|k-1}^{(j)}$.

end for

$J_k = J_{k|k-1}$.

output

$\Omega_k = \left\{ w_k^{(i)}, m_k^{(i)}, P_k^{(i)}, \mathrm{Id}_k^{(i)}, \mu_k^{(i)}, \rho_k^{(i)}, \tau_k^{(i)} \right\}_{i=1}^{J_k}$.

Algorithm 11 Duplication check.

given
$\Omega_k = \left\{ w_k^{(i)}, m_k^{(i)}, P_k^{(i)}, \mathrm{Id}_k^{(i)}, \mu_k^{(i)}, \rho_k^{(i)}, \tau_k^{(i)} \right\}_{i=1}^{J_k}$.
(Update the duplication time, $\rho_k^{(i)}$ for $i \in \{1, \ldots, J_k\}$)
for $i = 1$ **to** J_k **do**
  for $j = 1$ **to** J_k **do**
    if $i \neq j$ and $\left\| H_k m_k^{(i)} - H_k m_k^{(j)} \right\|_2 < D_{\mathrm{th}}$ **then**
      $\rho_k^{(i)} := \rho_k^{(i)} + 1$.
      break
    else
      if $i \neq j$ and $j = J_k$ and $\rho_k^{(i)} > 0$ **then**
        $\rho_k^{(i)} := \rho_k^{(i)} - 1$.
      end if
    end if
  end for
end for
$\Omega_k = \left\{ w_k^{(i)}, m_k^{(i)}, P_k^{(i)}, \mathrm{Id}_k^{(i)}, \mu_k^{(i)}, \rho_k^{(i)}, \tau_k^{(i)} \right\}_{i=1}^{J_k}$.
(Delete the duplicated targets)
$i = 0$.
while $J_k > 0$ **do**
  $i := i + 1$.
  if $\rho_k^{(1)} \leq \rho_{\max}$ **then**
    $\widetilde{w}_k^{(i)} = w_k^{(1)}, \quad \widetilde{m}_k^{(i)} = m_k^{(1)}, \quad \widetilde{P}_k^{(i)} = P_k^{(1)},$
    $\widetilde{\mathrm{Id}}_k^{(i)} = \mathrm{Id}_k^{(1)}, \quad \widetilde{\mu}_k^{(i)} = \mu_k^{(1)}, \quad \widetilde{\rho}_k^{(i)} = \rho_k^{(1)}, \quad \widetilde{\tau}_k^{(i)} = \tau_k^{(1)}.$
    Delete $\left\{ w_k^{(1)}, m_k^{(1)}, P_k^{(1)}, \mathrm{Id}_k^{(1)}, \mu_k^{(1)}, \rho_k^{(1)}, \tau_k^{(1)} \right\}$ from Ω_k.
    $J_k := J_k - 1$.
  else
    $L := \phi$.
    for $j = 1$ **to** J_k **do**
      if $\rho_k^{(1)}, \rho_k^{(j)} > \rho_{\max}$ and $\left\| H_k m_k^{(1)} - H_k m_k^{(j)} \right\|_2 < D_{\mathrm{th}}$ **then**
        $L := [L, j]$.
      end if
    end for
    $a = \arg\max_{j \in L} \tau_k^{(j)}$.
    $\widetilde{w}_k^{(i)} = w_k^{(a)}, \quad \widetilde{m}_k^{(i)} = m_k^{(a)}, \quad \widetilde{P}_k^{(i)} = P_k^{(a)},$
    $\widetilde{\mathrm{Id}}_k^{(i)} = \mathrm{Id}_k^{(a)}, \quad \widetilde{\mu}_k^{(i)} = \mu_k^{(a)}, \quad \widetilde{\rho}_k^{(i)} = \rho_k^{(a)}, \quad \widetilde{\tau}_k^{(i)} = \tau_k^{(a)}.$
    for $j \in L$ **do**
      Delete $\left\{ w_k^{(j)}, m_k^{(j)}, P_k^{(j)}, \mathrm{Id}_k^{(j)}, \mu_k^{(j)}, \rho_k^{(j)}, \tau_k^{(j)} \right\}$ from Ω_k.
    end for
    $J_k := J_k - \mathrm{length}(L)$.
  end if
end while
$\widetilde{J}_k = i$.
output updated $\widetilde{\Omega}_k = \left\{ \widetilde{w}_k^{(i)}, \widetilde{m}_k^{(i)}, \widetilde{P}_k^{(i)}, \widetilde{\mathrm{Id}}_k^{(i)}, \widetilde{\mu}_k^{(i)}, \widetilde{\rho}_k^{(i)}, \widetilde{\tau}_k^{(i)} \right\}_{i=1}^{\widetilde{J}_k}$.

Algorithm 12 Birth intensity generation for the next iteration.

given
$Z_{\mathrm{NA},k} = \left\{ z_{\mathrm{NA},k}^{(i)} \right\}_{i=1}^{M_{\mathrm{NA},k}}$,
$\mathrm{ID}_{\mathrm{unused}} = \left\{ \mathrm{Id}^{(i)} \right\}_{i=1}^{i=N_{\max}-J_{k-1}-J_{\gamma,k}}$,
$\left\{ \mathrm{Id}_k^{(i)} \right\}_{i=1}^{J_k}$.
(Birth target generation)
$J_{\gamma,k+1} = M_{\mathrm{NA},k}$.
for $j = 1$ **to** $J_{\gamma,k+1}$ **do**
    $w_{\gamma,k+1}^{(j)} = w_b, \quad m_{\gamma,k+1}^{(j)} = \begin{bmatrix} z_{\mathrm{NA},k}^{(j)} \\ \mathcal{O} \end{bmatrix}, \quad P_{\gamma,k+1}^{(j)} = P_b.$
    if $\mathrm{ID}_{\mathrm{unused}} \neq \phi$ **then**
        $\mathrm{Id}_{\gamma,k+1}^{(j)} =$ any $\mathrm{Id}^{(i)}$ where $\mathrm{Id}^{(i)} \in \mathrm{ID}_{\mathrm{unused}}$.
    else
        $\mathrm{ID}_{\mathrm{unused}} := \left\{ \forall \mathrm{Id}^{(l)} \right\}_{l=1}^{N_{\max}}$.
        for $i = 1$ **to** J_k **do**
            Delete $\mathrm{Id}_k^{(i)}$ from $\mathrm{ID}_{\mathrm{unused}}$.
        end for
        $\mathrm{Id}_{\gamma,k+1}^{(j)} =$ any $\mathrm{Id}^{(i)}$ where $\mathrm{Id}^{(i)} \in \mathrm{ID}_{\mathrm{unused}}$.
    end if
end for
output
$\Gamma_{k+1} = \left\{ w_{\gamma,k+1}^{(i)}, m_{\gamma,k+1}^{(i)}, P_{\gamma,k+1}^{(i)}, \mathrm{Id}_{\gamma,k+1}^{(i)} \right\}_{i=1}^{J_{\gamma,k+1}}$, and
updated $\mathrm{ID}_{\mathrm{unused}}$.

Algorithm 13 Multi-target state extraction.

given $\left\{ m_k^{(i)}, \mu_k^{(i)} \right\}_{i=1}^{J_k}$.
$\hat{X} := \phi$.
$l := 0$.
for $i = 1$ **to** J_k **do**
    if $\mu_k^{(i)} \leq 0$ **then**
        $l := l + 1$.
        $\hat{X} := \left[\hat{X}, H_k m_k^{(i)} \right]$
    end if
end for
$\hat{J}_k = l$.
output $\hat{X} = \left\{ \hat{x}_k^{(i)} \right\}_{i=1}^{\hat{J}_k}$.

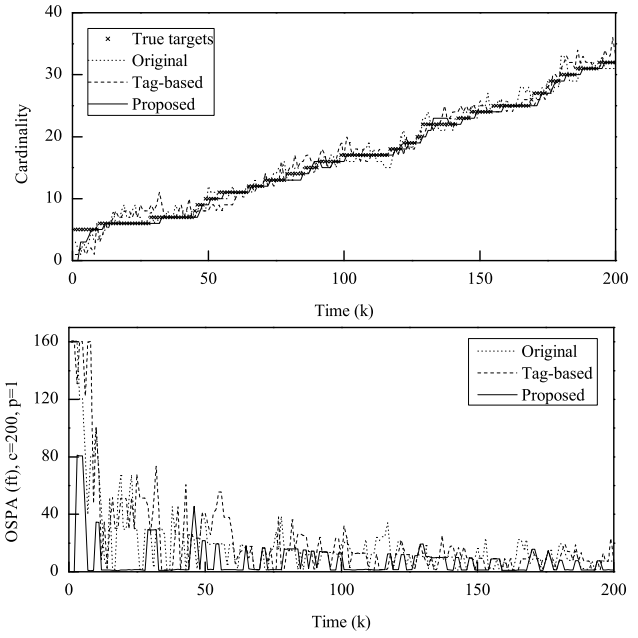

(a) $P_{d,k} = 0.9999,\ \lambda_c = 5$

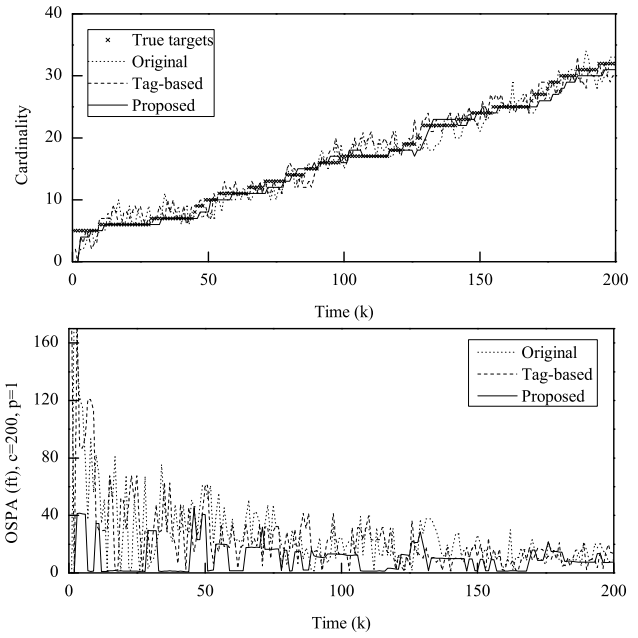

(b) $P_{d,k} = 0.9999,\ \lambda_c = 15$

Figure 4.8: Simulation results with $P_{d,k} = 0.9999$

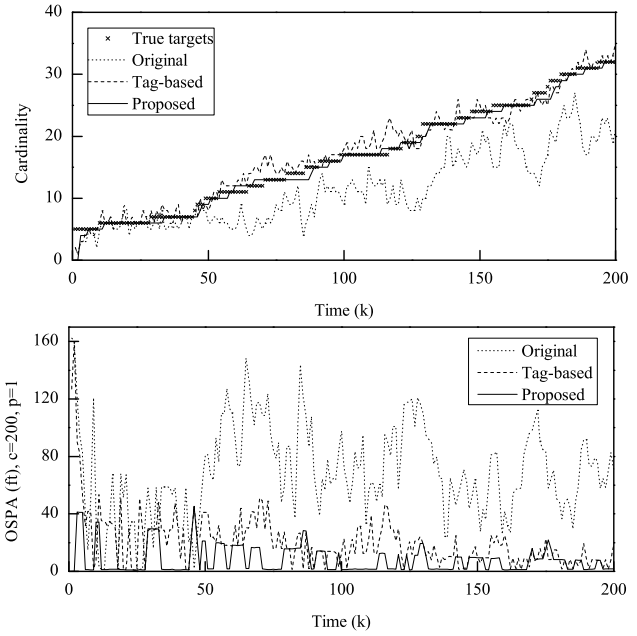

(a) $P_{d,k} = 0.9$, $\lambda_c = 5$

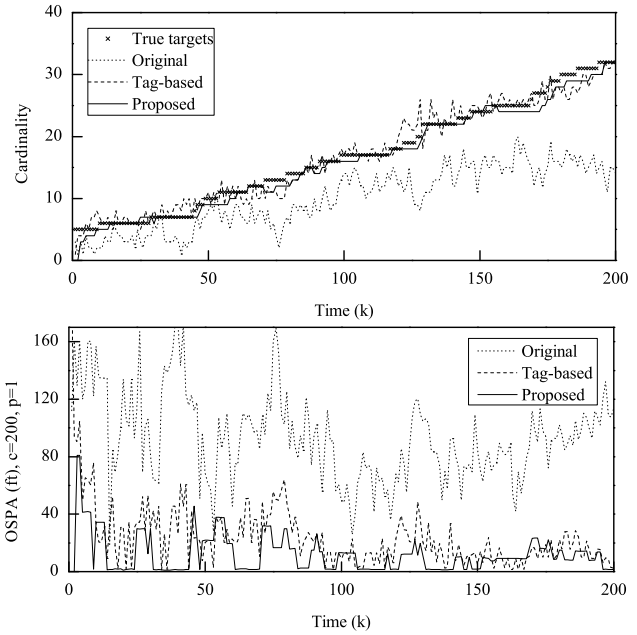

(b) $P_{d,k} = 0.9$, $\lambda_c = 15$

Figure 4.9: Simulation results with $P_{d,k} = 0.9$

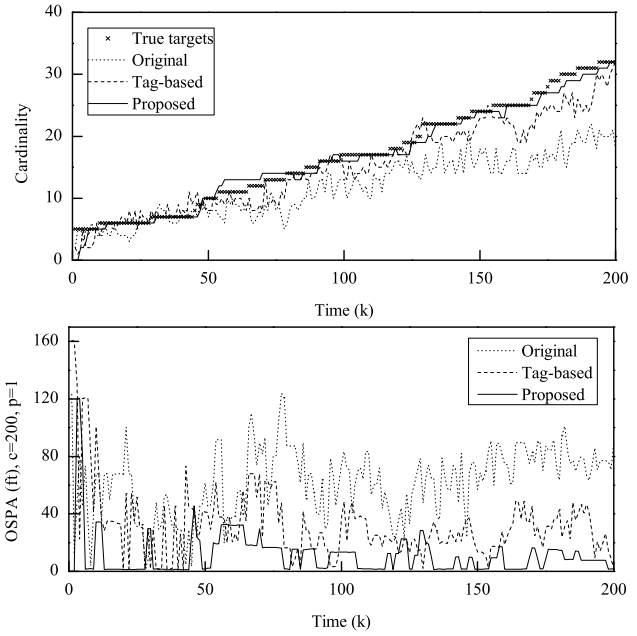

(a) $P_{d,k} = 0.75,\ \lambda_c = 5$

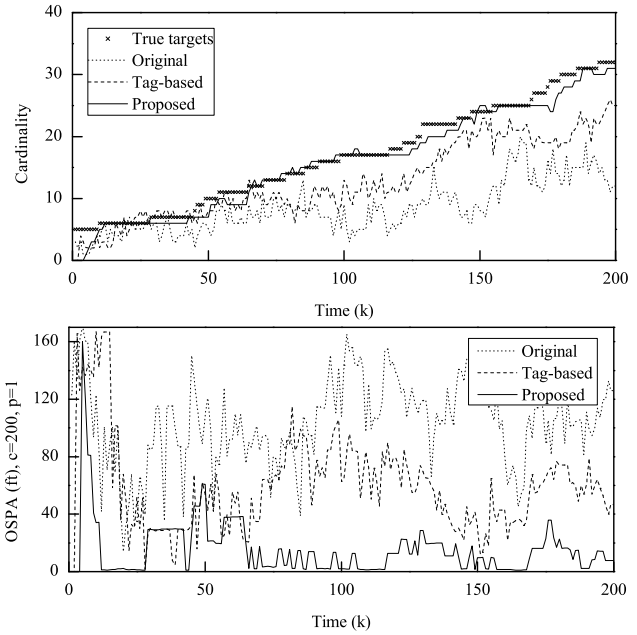

(b) $P_{d,k} = 0.75,\ \lambda_c = 15$

Figure 4.10: Simulation results with $P_{d,k} = 0.75$

Chapter 5

Conclusion and Future Work

In this dissertation, I focused on several issues for the intelligent electric vehicles. In Chapter 2, I proposed a method for the power control of the battery/SC HESS based on a convex optimization. The simulation results showed that the proposed method can effectively reduce the magnitude/fluctuation of the battery power that has an effect on a life of the battery. In Chapter 3, I proposed a real-time power control scheme for the battery/SC HESS in EVs. In the proposed scheme, the procedure of computing the SC reference voltage and the optimal SC power are included. The simulation results showed that the proposed scheme can effectively reduce not only the magnitude/variation of the battery power but also the power loss without future driving profiles. In Chapter 4, I proposed the multi-target tracking scheme, which is required for more accurately calculating the SC reference voltage. The proposed multi-target scheme based on the GM-PHD filter includes the step of the state/measurement evaluation and the birth state generation. The simulation results showed that the proposed multi-target tracking scheme can provide relatively accurate estimates even if there are many false negative/positive detections.

A number of open problems should be solved to develop the Intelligent Electric Vehicles that can be driven on roads. One such direction would be to investigate

assessing the impact of the multi-target tracking on the power control of the battery/SC HESS. For improving the power control scheme, the framework presented in this dissertation requires more precise power prediction scheme. For this, the model predictive control or Partially observable Markov decision process (POMDP) could be considered as a solution. The proposed multi-target tracking scheme can be applied for tracking the driving environments such as lanes, vehicles, or pedestrians. Since the states of vehicles and pedestrians can be defined by the position and speed, the proposed scheme can easily be adopted for estimating them with a slight modification of parameters. However, in case of the lane tracking, the state vectors and the target prediction model should be designed first.

Bibliography

[1] J. R. Miller, "Battery-Capacitor Power Source for Digital Communication Applications: Simulations using Advanced Electrochemical Capacitors," in *Proc. Electrochemical Soc.*, vol. 95-29, pp. 246-254, Oct. 1995.

[2] J. P. Zheng, T. R. Jow, and M. S. Ding, "Hybrid Power Sources for Pulsed Current Applications," *IEEE Trans. Aerosp. Electron. Syst.*, vol. 1, no. 1, pp. 288-292, Jan. 2001.

[3] H. W. Brandhorst Jr. and Z. Chen, "Achieving a High Pulse Power System through Engineering the Battery-Capacitor Combination," in *Proc. 16th Annu. Battery Conf. Applications Advances*, pp. 153-156, Jan. 2001.

[4] R. A. Dougal, S. Liu, and R. E. White, "Power and Life Extension of Battery-Ultracapactor Hybrids," *IEEE Trans. Compon. Packag. Technol.*, vol. 25, no. 1, pp. 120-131, Mar. 2002.

[5] D. Liu, and H. Li, "A Three-port Three-phase DC-DC Converter for Hybrid Low Voltage Fuel Cell and Ultracapacitor," in *Proc. Conf. Industrial Electronics*, pp. 1369-1374, Jun. 2003.

[6] S. Pay and Y. Daly, "Effectiveness of Battery-Supercapacitor Combination in Electric Vehicles," in *IEEE Proc. Power Tech. conf.*, vol. 3, pp. 1-6, Jun. 2003.

[7] A. C. Baisden and A. Emadi, "Advisor-based Model of a Battery and an Ultracapacitor Energy Source for Hybrid Electric Vehicles," *IEEE Trans. Vehic. Tech.*, vol. 53, no. 1, pp.199-205, Jan. 2004.

[8] L. Gao, R. A. Dougal, and S. Liu, "Power Enhancement of an Actively Controlled Battery/Ultracapacitor Hybrid," *IEEE Trans. Power. Electron.*, vol. 20, no. 1, Jan. 2005.

[9] A. D. Napoli, F. Crescimibini, F. G. Capponi, and L. Solero, "Constrol Strategy for Multiple Input DC-DC Power Converters Devoted to Hybrid Vehicle Propulsion Systems," in *Proc. 2002 IEEE International Symposium on Industrial Electronics*, pp. 1036-1041, May. 2002.

[10] S. M. Lukic, S. G. Wirasingha, F. Rodriguez, J. Cao, and A. Emadi, "Power Management of an Ultracapacitor/Battery Hybrid Energy Storage System in an HEV," in *IEEE Vehic. Power and Prop. Conf.*, pp.1-6, Sep. 2006.

[11] Y. Zhang, Z. Jiang. and X. Yu, "Control Strategies for Battery/Supercapacitor Hybrid Energy Storage Systems," in *IEEE Energy 2030 Conf.*, pp.1-6, Nov. 2008.

[12] J. Cao and A Emadi, "A New Battery/Ultra-Capacitor Hybrid Energy Storage System for Electric, Hybrid and Plug-in Hybrid Electric Vehicles," in *IEEE*, pp. . 2009.

[13] Z. Guoju, T. Xisheng, and Q. Zhiping, "Research on Battery Supercapacitor Hybrid Storage and its Application in MicroGrid" in *IEEE*, pp., 2010.

[14] W. Huang, D. M. Bevly, X. Li, and S. Schnick, "3D Road Geometry Based Optimal Truck Fuel Economy," in *Proc. ASME int. Mech. Eng. Congr. Expo.*, 2007.

[15] C. Zhang, A. Vahidi, P. Pisu, X. Li, K. Tennant, "Role of Terrain Preview in Energy Management of Hybrid Electric Vehicles," *IEEE Trans. Vehic. Tech.*, vol. 59, no. 3, pp. 1139-1147, Mar. 2010.

[16] V. H. Johnson, K. B. Wipke, D. J. Fhusen, "HEV Control Strategy for Real-Time optimization of Fuel Economy and Emissions," *Soc. of Autom. Eng.*, 2000-01-1543, 2000,

[17] E. D. Tate, S. P. Boyd, "Limits of Performance for Hybrid Electric Vehicles," *Soc. of Autom. Eng.*, 00FTT-50, 2000,

[18] A. Kleimaier, D. Schroder, "Design and Control of a Hybrid Vehicle by Optimal Control Theory," in *Proc. of IPEC-Tokyo 2000*, pp. 2186-2191, 2000.

[19] Karmarkar, Narendra, "A New Polynomial Time Algorithm for Linear Programming," *Combinatorica*, Vol 4, no. 4, pp. 373 395, 1984.

[20] S. Boyd, L. Vandenberghe,"Convex Optimization," Cambridge University Press, 2004.

[21] http://www.maxwell.com.

[22] J. Cao, and A. Emadi, "A New Battery/UltraCapacitor Hybrid Energy Storage System for Electric, Hybrid, and Plug-In Hybrid Electric Vehicles", in *IEEE Trans. Pow. Elect.*, vol. 27, no. 1, pp.122-132, Jan. 2012.

[23] O. C. Onar, and A. Khaligh, "A Novel Integrated Magnetic Structure Based DC/DC Converter for Hybrid Battery/Ultracapactor Energy Storage Systems", in *IEEE Trans. Smart Grid.*, vol. 3, no. 1, pp.296-307, Mar. 2012.

[24] M. B. Camara, H. Gualous, F. Gustin, and A. Berthon, "Design and New Control of DC/DC Converters to Share Energy Between Supercapacitors and Batteries in Hybrid Vehicles", in *IEEE Trans. Veh. Tech.*, vol. 57, no. 5, pp.2721-2735, Sep. 2008.

[25] M. B. Camara, H. Gualous, F. Gustin, A. Berthon, and B. Dakyo, "DC/DC Converter Design for Supercapacitor and Battery Power Management in Hybrid Vehicle Applications - Polynomial Control Strategy", in *IEEE Trans. Indust. Elect.*, vol. 57, no. 2, pp.587-597, Feb. 2010.

[26] A. D. Napoli, F. Crescimbini, F. G. Capponi, and L. Solero, "Constrol Strategy for Multiple Input DC-DC Power Converters Devoted to Hybrid Vehicle Propulsion Systems," in *Proc. 2002 IEEE International Symposium on Industrial Electronics*, pp. 1036-1041, May. 2002.

[27] Y. Zhang, Z. Jiang. and X. Yu, "Control Strategies for Battery/Supercapacitor Hybrid Energy Storage Systems," in *IEEE Energy 2030 Conf.*, pp.1-6, Nov. 2008.

[28] S. M. Lukic, S. G. Wirasingha, F. Rodriguez, J. Cao, and A. Emadi, "Power Management of an Ultracapacitor/Battery Hybrid Energy Storage System in an HEV," in *IEEE Vehic. Power and Prop. Conf.*, pp.1-6, Sep. 2006.

[29] R. Carter, A. Cruden, and P. J. Hall, "Optimizing for Efficiency or Battery Life in a Battery/Supercapacitor Electric Vehicle", in *IEEE Trans. Veh. Tech.*, vol. 61, no. 4, pp.1526-1533, May. 2012.

[30] J. Moreno, M. E. Ortuzar, and J. W. Dixon, "Energy-Management System for a Hybrid Electric Vehicle, Using Ultracapacitors and Neural Networks", in *IEEE Trans. Indust. Electr.*, vol. 53, no. 2, pp.614-623, Apr. 2006.

[31] L. Wang, E. G. Collins. Jr, and H. Li, "Optimal Design and Real-Time Control for Energy Management in Electric Vehicles", in *IEEE Trans. Veh. Tech.*, vol. 60, no. 4, pp.1419-1429, May. 2011.

[32] L. Wang, and H. Li, "Maximum Fuel Economy-Oriented Power Management Design for a Fuel Cell Vehicle Using Battery and Ultracapacitor", in *IEEE Trans. Indust. Appli.*, vol. 46, no. 3, pp.1011-1020, May/Jun. 2010.

[33] M. Zandi, A. Payman, J. P. Martin, S. Pierfederici, B. Davat , and F. M. Tabar, "Energy Management of a FuelCell/Supercapacitor/Battery Power Source for Electric Vehicular Applications", in *IEEE Trans. Veh. Tech.*, vol. 60, no. 2, pp.3882-3895, Feb. 2011.

[34] M. Choi, S. Kim, and S. Seo, "Energy Management Optimization in a Battery/Supercapacitor Hybrid Energy Storage System," in *IEEE Trans. Smartgrid*, vol. 3, no. 1, pp.463-472, Mar. 2012.

[35] M. Choi, and S. Seo, "Robust Energy Management of a Battery/Supercapacitor Hybrid Energy Storage System in an Electric Vehicle," in *IEEE Elec. Veh. Conf.*, pp.1-5, 2012.

[36] J. Bauman, and M. Kazerani, "An Analytical Optimization Method for Improved Fuel Cell-Battery-Ultracapacitor Powertrain," in *IEEE Trans. Veh. Tech.*, vol. 58, no. 7, pp.3186-3197, Sep. 2009.

[37] C. Romaus, D. Wimmelbucker, K. S. Stille, and J. Bocker, "Self-Optimzation Energy Management Considering Stochastic Influences for a Hybrid Energy Storage of an Electric Road Vehicle", in *IEEE Intern. Elect. Mach. and Driv. Conf.*, pp.67-74, 2013.

[38] B. Hredzak, V. G. Agelidis, and M. S. Jang, "A Model Predictive Control for a Hybrid Battery-Ultracapacitor Power Source", in *IEEE Trans. Power Electr.*, pp.1469-1479, 2014.

[39] J. P. Torreglosa, P. Garcia, L. M. Fernandez, and F. Jurado, "Predictive Control for the Energy Management of a Fuel-Cell-Battery-Supercapacitor Tramway", in *IEEE Trans. Indust. Inform.*, vol. 10, no. 1, pp.276-285, Feb. 2014.

[40] O. Laldin, M. Moshirvaziri, and O. Trescases, "Predictive Algorithm for Optimizaing Power Flow in Hybrid Ultracapacitor/Battery Storage Systems for Light Electric Vehicles", in *IEEE Trans. Power Electr.*, vol. 28, no. 8, pp.3882-3895, Aug. 2013.

[41] A. Sciarretta, M. Back, and L. Guzzella, "Optimal Conrol of Parallel Hybrid Electric Vehicles," in *IEEE Trans. Cont. Sys. Tech.*, vol. 12, no. 3, pp.352-363, May. 2004.

[42] A. Khaligh, and Z. Li, "Battery, Ultracapacitor, Fuel Cell, and Hybrid Energy Storage Systems for Electric, Hybrid Electric, Fuel Cell, and Plug-In Hybrid Electric Vehicles: State of the Art", in *IEEE Trans. Veh. Tech.*, vol. 59, no. 6, pp.2806-2814, Jul. 2010.

[43] E. Schaltz, A. Khaligh, and P. O. Rasmussen, "Influence of Battery/Ultracapacitor Energy-Storage Sizing on Battery Lifetime in a Fuel Cell Hybrid Electric Vehicle", in *IEEE Trans. Veh. Tech.*, vol. 58, no. 8, pp.3882-3891, Oct. 2009.

[44] H. Yeo, S. Hwang, and H. Kim, "Regenerative Braking Algorithm for a HEV with CVT Ratio Control During Deceleration," in *Proc. of the Inst. of Mech.*

Eng., Part D: Journal of Automobile Engineering, vol. 220, no. 11, pp.1589-1600, Nov. 2006.

[45] O. Tremblay, L. Dessaint, and A. Dekkiche, "A Generic Battery Model for the Dynamic Simulation of Hybrid Electric Vehicles," in *Proc. IEEE Vehicle Power Propuls. Conf.*, pp 284289, Sep. 2007.

[46] R. W. Erickson, "Fundamentals of Power Electronics, 2nd edition," 2004.

[47] T. A. Burress, S. L. Campbell, C. L. Coomer, C. W. Ayers, A. A. Wereszczak, J. P. Cunningham, L. D. Marlino, L. E. Seiber, and H. T. Lin, "Evaluation of the 2010 Toyota Prius Hybrid Synergy Drive System", in *Energy Efficiency and Renewable Energy FreedomCAR and Vehicle Technologies*, Mar. 2011.

[48] M. Ehsani, Y. Gao, A. Emadi,"Modern Electric, Hybrid Electric, and Fuel Cell Vehicles (Fundamentals, Theory, and Design)", CRC press, 2010

[49] D. Reid,"An Algorithm for Tracking Multiple Targets," in *IEEE Trans. Automatic Control*, Vol. 24, No. 6, PP, 843 - 854, Dec. 1979.

[50] S. Blackman,"Multiple Hypothesis Tracking for Multiple Target Tracking , " in *Aeros. and Elect. Sys. Magazine, IEEE*, Vol. 19, No. 1, PP, 5-18, Jan. 2004.

[51] I. Cox, and S. Hingorani,"An Efficient Implementation of Reid's Multiple Hypothesis Tracking Algorithm and Its Evaluation for the Purpose of Visual Tracking , " in *IEEE Trans. Pattern Analy. and Mach. Intel.*, Vol. 18, No. 2, PP, 138 - 150 , Feb. 1996.

[52] R. Mahler, "Multitarget Bayes filtering via first-order multitarget moments," in *IEEE Trans. Aeros. and Elect. Sys.*, Vol. 39, No. 4, PP. 1152-1178, Oct. 2003.

[53] B. Vo, S. Singh, and A. Doucet, "Sequential Monte Carlo Methods for Multi-Target Filtering with Random Finite Sets," in *IEEE Trans. Aeros. and Elect. Sys.*, Vol. 41, No. 4, pp, 1224-1245, Oct. 2005.

[54] B. Vo, and W. Ma,"The Gaussian Mixture Probability Hypothesis Density Filter, " in *IEEE Trans. Signal Proc.*, Vol. 54, No. 11, PP, 4091-4104, Nov. 2006.

[55] B. Vo, B. Vo, and A. Cantoni, "Analytic Implementations of the Cardinalized Probability Hypothesis Density Filter" in *IEEE Trans. Signal Proc.*, Vol. 55, No. 7, PP, 3553-3567, Jul. 2007.

[56] B. Ristic, D. Clark, B. N. Vo, and B. T. Vo, "Adaptive Target Birth Intensity for PHD and CPHD Filters," in *IEEE Trans. Aeros. and Elect. Sys.*, Vol. 48, No. 2, PP, 1656-1668, Apr. 2012.

[57] X. Zhou, Y. Li, B. He, and T. Bai, "GM-PHD-based Multi-Target Visual Tracking Using Entropy Distribution and Game Theory," in *IEEE Trans. Indust. Inform.*, Vol. 10, No. 2, PP, 1064-1076, May. 2014.

[58] K. Panta, B. Vo, and S. Singh, "Novel Data Association Schemes for the Probability Hypothesis Density Filter," in *IEEE Trans. Aeros. and Elect. Sys.*, Vol. 43, No. 2, PP, 556-570, Apr. 2007.

[59] E. Pollard, B. Pennetier, and M. Rombaut, "Hybrid Algorithms for Multitarget Tracking using MHT and GM-PHD," in *IEEE Trans. Aeros. and Elect. Sys.*, Vol. 47, No. 2, PP, 832-847, Apr. 2011.

[60] L. Lin, Y. Bar-Shalom, and T. Kirubarajan, "Track Labeling and PHD Filter for Multitarget Tracking," in *IEEE Trans. Aeros. and Elect. Sys.*, Vol. 42, No. 3, PP, 778-795, Jul. 2006.

[61] K. Panta, D. E. Clark, and B. Vo, "Data Association and Track Management for the Gaussian Mixture Probability Hypothesis Density Filter," in *IEEE Trans. Aeros. and Elect. Sys.*, Vol. 45, No. 3, PP, 1003-1016, Jul. 2009.

[62] C. Ouyang, and H. B. Ji,"Weight Over-estimation Problem in GMP-PHD Filter," in *Electronics Letters*, Vol. 47, No. 2, Jan. 2011.

[63] S, Blackman, and R. Popoli, "*Design and Analysis of Modern Tracking Systems*," Norwood, MA: Artech House, 1999.

[64] D. Schuhmacher, B-T. Vo, and B-N. Vo, "A consistent metric for performance evaluation of multi-object filters," in *IEEE Trans. Signal Processing*, Vol. 56, No. 8, PP, 3447-3457, Aug. 2008.

[65] NGSIM Web site at http://ngsim.fhwa.dot.gov.

[66] M. Brackstone, M. McDonald, "Car-following: a historical review," in Transportation Research Part F: Traffic Psychology and Behaviour, Vol. 2, No. 4, PP. 181196, Dec. 1999.

국문 초록

배터리는 상대적으로 낮은 파워 밀도를 가지고 있기 때문에, 높은 피크 파워와 갑작스런 파워 변화에 의해 수명이 단축될 수 있다. 이를 해결하기 위해 배터리/슈퍼캐패시터 하이브리드 에너지저장시스템 (battery/SC HESS)을 활용할 수 있다. 배터리/슈퍼캐패시터 하이브리드 에너지저장시스템 동작시 고려해야 할 주된 목표는 배터리 파워의 크기/변화량과 파워 손실을 최소화하는 것이다. 이러한 목표를 달성하기 위해 두 번째 챕터에서는 로드 동작 프로파일이 주어진 상황에서 배터리/슈퍼캐패시터의 최적 파워를 계산하기 위한 컨벡스 최적화 문제를 제시한다.

배터리/슈퍼캐패시터 하이브리드 에너지저장장치는 전기자동차에 효율적으로 적용할 수 있다. 왜냐하면 전기자동차 주행시 잦은 가/감속에 의해 발생하는 높은 피크파워와 충/방전이 배터리에 손상을 줄 수 있기 때문이다. 그러나 두 번째 챕터에서 제시한 최적 파워 제어 방식은 미래 주행 프로파일을 미리 알고 있다는 가정을 바탕으로 하고 있기 때문에 전기자동차의 실시간 파워 제어에 바로 적용하기에는 어려움이 있다. 이러한 한계를 극복하기 위해 세 번째 챕터에서는 슈퍼캐패시터의 레퍼런스 전압을 계산하는 방법과 이를 기반으로 파워 트레인, 차량 동적 특성을 고려하여 배터리, 슈퍼캐패시터의 최적 파워를 도출하는 최적화 기법을 제안한다. 이를 통해 전기자동차의 미래 주행 프로파일 없이도 배터리 파워의 크기/변화량과 파워 손실을 최소화 할 수 있다.

전기자동차의 배터리/슈퍼캐패시터 하이브리드 에너지저장장치를 보다 효율적으로 제어하기 위해서는 가까운 미래의 모터 파워를 미리 예측할 필요가 있다. 만약 미래의 속도 및 가속 정보를 예측할 수 있다면, 미래 모터파워는 두 번째 챕터에서 제시된 방법을 통해 도출 할 수 있다. 이를 위해서는 근본적으로 차량 주변 환경 (예, 차량, 보행자, 장애물 등)을 정확하게 추정할 필요가 있다.

다중 타겟 추정 정확도를 향상시키기 위해 네 번째 챕터에서는 GM-PHD필터를 기반으로 한 오탐에 강인한 다중 타겟 추적 기법을 제안한다. 제안되는 기법은 다중 상태 및 측정값 평가 단계와 새로운 상태값을 발생시키는 단계를 포함하고 있다. 제안된 방식은 비선형 가우시안 모델을 기반으로 한 예측/탐지 모델에도 적용할 수 있다.

주요어 : 최적 파워 제어, 배터리/슈퍼캐패시터, 하이브리드 에너지저장시스템, 전기자동차, 지능형자동차, 다중 타겟 추적

학 번: 2008-20990